Light-directed evolution of dynamic, multi-state, and computational protein functionalities

Vojislav Gligorovski[1], Marco Labagnara[1], Lorenzo Scutteri[1,2], Marius Blackholm[3], Andreas Möglich[3], Nahal Mansouri[4], Sahand Jamal Rahi[1,*]

[1]: Laboratory of the Physics of Biological Systems, Institute of Physics, EPFL, Switzerland

[2]: Laboratory of Protein and Cell Engineering, Institute of Bioengineering, EPFL, Switzerland

[3]: Department of Biochemistry, Universität Bayreuth, Germany

[4]: Division of Pulmonary Medicine, Department of Medicine, Lausanne University Hospital (CHUV), University of Lausanne (UNIL), Switzerland

[*]: sahand.rahi@epfl.ch

Abstract

Directed evolution is a powerful method in biological engineering. Current approaches draw on time-invariant selection mechanisms, ideal for evolving steady-state properties such as enzymatic activity or fluorescence intensity. A fundamental problem remains how to continuously evolve dynamic, multi-state, or computational functionalities, e.g., on-off kinetics, state-specific activity, stimulus-responsiveness, or switching and logic capabilities. These require selection pressure on all of the states of a protein of interest (POI) and the transitions between them. We realized that optogenetics and cell cycle oscillations could be leveraged for a novel directed evolution paradigm ('optovolution') that is germane for this need: We designed a signaling cascade in budding yeast where optogenetic input switches the POI between off (0) and on (1) states. In turn, the POI controls a Cdk1 cyclin, which in the re-engineered cell cycle system is essential for one cell cycle stage but poisonous for another. Thus, the cyclin must oscillate (1-0-1-0…) for cell proliferation. In this system, evolution can act efficiently on the POI's different states, input-output relations, and dynamics on the timescale of minutes in every cell cycle. Further, controlling the pacemaker, light, directs and tunes selection pressures. Optovolution is *in vivo*, continuous, self-selecting, and efficient. We first evolved two optogenetic systems, which relay 0/1 input to 0/1 output: We obtained 19 new variants of the LOV transcription factor El222 that were stronger, less leaky, or green light responsive *in vivo*. We demonstrate the utility of the latter mutations for orthogonal color-multiplexing with only LOV domains for the first time. Evolving the PhyB-Pif3 optogenetic system, we discovered that loss of *YOR1* makes supplementing the chromophore phycocyanobilin (PCB) unnecessary. Finally, we demonstrate the generality of the method by evolving a destabilized rtTA transcription factor, which performs an AND operation between transcriptional and doxycycline input. Optovolution makes coveted, difficult-to-change protein functionalities continuously evolvable.

Introduction

Directed evolution has been critical to improving and diversifying many of the molecular tools currently used in research and industry such as enzymes[1–5], fluorescent proteins[6,7], and antibodies[8,9]. The method relies on mutations from global or targeted mutagenesis[10–12] to diversify genetically encoded molecules. These are then screened for a desired function. The mutation-screen cycle is generally repeated to bring the molecules' functionalities closer to the desired goal.[13]

A key innovation in the field has been to couple a molecule of interest's functionality to organismal fitness obviating external intervention and screening. Such 'continuous' directed evolution methods rely on *in vivo* self-selection, which substantially simplifies and speeds up experiments, facilitating scale-up.[1,14–18] Current continuous directed evolution methods, however, use time-invariant selection mechanisms based on, for example, the strength of binding or of transcriptional activation, which are steady-state functionalities. These mechanisms can be combined to achieve complex but non-dynamic functionalities by simultaneously selecting for and against different goals[19–27] (see **Supplementary Note 1** for a partial list of previous continuous multiple-goal directed evolution experiments).

Thus, existing continuous directed evolution paradigms are poorly suited for the many natural and synthetic biological molecules that can be in different states and can dynamically switch between them. In fact, all signal transduction, control, and computation necessarily involve changes between states, usually, on (1) or off (0). For example, many transcription factors and kinases are controlled by upstream signals. In addition to relaying signals, proteins and circuits often integrate multiple inputs for cellular decisions, e.g., the amount of DNA damage and arrest times jointly determine the DNA damage checkpoint override decision.[28] Such computational capabilities are highly desirable. Building cells with more sophisticated decision-making capabilities needs logic gating, which has been created by rational design.[29–33] Evolving such proteins requires, in principle, that selection pressure is simultaneously applied on all of the computations, that is, all input-output relationships of the POI. Otherwise, if directed evolution is performed for only one state, the other states or the ability to switch to them can be corrupted.[34] For example, long-term directed evolution of GPCRs under step-wise constant ligand concentrations reduces ligand responsiveness.[35]

To address this need, researchers have developed non-continuous directed evolution methods, in which time-invariant selection mechanisms are alternated to screen each POI state sequentially[36–70] (see **Supplementary Note 2** for a partial list of past alternating selection/counterselection experiments). In these methods, two steps are typically repeated: an assay for on (1) activity is performed under inducing conditions, then an assay for off (0) activity under non-inducing conditions. In practice, selection and counterselection are performed with alternating media conditions, e.g., -uracil and +5-fluoroorotic acid[71], or changing fluorescence-activated cell sorting (FACS) gates. While creative, these approaches require interventions involving labor or specialized

instrumentation or both. Furthermore, one cycle of selection and counterselection based on media switches and cell proliferation took 8-64 hrs with bacteria or 2-5 days with yeast. This timescale determines the selection pressure placed specifically on the kinetics of the POI switch cycle, which is typically desired to be much shorter.

The ability to perform directed evolution for dynamic, multi-state, and computational protein functionalities would advance biological engineering. Here, we present the first such paradigm, which we name 'optovolution'. In contrast to previous approaches, optovolution was designed with a mechanism to evolve all input-output relationships of a POI as well as switches among them continuously. Two conceptual advances underlie optovolution (**Discussion**): By engineering a POI to control a cell cycle regulator that is essential for one step of cell proliferation but toxic to another, the POI must evolve or maintain the ability to switch the output between 0 to 1 and back rapidly, once per cell cycle. The selection mechanism is cell-intrinsic and inherently dynamic. Secondly, by controlling the input to the POI with light and optogenetics, the selection pressure is shaped by an external signal that is changing at the timescale of a cell cycle.

We apply optovolution to three systems, the optogenetic transcriptional system El222 and the optogenetic protein-protein interaction system PhyB-Pif3, which relay light input by switching on (1) or off (0), and an AND gate, in which a degron-tagged rtTA transcription factor is controlled by transcription and doxycycline. The dynamic, multi-state properties of these proteins make them unsuitable for existing continuous directed evolution paradigms:

1) LOV domains make up the core of most non-ion-channel optogenetic systems[72–80,80–86], presumably because they are small, reliable, and do not need exogenous chromophores. Interest in LOV domains has spurred past diversification work[54,87–89]. While usually controlled with light, LOV domains have also been developed as temperature sensors[90,91]. The LOV transcription factor El222, in particular, is widely used in many biological models from cell-free systems[92], to bacteria[93], yeast[94,95], mammalian cell lines[96,97], and zebrafish[98]. (See **Supplementary Note 3** for additional information regarding El222.) In comparison to other inducible transcriptional systems, El222 controlling the standard *light-inducible promoter* (*LIP*) has both more off-state leakiness and lower on-state strength than, for example, the *GAL1* promoter, demonstrating potential room for improvement.[88] Less leaky or more light-sensitive variants are desirable for different applications: Low leakiness is necessary when controlling toxic genes such as endonucleases; on the other hand, higher output under less light allows reducing phototoxicity.[88] Further, all existing LOV systems are thought to be activated exclusively by blue light, which limits their use for independently controlling multiple optogenetic systems within the same organism. Ideally, one could build optogenetic systems based on LOV domains, change their color responsiveness by mutation, and thus straightforwardly combine different systems. Instead, for independent multiplexing, one LOV domain protein has to be used together with other light-sensitive domains, each representing a challenging engineering endeavor.[99–102] In fact, substantially changing the color responsiveness of LOV domains was conjectured to be "likely impossible" based on the lack of such known natural or

111 engineered examples and physicochemical considerations.[103] Previous work to shift the absorption
112 spectrum of LOV domains with targeted mutations achieved a maximal shift of 8 nm further toward
113 UV in the absorption peak *in vitro*[104]. Shifts in the emission spectrum for use as fluorescent proteins
114 have also been attained.[105] Using optovolution, we evolved 19 new variants of El222, including more
115 light sensitive, less leaky, or *in vivo* green-light responsive mutants, paving the way for new
116 applications. Furthermore, we built a circuit for green-light-only activation of transcription,
117 demonstrating the possibility of independent addressing of LOV proteins with green and blue light.

118 2) In the widely used PhyB-Pif3 system, PhyB and Pif3 dimerize in response to red light,
119 dissociate rapidly with far-red light, or more slowly in darkness. The system is often used to change
120 the intracellular localization of proteins by fusing them to PhyB or Pif3 and anchoring the other
121 dimerization partner to a specific intracellular compartment[106,107]. (See **Supplementary Note 4** for
122 additional information regarding the PhyB-Pif3 system.) For transcriptional induction, PhyB and Pif3
123 are fused to the Gal4 transcriptional activation domain (TAD) and the Gal4 DNA binding domain
124 (DBD), respectively.[108–110] For use in yeast, *Caenorhabditis elegans*, and mammalian cells, the
125 chromophore PCB has to be supplemented.[106,108,111] The co-factor is expensive as well as light- and
126 temperature-sensitive, complicating experiments. In previous work, a biochemical pathway to
127 convert heme to PCB was introduced in different organisms.[111–114] This involved substantial genetic
128 manipulation of the host genome: Several transgenes had to be introduced, some of which needed
129 to be targeted to mitochondria, their expression levels needed to be optimized, and, in certain
130 cases, endogenous genes needed to be deleted. It is unclear whether there are pathways in cells
131 that could be modified for PhyB-Pif3 to work without supplemental PCB. Using optovolution, we
132 found that loss of function of *YOR1* makes PCB unnecessary in budding yeast. The use of *yor1Δ*
133 substantially simplifies applications and further directed evolution experiments.

134 3) While optovolution leverages light for directing evolution, we demonstrate the more general
135 applicability of optovolution by evolving a non-optogenetic logic gate. It is often desirable to
136 condition the activity of molecules on two inputs. This requires AND logic, which is relatively difficult
137 to create in biological systems. To construct such a system, we used the doxycyclin-controlled
138 transcription factor rtTA[115] and fused it to a PEST degron[116]. (See **Supplementary Note 5** for
139 additional information regarding rtTA.) This double-lock control represents an AND gate function
140 between transcriptional and doxycycline input. Without the degron, rtTA protein would be stable
141 and thus, after translation, only controlled by doxycycline; responsiveness to further transcriptional
142 input could only happen in proliferating cells at the relatively slow timescale of dilution. However,
143 the PEST-rtTA fusion protein initially produced very weak output. With optovolution, we evolved
144 two mutants that conferred substantial output from the *tetO* promoter while maintaining minimal
145 leakiness.

146 Optovolution is the first continuous directed evolution paradigm for dynamic, multi-state, and
147 computational functionalities. We demonstrate its utility by uncovering unexpected and useful
148 mutations improving three different important molecular tools.

149 # Results

150 ## Requirements for evolving dynamic, multi-state, and computational properties

151 We considered how to evolve a POI with one or more inputs and one output, each of which can be
152 in the 0 or 1 state (Fig. 1 A). Specifically, there can be a single input *i* to the POI, for example,
153 transcriptional induction of the POI, or a complex input vector $\boldsymbol{i}=(i_1,\ldots,i_n)$ such as specific
154 phosphorylation patterns at *n* residues of the POI. For such a set of possible inputs and outputs, the
155 main conceptual challenge was to find a mechanism to perform selection on each input-output
156 relationship of the POI and the kinetics of the transitions. We suppose that the input vectors are
157 labeled $\boldsymbol{i_a}$, $\boldsymbol{i_b}$, $\boldsymbol{i_c}$, $\boldsymbol{i_d}$, … and correspond to desired POI outputs 1, 0, 1, 0, … We realized that we could
158 perform continuous directed evolution on this system if we made the POI fully control a cellular
159 regulator that was essential for one step in cell proliferation but poisonous for another (Fig. 1 B, C).
160 In such a system, if the POI switches between 1-0-1-0-… outputs, driven by repeated cycles of inputs
161 $\boldsymbol{i_a}$-$\boldsymbol{i_b}$-$\boldsymbol{i_c}$-$\boldsymbol{i_d}$-…, then cells will proliferate maximally (Fig. 1 D). Any error, either in switching speed or
162 state, e.g., POI output sequence 1-1-1-0-…, causes skipped cell cycles, incurring a substantial fitness
163 penalty and giving an advantage to mutants with better fidelity to the desired input-output
164 relationships.

165 The inputs to the POI must be exogenously controllable. Optogenetic control of the POI inputs is
166 compatible with continuous directed evolution since administering light, even for weeks, is precise,
167 fast, easily tunable, cheap, straightforward, and scalable. For control of non-optogenetic POIs, light
168 input can be indirectly mediated through the rapidly expanding optogenetics toolkit, which includes
169 light-sensitive transcription factors, localization signals, degrons, and kinases, acting on the POI.[117–
170 122] On the other side, cell proliferation must be fully dependent on the POI's 1-0-1-0-… output. The
171 key idea was to find a regulator of cell proliferation, which would be required for one step in
172 proliferation but block another (Fig. 1 B-D). By engineering the POI to fully control this regulator,
173 the POI would drive one cell cycle for each 1-0 output oscillation of the POI.

174

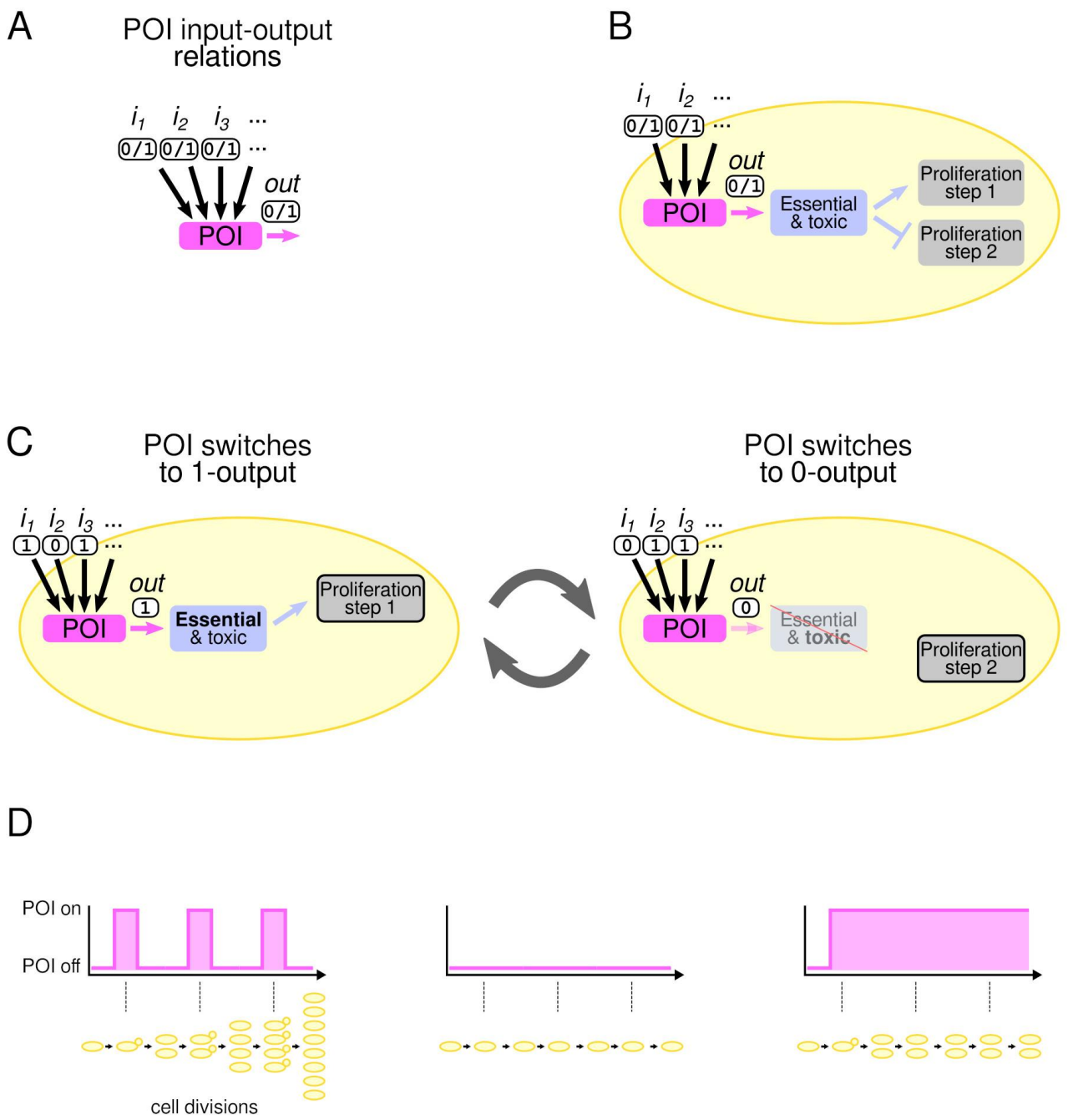

Fig. 1. Conceptualization of optovolution. A. The POI has one or multiple inputs and one output. Inputs and output are idealized as having two states, on (1) or off (0). B. In optovolution, the POI controls a cellular regulator that is essential for one step in cellular proliferation but poisonous for another. The inputs to the POI are most conveniently controlled by light, mediated by optogenetic systems, which are not shown. C. By cycling the inputs to the POI, the POI switches output states and drives cycles of cellular proliferation. D. Cells only proliferate with repeated 1-0-1-0-… output pulses of the POI, not continuously on (1) or off (0) output, in a mutationally robust manner. (Cell death and size growth not shown.)

184 ## Implementation in budding yeast

185 We engineered the system in budding yeast because it has a relatively fast cell cycle (≈ 90 min period
186 in glucose medium). A short generation time is important since it sets the maximum speed with
187 which selection pressure can be exerted on POI state switching.

188 In search of a gene that is essential for one proliferative step but poisonous for another, we
189 considered cell cycle control regulators that oscillate once per cell cycle. However, it is not obvious
190 which to choose since the cell cycle control system is remarkably robust. For example, constitutive
191 expression of *CLN2* and *CLB2* in the absence of all other Cdk1 cyclins (*cln1-3Δ clb1-6Δ*) suffices for
192 cell cycles[123]. Even in such a highly stripped-down cell cycle control system, the remaining two Cdk1
193 cyclins do not need to oscillate transcriptionally.

194 However, past experiments showing that constant transcriptional induction suffices for cell
195 proliferation were often performed with relatively weak promoters such as *GALL*[88]. Thus, we re-
196 examined elements of cell cycle control for being essential for one part of the cell cycle but
197 poisonous for another, at least, when over-expressed. Once found, we could engineer cells to be
198 even more sensitive to both the need for the cell cycle regulator at one cell cycle stage and
199 poisonous for the other.

200 For our search, we used the relatively strong blue-light-induced LOV transcription factor El222 and
201 the El222-controlled *LIP* (**Supplementary Note 3**). This system allowed us to test rapid switches in
202 target gene expression in glucose medium, where proliferation is relatively fast. We transformed
203 yeast with constructs in which *LIP* controlled the transcription of cell cycle regulators we wished to
204 test (Table 1, column 1). In these cells, we had deleted endogenous cell cycle control genes whose
205 absence makes the corresponding inducible cell cycle gene essential. Further, cells were kept viable
206 before our tests by inducible transcriptional constructs that could be shut off for the test (Table 1,
207 column 2). For more details on cell cycle regulation in budding yeast generally and in our final strain,
208 see **Supplementary Note 6**.

Candidate cell cycle regulator controlled by El222/*LIP*	Genetic background for tests	Result
CLB2	*clb1,2Δ* *GALL-CLB2*	Constitutive overexpression failed to arrest cell cycle
CLB2kd	*clb1-6Δ swe1Δ* *GALL-CLB2*	No pulsatile expression regime could be found for periodic cell cycles
CDC20	*cdc20Δ cdh1Δ* *MET3pr-CDC20*	Constitutive overexpression failed to arrest cell cycle
CLN2	*cln1-3Δ* *MET3pr-CLN2*	Constitutive overexpression failed to arrest cell cycle

CLB5	*cln1-3Δ* *MET3pr-CLN2*	Oscillatory induction needed for cell cycles
CLB5	*cln1-3Δ clb3,4,6Δ* *MET3pr-CLN2*	Oscillatory induction needed for cell cycles

Table 1: Tests to identify cell cycle regulators which are needed for one part of the cell cycle but toxic for another in specially engineered genetic backgrounds. During the tests, we turned off the nutrient-inducible promoters *MET3pr* and *GALL*.

We tested for three different properties: inviability given continuous off (0) or on (1) expression as well as proliferation under periodic expression. We started with the key components of the core cyclin-Cdk/APC negative feedback loop of the cell cycle (Table 1, Fig. 2 A). First, we tested optogenetic control of *CLB2*, the major M cyclin in budding yeast[124], in a *clb1,2Δ* background. As expected, in darkness, the lack of *CLB1* and *CLB2* caused cells to arrest before mitosis. However, continuous expression of *LIP-CLB2* did not prevent cells from cycling in glucose medium. Since Clb2 activity has to be reduced for cell cycle exit[125], we next tested whether Clb2kd, an undegradable variant of Clb2 was more suitable. Clb2kd continued to be needed for entry into mitosis and anaphase in a *clb1,2Δ* background. However, we could not find a regime of pulsing light under which cells performed periodic cell cycles. After a few cell cycles, Clb2kd blocked mitotic exit nearly permanently presumably because Sic1 inhibition and dilution did not reduce Clb2kd activity sufficiently. (Budding yeast cells have been shown to be very sensitive to the duration and period of joint Start cyclin and *GAL1pr-CLB2kd* pulsing over only a few cell cycles; this was interpreted as a signature of an artificial incoherent feedback loop[126].) Next, testing the B-type cyclin inhibitor *CDC20*, whose deletion leads to metaphase arrest, we found that it was similarly not suitable since *LIP-CDC20* overexpression did not arrest cells.

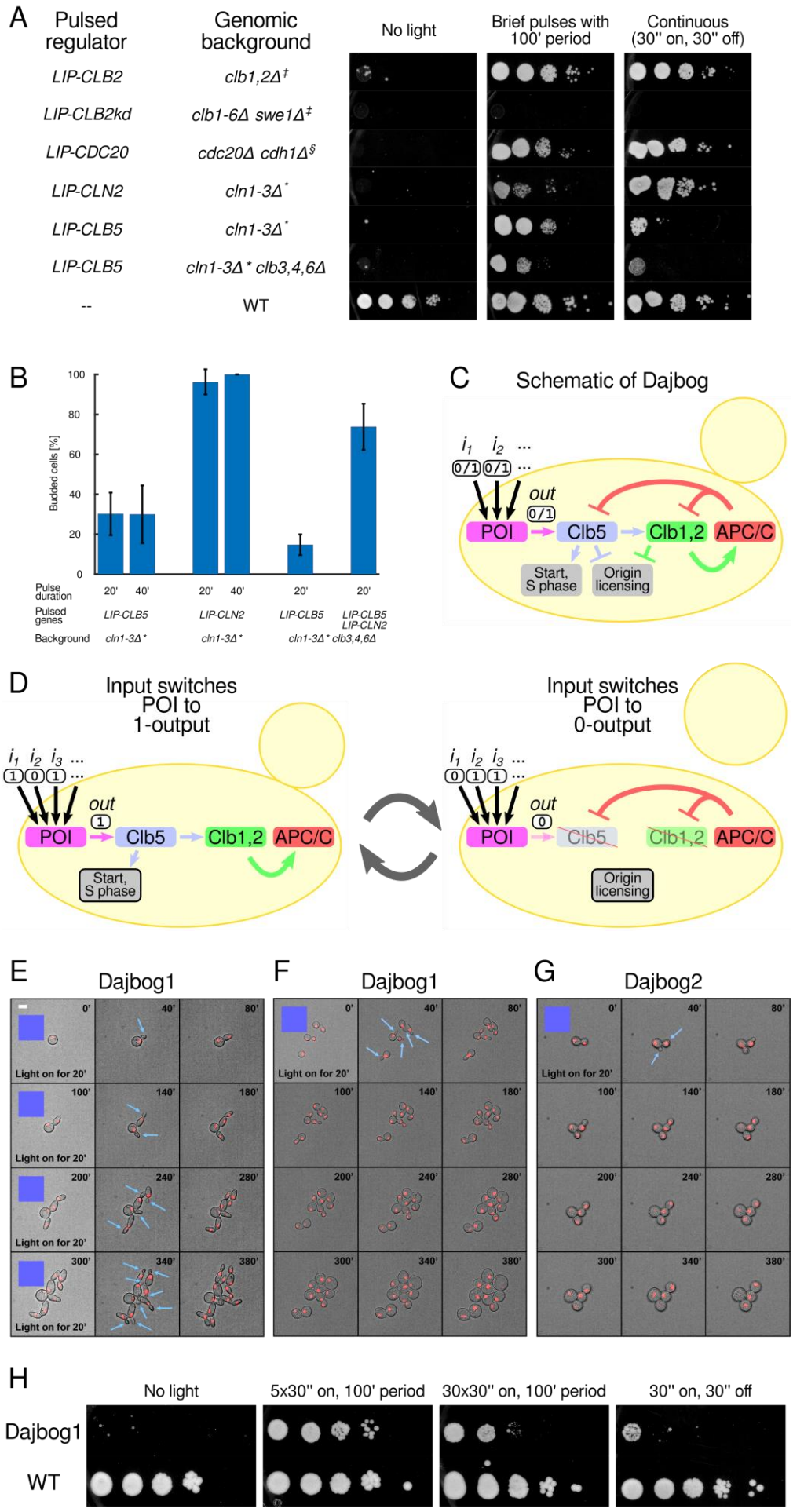
A
Pulsed regulator
Genomic background
No light
Brief pulses with 100' period
Continuous (30'' on, 30'' off)
LIP-CLB2
clb1,2Δ‡
LIP-CLB2kd
clb1-6Δ swe1Δ‡
LIP-CDC20
cdc20Δ cdh1Δ§
LIP-CLN2
cln1-3Δ*
LIP-CLB5
cln1-3Δ*
LIP-CLB5
cln1-3Δ* clb3,4,6Δ
--
WT
B
Budded cells [%]
Pulse duration
Pulsed genes
Background
20' 40' 20' 40' 20' 20'
LIP-CLB5 LIP-CLN2 LIP-CLB5 LIP-CLB5 LIP-CLN2
cln1-3Δ* cln1-3Δ* cln1-3Δ* clb3,4,6Δ
C
Schematic of Dajbog
out
POI
Clb5
Clb1,2
APC/C
Start, S phase
Origin licensing
D
Input switches POI to 1-output
Input switches POI to 0-output
E
Dajbog1
F
Dajbog1
G
Dajbog2
Light on for 20'
H
No light
5x30'' on, 100' period
30x30'' on, 100' period
30'' on, 30'' off
Dajbog1
WT

Fig. 2. Engineering budding yeast strains for optovolution. A. Evaluation of different cell cycle regulators for three properties: essential for proliferation (cells inviable when regulator is off), sufficient for proliferation when pulsed with cell cycle period (5 light pulses of 30 sec on, 30 sec off administered every 100 min, except for *cln1-3Δ clb3,4,6Δ* when we used 30 such light pulses), and lethal when expressed continuously (30 sec on, 30 sec off). (We used a 50% duty cycle, that is, 30 sec on and 30 sec off, to reduce light toxicity to a negligible level, see wild type in panel A.) All cells expressed *EL222*, which induces *LIP*. Spot tests were performed with ten-fold dilutions. (Note that panel F shows tests for the Dajbog1 (*cln1-3Δclb3-6Δ*) strain, which has been improved with respect to these three properties.) B. Efficiency of cell cycle initiation (budding) when different light-inducible cell cycle regulators are activated, assessed by timelapse microscopy. Error bars show 5-95% confidence intervals. Number of scored cells are given in Supplementary Table 3. C. Schematic of cell cycle regulators in Dajbog strains. A subset of key cell cycle elements is shown only. Cln2 and Sic1 were omitted for clarity. D. Illustration of cell cycle states of the Dajbog strains when the POI output is on (1) or off (0). E. Timelapse recording of Dajbog1 strain, exposed to diascopic microscope light every 100 min for 20 min (Supplementary Figure 1 C). Cells carry the red fluorescent nuclear marker Htb2-mCherry. Blue arrows point to buds. Scale bar, 5 µm. Blue square, time point with optogenetic light induction. F. Timelapse recording with only one light pulse administered for 20 min. G. Timelapse recording of Dajbog2 cells (Dajbog1 with *sic1Δ* deletion) with only one 20 min light pulse. H. Spot test of Dajbog1 strain under different light pulse regimes, revealing 5 times 30 sec on, 30 sec off every 100 min to be optimal among the conditions tested. In the middle two panels, five or thirty 30 sec light pulses, respectively, are separated by 30 sec of no light (off). In the right panel, 30 sec on, 30 sec off light pulses are administered continuously. Spot tests were performed with ten-fold dilutions. To keep cells proliferating before the tests, cells carried nutrient-inducible *MET3pr-CLN2* (*), *GALL-CLB2* (‡), or *MET3pr-CDC20* (§) constructs, which were shut off during the tests by glucose or methionine in the agar plates.

The cell cycle regulators discussed thus far control mitotic transitions, where arrest and release often induce aneuploidy. We next shifted our focus to cyclins which control the G1-to-Start transition, which is less perilous for genomic stability. While pulsing of the G1/S cyclin *CLN2* has been extensively tested,[126] constitutive over-expression of *CLN2* from El222/*LIP* in the *cln1-3Δ* background, where *CLN2* is essential, did not kill cells. Thus, we turned to the S-phase cyclin *CLB5*. We first tested *LIP-CLB5* in a *cln1-3Δ* strain since *CLB5* expression is known to override *cln1-3Δ* G1 arrest[127], although with lower efficiency than the G1/S cyclin *CLN2*. In darkness, cells were arrested in G1. Light pulses with a 100 min period led to repeated cell cycles. Fortuitously, we found that constitutive *CLB5* expression by El222/*LIP* severely impeded proliferation and was lethal over multiple cell cycles . (In contrast, *GAL1pr-CLB5* overexpression in galactose medium, as opposed to glucose medium, where cell cycles are substantially slower, is tolerated.[128]) Thus, *CLB5* was a promising candidate for tightly coupling the cell cycle to the POI.

Next, we engineered the system for mutational robustness. To further increase the cells' dependence on *LIP-CLB5* expression, we deleted the four chromosomal *CLB3,4,5,6* gene copies, which can be functionally redundant with light-induced *CLB5*[129,130]. No mutations are known that can bypass the requirement for Clb5 in a *cln1-3Δ clb3-6Δ* background[131], where Clb5 triggers Start, S phase, and mitotic entry. We named this genotype Dajbog1 (including appropriate constructs for *CLB5* and *CLN2* control) after the mythological Slavic deity coupling astronomical cycles and light to life[132].

271 The reliability of cell cycle initiation in response to a *LIP-CLB5* pulse, however, was low (Fig. 2 B).
272 Only 30% of *cln1-3Δ* cells budded in response to a *LIP-CLB5* pulse. In *cln1-3Δ clb3,4,6Δ* cells, light-
273 induced *LIP-CLB5* led to budding in even fewer (15%) G1-arrested cells. This fraction was much
274 higher (>90%) for *cln1-3Δ* cells with *LIP-CLN2*. Increasing the duration of the light pulse did not
275 change the fraction of *cln1-3Δ LIP-CLB5* cells that committed to the cell cycle. Guided by these
276 results, we sought to increase the reliability of the response to light pulses by adding a *LIP-CLN2*
277 construct. This does not undermine the dependence on *LIP-CLB5*, which continues to be essential
278 for S phase and triggering entry into mitosis in the *cln1-3Δ clb3-6Δ* background. Simultaneous
279 expression of *LIP-CLN2* and *LIP-CLB5* in the *cln1-3Δ clb3,4,6Δ* background led to a more reliable >70%
280 of cells budding in response to a 20 min pulse of light. Altogether, the Dajbog background (Fig. 2 C,
281 D) allowed reliable control by external light pulses, with cell cycle Start only initiated in response to
282 a light pulse (Fig. 2 E-H).

283 After deleting *CLB3-6* to make the Dajbog1 strain more strongly depend on *LIP-CLB5* induction, we
284 could next also make the strain less tolerant to continuous *LIP-CLB5* expression. This would further
285 increase the need for Clb5 to oscillate on and off for proliferation. We accomplished this by deleting
286 *SIC1*, a B-type cyclin inhibitor. *SIC1* is part of a circuit that can oscillate when cyclin levels are
287 constant and can rescue such cell cycles[123]. When *SIC1* is deleted, the *cln1-3Δ* arrest becomes
288 leaky[133]. However, we found that this depends on at least one of the *CLB3-6* genes being present.
289 *cln1-3Δ clb3-6Δ sic1Δ* cells continued to be tightly blocked in darkness (Fig. 2 G). We named this
290 strain background Dajbog2[132].

291 To enable routine propagation of these cells prior to directed evolution campaigns, we created a
292 'training-wheel plasmid'. This plasmid allowed cells to grow without exogenously induced Clb5
293 oscillations, and the directed evolution campaign begins with counter-selection against the plasmid.
294 This increases the method's tolerance for POIs that initially cannot control *CLB5* sufficiently well.
295 We used a *URA3*-marked CEN/ARS plasmid, which can be selected against with 5-FOA, containing a
296 *CLB5* copy and *MET3pr-CLN2*. Finally, to increase the mutation rate for directed evolution, we
297 introduced the *pol3-L523D*[134–136] mutation that is reported to increase the global mutation rate
298 about one-hundred fold.

299 In summary, we achieved tight coupling of the cell cycle machinery to externally applied periodic
300 on-off light signals using Clb5 (aided by Cln2) in a *cln1-3Δ clb3-6Δ SIC1/sic1Δ* background (Fig. 2 C-
301 H). In principle, any POI controlling *CLB5* (and *CLN2* for higher efficiency) can be inserted for directed
302 evolution.

303 Overview of directed evolution experiments

304 We performed six directed evolution campaigns with the Dajbog strains, in which we inserted
305 different POI genes to control cell-cycle progression (four campaigns with El222, one with PhyB-Pif3,
306 and one with PEST-rtTA). All campaigns followed the same procedure (Fig. 3): The Dajbog strains
307 were transformed with genetic constructs controlling both *CLN2* and *CLB5* simultaneously in *trans*,

308 and were selected for loss of the training wheel plasmid under a permissive light pulse regime
309 (preparatory strain manipulation not shown in illustration). Next, the cells were spread on agar
310 growth medium plates (Fig. 3 A, G) and allowed to proliferate until the plate was covered by a lawn
311 of cells (Fig. 3 B, H). The plate was then briefly exposed to a 30 W, 254 nm UV lamp. Immediately
312 afterwards, cells were either spread in a thin layer on agar plates (Fig. 3 C, I) or suspended at low
313 optical density (OD_{660} = 0.1) in liquid growth medium (Fig. 3 E, K, L), depending on the campaign.
314 (Since we wished to explore the diversity of mutational solutions, we opted for the agar plate format
315 in five out of our six campaigns.) Then, the desired selection pressure was imposed by changing to
316 a restrictive light pulse pattern under which the initial cells could not proliferate. We chose both
317 initial and final light pulse patterns without fine-tuning: Starting with the light pulse regime where
318 cells clearly proliferated well during strain construction, we chose a very different regime in which
319 the desired POI property was necessary for proliferation and the vast majority of Dajbog cells were
320 obviously arrested.

321 On agar plates, mutant colonies emerged after 2 days and were then analyzed (Fig. 3 D, J); the death
322 of all other cells on the plate was evidence for the stringency of our selection pressure. Because
323 optovolution does not require intervention and media changes, cells can remain on the same agar
324 plate. While we stopped evolution here to analyze the mutations by Sanger or whole-genome
325 sequencing, colonies could be propagated by standard replica plating. For the liquid culture
326 experiments, the cell culture was diluted twice per day into fresh medium to maintain log phase
327 (Fig. 3 E, F), unless the OD did not change substantially compared to the previous timepoint. After
328 the switch to a restrictive light pulse regime, the OD rose for 1.5 days, presumably due to cell growth
329 without proliferation (Fig. 3 K, L), and then plateaued until about day 3. The lack of change of OD
330 indicated that the restrictive light pulsing conditions and resulting long arrests had killed the
331 majority of cells. After this period, we observed a more typical OD rate of increase, when adaptive
332 mutants took over the cell culture. After passaging cells for another 3 days, we analyzed the bulk
333 cell culture for mutations in the POI gene. The frequency of mutations from standing variation,
334 error-prone DNA replication, and additional exposure to 10 sec of UV sufficed to find desired
335 mutations in every campaign (**Supplementary Table 4**).

336

337

338

339 Fig. 3. Procedure of optovolution experiments. A-F. Illustration of optovolution experiments on agar plates or in liquid
340 cell culture. G-J. Representative pictures of plates of Dajbog cells: G, at the beginning of the experiment; H, after 2 days
341 of proliferation without selection pressure; I, after spreading on fresh agar plates; and J, after three days subjected to
342 selection pressure. K. OD_{660} measurements during two independent liquid culture experiments. Black circles indicate
343 measurement points. Lines solely serve to guide through the sequence of measurements. Dilutions are marked by
344 dashed red lines. L. Representative images of cells at different days of optovolution in liquid culture. Red, Htb2-mCherry.
345 Scale bar, 5 µm.

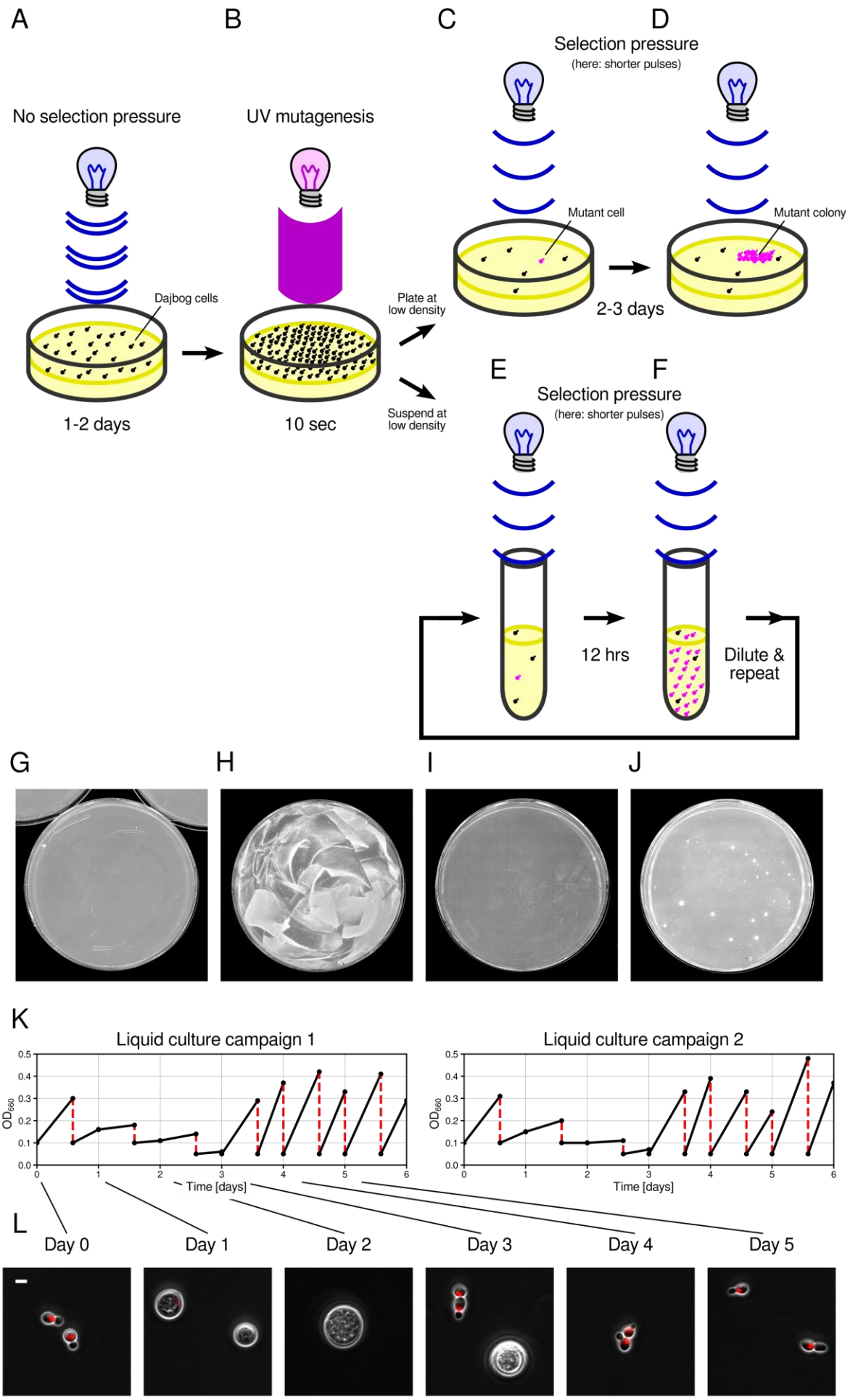
A
B
C
D
No selection pressure
UV mutagenesis
Selection pressure
(here: shorter pulses)
Dajbog cells
Mutant cell
Mutant colony
Plate at low density
2-3 days
1-2 days
10 sec
Suspend at low density
E
F
Selection pressure
(here: shorter pulses)
12 hrs
Dilute & repeat
G
H
I
J
K
Liquid culture campaign 1
Liquid culture campaign 2
OD660
Time [days]
L
Day 0
Day 1
Day 2
Day 3
Day 4
Day 5

Validation of mutants

We functionally validated the mutations *in vivo*: We cloned all mutations that emerged and introduced them in wild-type budding yeast cells where the POI drove transcription of the bright, yeast-optimized *yEVenus* or *ymScarletI* fluorescent protein genes (**Methods**). We followed the characterization procedure of ref.[88], using degron-destabilized fluorescent proteins for dynamic time course measurements, fluorescence microscopy for relatively high precision, and unbiased neural network-based image processing[137]. All fluorescence levels are expressed in maxGAL1 units[88], the maximal transcriptional output from the well-known *GAL1* promoter, which provides a straightforward, intuitive means to gauge the strength of transcriptional induction across different systems and publications.

Crucially, potential mutations elsewhere in the genome of the Dajbog cells, which could have emerged in the directed evolution campaign, could not affect our characterizations of the mutations. We thus established the causal effects of the evolved mutations independently of their ability to support proliferation under the restrictive light pulsing regime in the Dajbog strains.

Directed evolution of a LOV-transcription factor

We first applied the method to optogenetic systems, i.e., the POI itself was light sensitive. Optogenetic systems relay external on (1) or off (0) light states to on (1) or off (0) cellular activity, i.e., they have two input-output states. Optogenetic systems have been challenging to evolve, requiring repeated, sequential campaigns for the on (1) and off (0) output states since mutations improving one output state may destroy the other.[138] Given that El222 is itself widely used and that LOV domains are of broad interest, we chose to evolve El222 in three different directions, toward i) greater light sensitivity, ii) less leakiness, or iii) sensitivity to different colors for multiplexing and reduced phototoxicity.

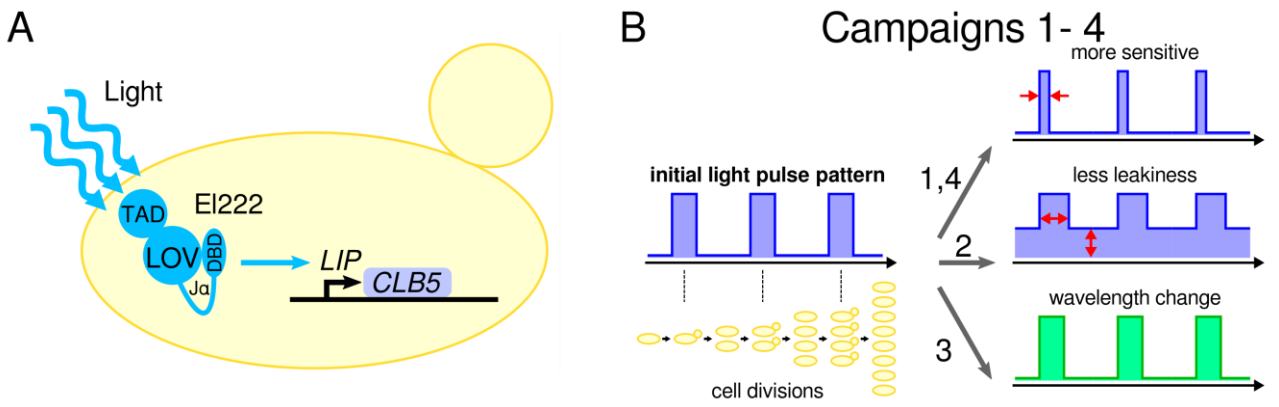

Fig. 4. Directed evolution campaigns 1-4 with LOV-transcription factor El222 as POI. A. Schematic of the wiring diagram for El222 evolution. *CLN2*, which is controlled by the same copy of the *EL222* gene, and other cell cycle regulators omitted for clarity. TAD, transcriptional activation domain; LOV, LOV domain; Jα, Jα helix; DBD, DNA binding domain. B. Schematic of four directed evolution campaigns. The initial light pulse pattern was switched to very brief pulses

376 (campaigns 1 and 4), long pulses with additional ambient light (campaign 2), or green and longer-wavelength light pulses
377 (campaign 3). Campaign 4 was a long-term campaign in liquid culture. Under each final light pulse regime, wild-type
378 Dajbog cells did not proliferate (see representative spot tests for each campaign, Fig. 5 A, E, Fig. 6 A).

379

380 We used the Dajbog strains with one copy of *EL222* directly controlling the transcription of both
381 *CLN2* and *CLB5* in *trans* in the same configuration as for testing and developing our method (Fig. 4
382 A). We used the experimental procedure illustrated in Fig. 3. Cells initially proliferated under a
383 permissive light pulse regime (5 times 25 sec on, 35 sec off every 100 min). Then, we changed the
384 light pulse regime to apply one of three selection pressures, in which cells with wild-type El222 could
385 not proliferate (Fig. 4 B). (See Supplementary Figure 1 for the excitation and imaging light spectra.)

386 In the first directed evolution campaign, we sought to enhance the 1-output (on) state of El222. This
387 would allow higher output under low light conditions. To evolve more light-sensitive mutants, we
388 exposed cells to very brief light pulses (1 sec on every 100 min, Fig. 4 B), which was insufficient for
389 viability of the wild-type Dajbog cells (Fig. 5 A). In the colonies that grew under these conditions (Fig.
390 5 A), we found 11 different El222 mutations (Fig. 5 B). (Interestingly, the light-sensitizing mutations
391 did allow extremely slow growth (about 1%) to occur in darkness (Fig. 5 A).) Remarkably, using
392 Dajbog2 (with *sic1Δ*) we observed 96% (n = 247) of colonies had a mutation in *EL222* while Dajbog1
393 (with *SIC1*) permitted mutations elsewhere in the genome to rescue cells (10% in *EL222*, n = 816).
394 Evaluating the new El222 variants cloned into our reporter strain, we found that they showed
395 improved light sensitivity, with levels of transcription under low-intensity light up to 16 times higher
396 than with wild-type *EL222* (Fig. 5 B). Several variants were comparable or more light sensitive than
397 the most sensitive El222 mutant to date, strongLOV (E84D), which we had engineered previously[88]
398 and rediscovered here.

399 To characterize the dynamic properties of the evolved El222 variants, we monitored their activity
400 by fluorescence timelapse microscopy where we induced them with diascopic white light for 3.5 h
401 (Fig. 5 C, Supplementary Figure 1 C). All tested variants showed increased activity compared to wild-
402 type El222 under a constant light source of 8.4 mW/cm^2. For most variants, we observed a trade-
403 off between strength and turn-off dynamics, similar to strongLOV[88]. However, remarkably, the
404 highly light-sensitive variant A157V, containing a mutation in the Jα helix (Supplementary Figure 2),
405 showed turn-off dynamics comparable to wild-type El222. (All references to mutant residue
406 numbers in El222 are conventionally given with respect to bacterial El222 to match the numbering
407 used in previous work[88,139,140]). This mutant is further interesting because it is the only one outside
408 the core of the LOV domain of El222 (Fig. 5 D, Supplementary Figure 2). Within the core of the LOV
409 domain, the Fα helix, which is adjacent to the chromophore, was particularly enriched for light-
410 sensitizing mutations.

411

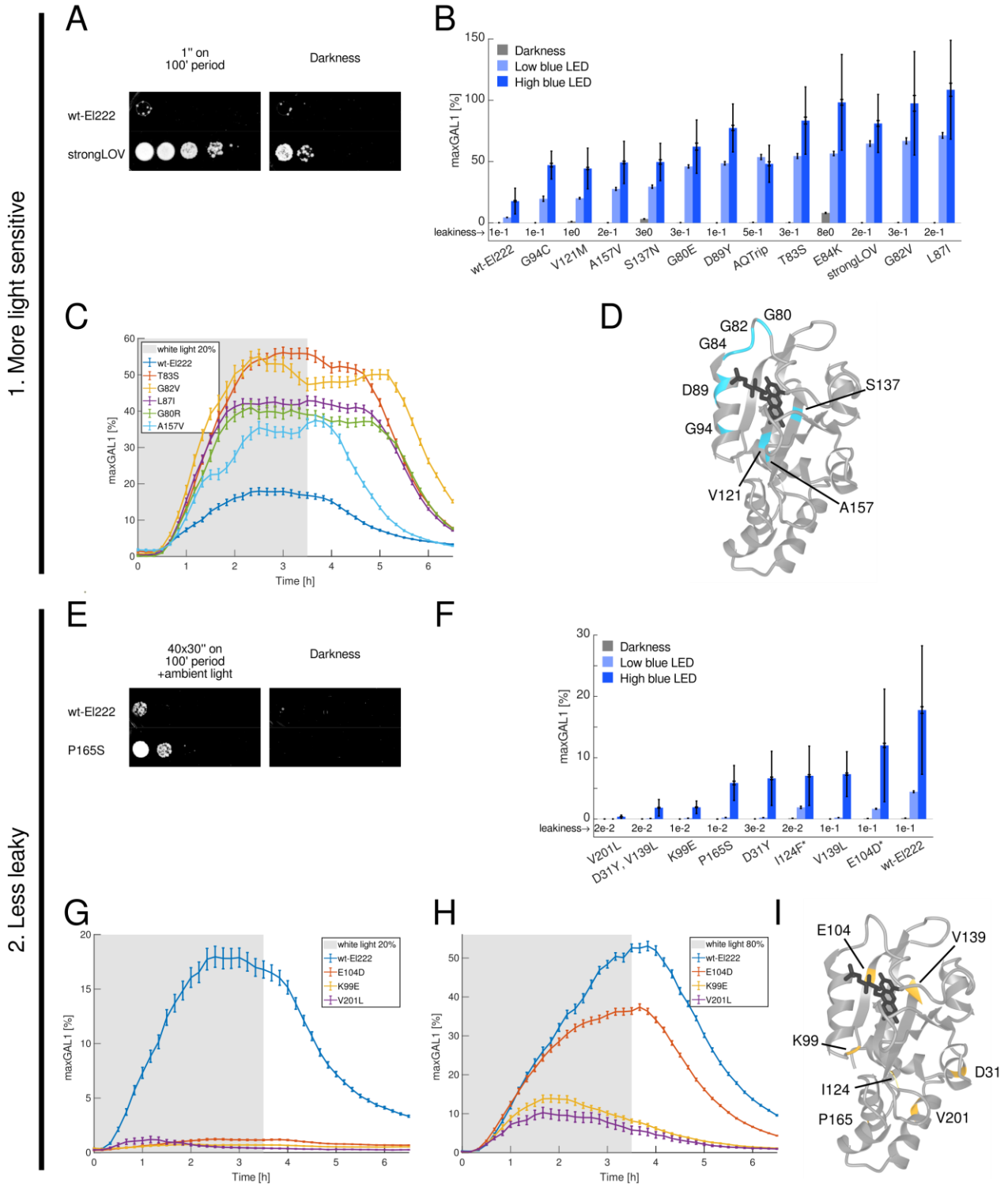

Fig. 5. Results of directed evolution campaigns of El222 for higher sensitivity and lower leakiness. A, E. Spot tests for the wild-type Dajbog strain (ancestor) and typical evolved mutants. Spot tests were performed with ten-fold dilutions. B, F. *In vivo* steady-state expression levels of the transcriptional fluorescent reporter *LIP-yEVenus* under different light exposure conditions, as indicated, driven by mutant *EL222*, which was cloned from the Dajbog strains and introduced into the reporter strain. The inner error bars represent the standard error of the mean (SEM); the outer error bars represent the standard deviation (STD). The mean leakiness values in the dark are explicitly stated for each mutant. In panel B, we included AQTrip[140] for reference. In panel F, * refers to mutants obtained with variations of the low-leakiness campaigns (main text). C, G, H. Time courses of El222 mutants, driving a destabilized fluorescent transcriptional reporter

421 with the PEST degron. The optogenetic systems were induced from 0 h to 3.5 h (grey region) by diascopic light
422 (Supplementary Figure 1)[88]. Error bars, SEM. G and H differ by the intensity of the induction light, as indicated. D, I.
423 Locations of a subset of the mutations (blue or yellow) in the dark-state 3D structure of El222 (PDB ID: 3P7N)[139]. All
424 references to mutant residue numbers in El222 are given with respect to bacterial El222 to match the numbering used
425 previously[88,139,140]. B, C, F, G, H. Numbers of analyzed cells are given in Supplementary Tables 5-7. All values are in
426 %maxGAL1 units[88]. All measured characteristics of the new El222 mutants have been added to the Inducible
427 Transcriptional Systems Database (https://promoter-benchmark.epfl.ch/)[88].

428

429 In the second campaign, we sought to reduce the leakiness of El222, that is, suppress activity in the
430 0-output (off) state. This is particularly important for applications where baseline expression needs
431 to be minimized, e.g., when controlling toxic genes. We exposed cells to very long duration pulses
432 of light (40 times 30 sec on, 30 sec off every 100 min, Fig. 4 B) in addition to continuous, dim
433 background light (Fig. 5 E-H). This condition was lethal to Dajbog strains with wild-type El222 (Fig. 5
434 E). In a preliminary run, we found many mutations in *LIP-CLB5*, which presumably maintained Clb5
435 function but with reduced activity that blunted the selection pressure. Thus, we introduced
436 additional copies of *LIP-CLB5* to block this evolutionary avenue (**Discussion**). Among the mutant
437 colonies that emerged in this campaign, the frequency of mutations in the *EL222* ORF was 36% (n =
438 44).

439 We identified five new mutations whose leakiness was nearly indistinguishable from baseline
440 transcription from *LIP* in the absence of El222 (Fig. 5 F, Supplementary Figure 3). As expected, they
441 were also overall less strongly induced by light. One of the colonies that emerged had fixed two
442 mutations in the LOV domain (D31Y, V139L). To understand their individual contributions to the
443 phenotype, we tested them separately. The mutations contributed independently and about
444 equally under high blue LED light. We also measured the on-off dynamics of low-leakiness mutants
445 by fluorescence microscopy. Using continuous light of 8.4 mW/cm^2 intensity as in the case for light-
446 sensitized mutants led to little observable activity in the low-leakiness mutants (Fig. 5 G). Under
447 much stronger light (97 mW/cm^2), the mutants responded noticeably (Fig. 5 H). The low-leakiness
448 mutations were both in the LOV domain as well as the DNA binding domain (Fig. 5 I). To test whether
449 the combination of long induction light pulses and background light had been necessary to discover
450 these mutants, we performed additional campaigns with only the long duration pulses or only
451 background light. We discovered two additional mutations (marked with * in Fig. 5 F) in these
452 campaigns. Their properties were comparable to the mutations found previously.

453

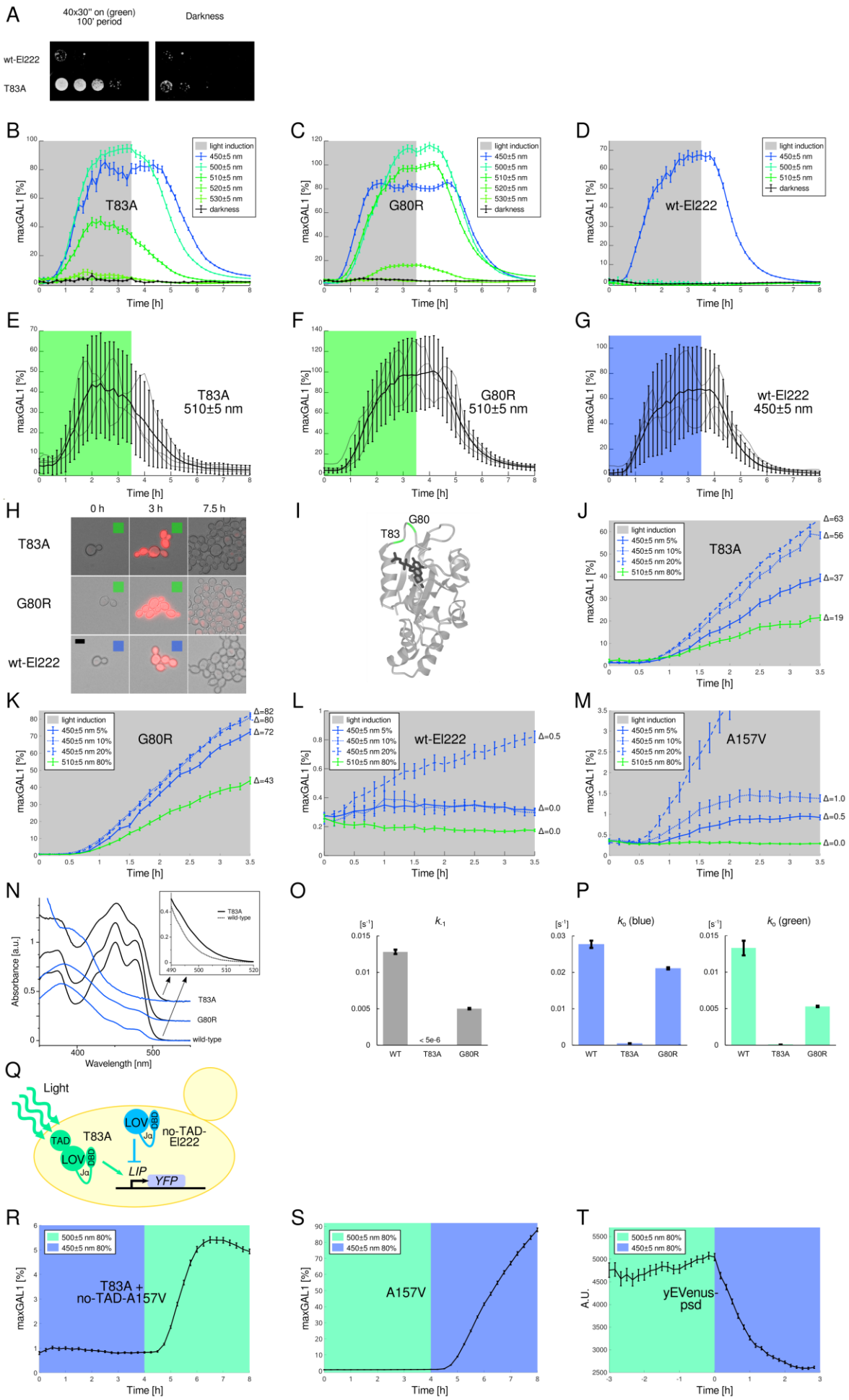
A
40x30" on (green)
100' period
Darkness
wt-El222
T83A
B
T83A
light induction
450±5 nm
500±5 nm
510±5 nm
520±5 nm
530±5 nm
darkness
maxGAL1 [%]
Time [h]
C
G80R
D
wt-El222
E
T83A
510±5 nm
F
G80R
510±5 nm
G
wt-El222
450±5 nm
H
0 h
3 h
7.5 h
T83A
G80R
wt-El222
I
G80
T83
J
T83A
450±5 nm 5%
450±5 nm 10%
450±5 nm 20%
510±5 nm 80%
Δ=63
Δ=56
Δ=37
Δ=19
K
G80R
Δ=82
Δ=80
Δ=72
Δ=43
L
wt-El222
Δ=0.5
Δ=0.0
Δ=0.0
M
A157V
Δ=1.0
Δ=0.5
Δ=0.0
N
Absorbance [a.u.]
Wavelength [nm]
T83A
wild-type
G80R
O
k_{-1}
[s⁻¹]
< 5e-6
WT
T83A
G80R
P
k_0 (blue)
k_0 (green)
Q
Light
TAD
T83A
LOV
DBD
Jα
no-TAD-El222
LIP
YFP
R
500±5 nm 80%
450±5 nm 80%
T83A +
no-TAD-A157V
S
A157V
T
A.U.
yEVenus-psd

455 Fig. 6. Results of optovolution campaigns for spectrally modified El222. A. Spot tests for the wild-type Dajbog strain
456 (ancestor) and the evolved T83A mutation. Spot tests were performed with ten-fold dilutions. B, C. Time courses of the
457 T83A and G80R El222 mutants cloned from evolved Dajbog strains and introduced into the reporter strain driving *LIP-*
458 *ymScarletI-PEST*. The optogenetic systems were induced from 0 h to 3.5 h (grey region) by diascopic white light
459 (Supplementary Figure 1) filtered through different 10 nm bandpass filters. Plot colors correspond to the center
460 wavelength of the filters. D. Time course for wild-type El222. Error bars in B-D indicate the standard error of the mean
461 (SEM). E-G. Mean, standard deviation, and three representative single-cell time courses for the T83A and G80R mutants
462 induced by green light and wild-type El222 induced by blue light. The mean time course with SEM error bars is also
463 shown in panels B-D. H. Snapshots of different reporter cell strains (different rows) at three time points in the timelapse
464 recordings (different columns). Colored squares indicate exposure to optogenetic induction light at the respective time
465 points. Scale bar, 5 µm. I. Locations of the mutations in the dark-state 3D structure of El222 (PDB ID: 3P7N)[139]. J-M.
466 Sensitivity of the T83A, G80R, A157V mutants, and wild-type El222 to green light and different intensities of blue light
467 measured using a *LIP-ymScarletI* reporter. Δ values on the right side of the plots indicate the difference between final
468 values at 3.5 h and initial values at 0 h in %maxGAL1 units. Error bars, SEM. N. Normalized dark- and light-state
469 absorption spectra of purified El222 variants, offset along the vertical axis for clarity. Inset presents a superposition of
470 the T83A and wild-type spectra at the long-wavelength tail. O. Dark reversion rate constants of the purified El222
471 variants. The value for the T83A mutant represents an upper bound. P. Observed photoactivation rate constants k_o of
472 purified El222 variants under blue and green light. Q. Schematic for green-only transcriptional activation system using
473 El222(T83A) and a no-TAD-El222. R. Time course of T83A-driven *LIP-ymScarletI* expression under simultaneous
474 expression of *GAL1pr-no-TAD-EL222(A157V)* in raffinose + galactose medium and a switch from blue to green light. S.
475 Time course of the A157V mutant under the same conditions as in panel R but without a competitor. T. Time course of
476 yEVenus tagged with *At*LOV2-based photo-sensitive degron (psd)[120] and expressed under the control of the *PGK1*
477 promoter. Error bars in panels O, P, R-T represent SEM. All references to mutant residue numbers in El222 are given
478 with respect to bacterial El222 to match the numbering used previously[88,139,140]. Numbers of analyzed cells are given in
479 Supplementary Table 6. All values are in %maxGAL1 units[88]. All measured characteristics of the new El222 mutants have
480 been added to the Inducible Transcriptional Systems Database (https://promoter-benchmark.epfl.ch/)[88].

481

482 In our third campaign, we sought to modify the nature of the 1-output state with respect to color
483 responsiveness. After proliferating Dajbog cells under blue light pulses, we evolved them under
484 green, orange, and red light combined (40 times 30 sec on, 30 sec off every 100 min). (Figs. 4 B, 6,
485 Supplementary Figure 1 for details regarding light sources). Among the mutant colonies that
486 emerged, we discovered mutations in *EL222* that allowed cells to proliferate under these LED light
487 pulses (Fig. 6 A). Optovolution was highly efficient: 96% (n=247) of mutations were in the *EL222* ORF
488 when Dajbog2 (with *sic1Δ*) was used and 10% (n = 816) with Dajbog1 (with *SIC1*). As before, we
489 validated the mutations functionally by cloning the evolved *EL222* genes into a reporter strain. To
490 monitor turn-on and turn-off dynamics longitudinally at the single-cell level, we characterized the
491 mutant El222 proteins in the reporter strains by timelapse microscopy (Fig. 6 B-H, J-M). As
492 transcriptional reporter, we chose *LIP-mScarletI-PEST*, which was excited by 562±20 nm light for 100
493 ms every 10 min for imaging, minimizing unwanted potential optogenetics activation. We covered
494 the relevant part of the light spectrum for inducing the optogenetic system using 10 nm bandpass
495 filters and the microscope's white light source (Supplementary Figure 1). In the following, we

496 indicate the optogenetic induction light by the central wavelength of the filter and the width of ±5
497 nm.

498 We discovered two mutants, G80R and T83A, which responded strongly to green light, only
499 markedly reducing in activity at 520±5 nm and above (Fig. 6 B, C). In contrast, wild-type El222
500 showed no responsiveness at 500±5 nm or longer wavelengths, even at the highest light intensity
501 we could achieve (80% = 0.26 mW/cm^2) (Fig. 6 D). Variability and noise were similar in T83A and
502 G80R in green light as wild-type El222 in blue (Fig. 6 E-H). Both G80 and T83 residues are in close
503 proximity to the chromophore (Fig. 6 I).

504 To investigate whether responsiveness to green light was merely a consequence of overall higher
505 sensitivity to light, we sought to measure the ratio of the response to blue and green light (Fig. 6 J-
506 M). We exposed our reporter cells to 510±5 nm light and to different intensities of 450±5 nm light.
507 To maximize measurement sensitivity, we used the *LIP-mScarletI* construct, i.e., without the PEST
508 degron. (We only show induction in Fig. 6 J-M since the long lifetime of the reporter is not
509 informative of the turn-off dynamics of the optogenetic system, which is already shown in panels B-
510 H.) Without the PEST degron, the baseline activity of each mutant was precisely detectable and is
511 represented by the first timepoint in the time courses. For green 510 nm light induction, we applied
512 the highest intensity we could achieve with our light source (0.26 mW/cm^2). Nevertheless, this green
513 light elicited no detectable response with wild-type El222 (the fluctuations in Fig. 6 L are small, on
514 the scale of ~0.1% maxGAL1). However, this green light led to robust expression of the fluorescent
515 reporter with T83A and G80R (Fig. 6 J, K). On the other hand, the intensities of blue light that were
516 sufficient to strongly activate and saturate T83A and G80R (10%-20%, Fig. 6 J, K) were just high
517 enough to activate wild-type El222 (only 20% led to detectable activation, Fig. 6 L). The relative
518 insensitivity of El222 to light overall prevented us from making a definitive comparison of relative
519 green-to-blue responsiveness. Thus, we utilized the A157V mutation, which led to greater light
520 sensitivity than wild-type El222 (Fig. 5 B, C) but whose location far from the chromophore
521 (Supplementary Figure 2) was unlikely to differentially affect color sensitivity. Indeed, A157V
522 responded with all blue light intensities tested (5%, 10%, and 20%) but, again, showed no response
523 to green light (Fig. 6 M). Thus, our mutants show differential sensitivity to 510±5 nm light *in vivo*
524 compared to wild-type El222 or A157V, neither of which showed a detectable response to clearly
525 visible, strong green light.

526 To investigate the biophysical characteristics of the *in vivo* green-responsive mutants, we produced
527 wild-type El222, and the T83A and G80R variants by heterologous expression in *E. coli* and
528 purification. UV/Vis absorption spectroscopy revealed that in their dark-adapted states all three
529 El222 receptors bind flavin-nucleotide chromophores and exhibit characteristic LOV absorbance
530 spectra with peaks around 450 nm and two shoulders at about 430 and 475 nm (Fig. 6 N,
531 Supplementary Figure 5 A). Compared to the other proteins, the spectrum of T83A had a less
532 pronounced fine structure which could be indicative of looser flavin binding. Crucially, the T83A (but

533 not G80R) spectrum revealed a broader tail at long wavelengths that incurred higher relative
534 absorbance in the 500-520 nm range (Fig. 6 N inset).

535 Once exposed to strong blue light, all El222 proteins adopted their light-adapted state characterized
536 by a shallow absorbance peak around 390 nm. Returned to darkness, wild-type El222 thermally
537 recovered its dark-adapted state in a single-exponential manner with a rate constant k_{-1} of 1.28 ×
538 10^{-2} s^{-1} at 25 °C (Fig. 6 O, Supplementary Figure 5 B), corresponding to a time constant τ of around
539 75 s. Owing to a different buffer composition and pH, the kinetics are slower than originally
540 reported[139]. The G80R variant recovered around 2.5-fold more slowly to its dark-adapted state with
541 a rate constant of 5.0 × 10^{-3} s^{-1}. By contrast, the dark recovery reaction of the T83A variant was
542 exceedingly slow and incomplete even after extended times (Supplementary Figure 5 B). Based on
543 the observation that after around 16 h only 20% of the initial absorbance at 450 nm was regained,
544 we estimate an upper limit of the recovery rate constant k_{-1} of around 5 × 10^{-6} s^{-1}.

545 We next addressed to which extent El222 is photoactivated by blue versus green light (Fig. 6 P,
546 Supplementary Figure 5 C, D). To this end, we tracked the gradual decrease of the dark-adapted
547 state upon exposure to light passed through 450-nm and 510-nm filters (10 nm bandwidth in both
548 cases) at powers of 0.75 mW cm^{-2} and 1.5 mW cm^{-2}, respectively. The observable rate constant k_o
549 obtained by evaluating the photoactivation time courses according to single-exponential functions
550 is a sum of the light-driven forward rate constant k_1 and the reverse dark-recovery rate constant k_{-}
551 $_1$. For instance, under 450-nm light the dark-adapted state of wild-type El222 decayed with an
552 observable rate constant k_o = 2.77 × 10^{-2} s^{-1} from which a forward rate constant k_1 of 1.5 × 10^{-2} s^{-1}
553 results. Consistent with the similar magnitude of k_1 and k_{-1}, for these experimental settings a
554 photostationary state resulted with around 51% population of the light-adapted state. Green light
555 also drove the transition to the light-adapted state but with much slower observable kinetics of 1.3
556 × 10^{-2} s^{-1} and only 5% amplitude, from which a value of around 5 × 10^{-4} s^{-1} results for k_1 of green-
557 light-driven photoactivation. Considering the individual light powers used in the experiments, green
558 light thus proved around 60 times less efficient at activating the wild-type LOV receptor compared
559 to blue light. LOV activation by green light is thus possible, in principle, although too inefficient to
560 lead to sufficient photoactivation as observed *in vivo*. For G80R, blue and green light promoted
561 conversion to the light-adapted state with observable kinetics of 2.1 × 10^{-2} s^{-1} and 5.3 × 10^{-3} s^{-1} and
562 amplitudes of 66% and 14%, respectively. From these data, we determine photoactivation kinetics
563 similar to those of wild-type El222 with k_1 amounting to 1.6 × 10^{-2} s^{-1} and 3 × 10^{-4} s^{-1} under blue and
564 green light, respectively. While the photoactivation therefore did not substantially differ between
565 El222 wild-type and G80R, the much slower dark recovery in G80R gives rise to a 2- to 3-fold higher
566 population of the light-adapted state under constant illumination at the conditions investigated,
567 which at least qualitatively accounts for the higher effective light sensitivity seen above for the *in*
568 *vivo* data[141]. In the case of the T83A variant, the activation by both blue and green light was
569 remarkably slower than for the other two El222 proteins with observable rate constants k_o of 5.6 ×
570 10^{-4} s^{-1} and 9.1 × 10^{-5} s^{-1}. Given that the dark recovery in T83A proceeds with a rate constant of 5 ×

571 10^{-6} s^{-1} or less, these kinetics are dominated by the forward rate constant k_1. That is, k_1 is essentially
572 equal to the observable rate constants k_o, and T83A is therefore only 12 times less efficiently
573 activated by green than blue light, explaining the observed *in vivo* differential green responsiveness
574 and consistent with the long-wavelength tail of the dark-adapted T83A absorbance spectrum (Fig.
575 6N inset). We note that modulation of the dark-recovery kinetics is well developed in LOV
576 receptors[89] but only scarce information exists for the variation of the photoactivation kinetics[142].

577 We wished to showcase the utility of the *in vivo* green-responsive mutants for orthogonal color-
578 multiplexing with LOV domains only. The key obstacle to achieving independent control was that
579 the green-responsive mutants remained responsive to blue light. We thus pursued a strategy of
580 combining the T83A mutant with a spectrally wild-type El222 which lacked the transcriptional
581 activation domain (TAD) and should competitively inhibit binding of El222(T83A) to DNA in blue light
582 only (Fig. 6 E). In green light, on the other hand, El222(T83A) could continue to activate transcription.
583 The first inhibitor that we constructed, no-TAD-El222, could not suppress transcription in blue light,
584 even when overexpressed from the *GAL1* promoter (Supplementary Figure 4 A, B). However, using
585 the light-sensitized A157V mutant, we found no-TAD-El222(A157V) to fully suppress transcription
586 in blue 450±5 nm light but permit transcription in 500±5 nm or 510±5 nm light (Fig. 6 R,
587 Supplementary Figure 4 C). Under the same conditions, wild-type El222 and A157V only activate
588 under blue 450±5 nm light (Fig. 6 S, Supplementary Figure 4 B). These results establish the first
589 demonstration of two-color, orthogonal transcriptional control using only LOV domains, providing
590 a modular strategy for optogenetic multiplexing.

591 An important question about green sensitivity, both for multiplexing and for mechanistic
592 understanding, is whether other LOV proteins are generically green responsive. The long-
593 wavelength tail (500-520 nm) of the wild-type El222 absorption spectrum is clearly below that of
594 the T83A variant – but could still be detected (Fig. 6 N inset). This raises the possibility that El222 is
595 'close' to being green responsive and differences in individual amino acids could make other existing
596 LOV proteins green responsive. On the other hand, if other LOV domains are not generally green
597 responsive, our evolved mutations, which enable the green-only inducible transcriptional circuit
598 (Fig. 6 Q-S), will be particularly valuable for multiplexing, since other LOV domains would be only
599 activated by blue light. Thus, we tested *in vivo* green responsiveness in the widely used wild-type
600 *At*LOV2 domain. We tagged a constitutively expressed yEVenus gene with psd[120], an *At*LOV2-based
601 degron, and tested its response under blue 450±5 nm and green 500±5 nm light, as used previously
602 (Fig. 6 Q-S). We observed degron activity only in blue light, not in green light (Fig. 6 T). We also
603 verified the absence of a response at 510±5 nm (Supplementary Figure 4 D). The absence of green
604 responsiveness in two widely used LOV systems, wild-type El222 and *At*LOV2 suggests that the T83A
605 and G80R mutations unlock in El222 a highly useful and not commonly shared property.

606 In total, we discovered 19 new El222 mutations, mostly in the core of the LOV domain, one in the
607 Jα helix, and two in the DNA binding domain (Figs. 5 D, 5 I, 6 I). The analysis of the mutation spectrum

608 in the first three campaigns showed that we observed transitions (A-G, C-T) and transversions
609 (purine-pyrimidine) with about equal probability (**Supplementary Table 4**).

610 LOV domain proteins such as El222 are ubiquitous across the tree of life and control a variety of
611 cellular processes. Most approaches to altering LOV-optogenetic tools have involved introducing
612 mutations from other known natural LOV domains, which were faster or slower cycling[87,89,140]. To
613 gauge how realistic it would have been to discover our evolved mutants rationally, we quantified
614 the novelty of our mutants by searching a catalog of 7000 known and putative LOV-domains[143]
615 (Supplementary Figure 6 A) as well as by aligning their sequences with the well-studied LOV-domain
616 proteins FKF1 from *Arabidopsis thaliana*, VVD from *Neurospora crassa*, YtvA from *Bacillus subtilis*,
617 *Ds*LOV from *Dinoroseobacter shibae*, and the LOV2 domain of phot1 from *Avena sativa*
618 (Supplementary Figure 6 B). We discovered that the majority of the mutations (15/19) were rare
619 (≤10%) in putative LOV domains, and 6 are present in LOV domains whose kinetics had previously
620 been characterized. V121M found in VVD is part of the rationally-designed El222 variant AQTrip[140].
621 Similarly, another mutation (E84D) was used to construct the more light-sensitive strongLOV mutant
622 protein by us recently[88]. Interestingly, the other two mutations, K99E and V139L, would have been
623 expected to lead to more stable light-adapted states based on previously measured off-kinetics[87].
624 We found them, instead, to lead to lower leakiness and overall weaker responses. None of the LOV
625 proteins with characterized kinetics contained the T83A or the G80R mutation, which lead to green
626 sensitivity in El222. These results further underscore the power of directed evolution to uncover
627 functional mutations with specific desired properties.

628 Long-term optovolution of light-sensitized LOV domains

629 The directed evolution campaigns described thus far were unbiased by design: Any El222 mutant
630 which emerged and which could switch on and off repeatedly for ≈2 days under the respective
631 selection pressure would generate a colony and be detected by us. In our fourth campaign, we
632 wished to test whether optovolution could be used for directed evolution over longer periods of
633 time in liquid culture, where mutations could compound and compete against one another, in
634 principle. The fittest mutant would take over the cell culture.

635 We implemented the experimental approach presented in Fig. 3 A, B, E, F (additional details in
636 **Methods**). We again sought to boost the 1-output activity of El222, this time over one week. We
637 evolved the Dajbog2 strain under 5 sec of light, administered every 100 min. The OD time course
638 (Fig. 3 K) showed an initial increase likely from arrested cells growing in size (Fig. 3 L). Between days
639 1.5 to 3, the OD did not change noticeably, reflecting the inability of the majority of cells to grow or
640 proliferate. Subsequently, the growth in OD returned to normal, indicating that mutant Dajbog2
641 cells had taken over the cell culture. At the end of the week, we stopped the experiment and
642 sequenced *EL222*. We observed three mutations that won in four different long-term experiments,
643 E84D, G82V (twice), and V121M, which we had already discovered using the previous unbiased
644 approach.

645 ## Directed evolution of PhyB-Pif3 for independence from supplemental chromophore

646 In our fifth directed evolution campaign, we wished to improve the usability of the red-/far-red-light
647 controlled optogenetic switch PhyB-Pif3. For this purpose, we put *CLN2* and *CLB5* under the control
648 of the *GAL1* promoter and introduced single copies of *ADH1pr-PHYB-GAL4BD* and *ADH1pr-GAL4AD-*
649 *PIF3* constructs, which controlled both cyclin genes in *trans* (Fig. 7 A). We screened for mutations
650 allowing cell proliferation without supplementing PCB (Fig. 7 B). In ten out of ten mutants, which
651 we analyzed by whole-genome sequencing, we found mutations in the *YOR1* (also known as *YCF1*)
652 gene, of which five were nonsense mutations, two were single-nucleotide deletions, and one was a
653 single-nucleotide insertion (Q64*, E421K, E538*, W570*, K676*, G713S, E1318*, A1306>, A1834>,
654 A4690>AA).

655 We validated that a *YOR1* deletion suffices to obviate the need to supplement PCB for PhyB-Pif3
656 function in two reporter strains from other laboratories. We deleted *YOR1* in a strain from ref.[110], in
657 which PhyB-Pif3 drives the transcription of a fluorescent reporter (Fig. 7 C, D). In the absence of PCB,
658 the fluorescent reporter responded as strongly in the *yor1Δ* background as with PCB and wild-type
659 *YOR1*. Leakiness was comparable with and without *YOR1*. Since PhyB-Pif3 is frequently used to
660 control the localization of proteins to different cellular compartments, we tested if the *yor1Δ*
661 deletion sufficed to obviate supplemental PCB for this purpose as well. We deleted *YOR1* in a yeast
662 strain from ref.[144] in which PhyB is anchored to mitochondria, labeled with mCherry, and Pif3 is
663 fused to a yellow fluorescent protein and Bem1 (PhyB-mCherry-Tom7, Bem1-mCitrine-Pif3).
664 Exposing this strain with the *yor1Δ* deletion to red light led to colocalization of PhyB and Pif3 without
665 supplemental PCB, comparable to *YOR1* cells with supplemental PCB in extent and reversibility (Fig.
666 7 E-G).

667

668

669 Fig. 7. Directed evolution campaign 6 to lose the dependence of PhyB-Pif3 on supplemental PCB. A. Schematic of the
670 wiring diagram relevant for the campaign. (*CLN2* and other cell cycle regulators omitted for clarity.) TAD, transcriptional
671 activation domain; DBD, DNA binding domain. B. Schematic of the campaign. C. *GAL1pr-yEVenus* induction in the
672 presence or absence of different genes involved in biliverdin metabolism and of supplemental biliverdin derivatives.
673 The inner error bars represent the standard error of the mean (SEM); the outer error bars represent the standard
674 deviation (STD). Numbers of analyzed cells are given in Supplementary Tables 8-10. D. Representative images of cells in
675 experiments for panel C. E. Representative images of cells used for testing co-localization of Pif3 to mitochondrially
676 anchored PhyB with or without *YOR1*. Cells were exposed to red LEDs, an image was taken, then cells were exposed to
677 far-red LEDs for 30 sec, after which another image was taken. F. Scatter plot and linear regression fits for mCitrine versus
678 mCherry fluorescence for each intracellular pixel. G. Pearson correlation coefficients for the linear regression fits in
679 panel F. H. iRFP fluorescence in *YOR1* and *yor1Δ* cells at different extracellular biliverdin concentrations. All scale bars,
680 5 µm. Panels C-G, the supplemental PCB and BV concentrations were 30 µM and 100 µM, respectively. In panels G, H,
681 error bars indicate the standard error of the mean (SEM). For the spectra of the LED lights see Supplementary Figure 1.
682 The measured characteristics of PhyB-Pif3 with and without *YOR1* have been added to the Inducible Transcriptional
683 Systems Database (https://promoter-benchmark.epfl.ch/)[88].

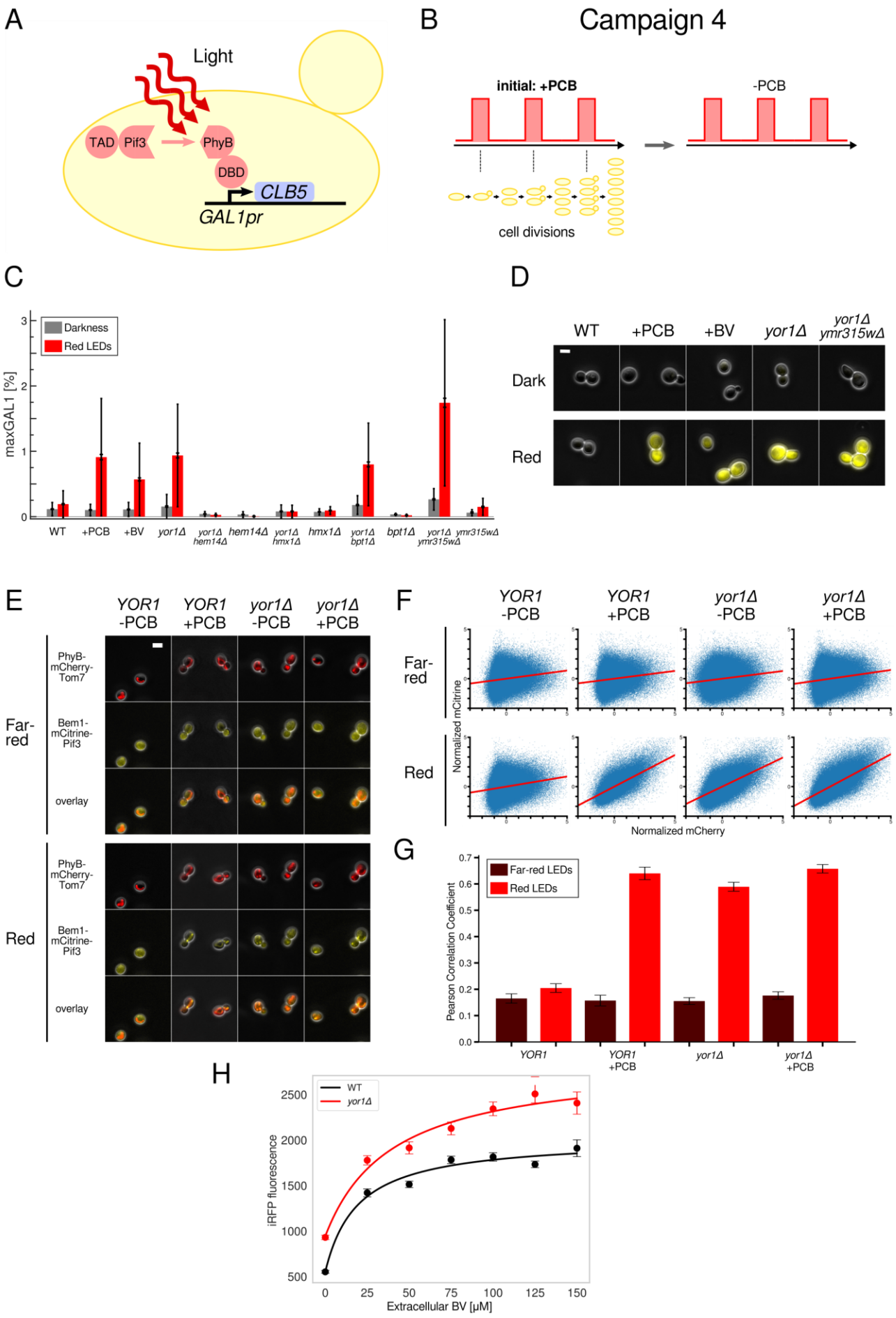
A
Light
TAD
Pif3
PhyB
DBD
CLB5
GAL1pr
B
Campaign 4
initial: +PCB
-PCB
cell divisions
C
Darkness
Red LEDs
maxGAL1 [%]
WT
+PCB
+BV
yor1Δ
yor1Δ hem14Δ
hem14Δ
yor1Δ hmx1Δ
hmx1Δ
yor1Δ bpt1Δ
bpt1Δ
yor1Δ ymr315wΔ
ymr315wΔ
D
WT
+PCB
+BV
yor1Δ
yor1Δ ymr315wΔ
Dark
Red
E
YOR1 -PCB
YOR1 +PCB
yor1Δ -PCB
yor1Δ +PCB
Far-red
Red
PhyB-mCherry-Tom7
Bem1-mCitrine-Pif3
overlay
F
YOR1 -PCB
YOR1 +PCB
yor1Δ -PCB
yor1Δ +PCB
Far-red
Red
Normalized mCitrine
Normalized mCherry
G
Far-red LEDs
Red LEDs
Pearson Correlation Coefficient
YOR1
YOR1 +PCB
yor1Δ
yor1Δ +PCB
H
WT
yor1Δ
iRFP fluorescence
Extracellular BV [μM]

684

685 Yor1 is an ABC plasma membrane exporter[145], a homolog of human cystic fibrosis transmembrane
686 receptor (CFTR)[146]. We speculated that budding yeast produces a chromophore that can accumulate
687 sufficiently for PhyB-Pif3 function unless Yor1 exports it out of the cell. Because PCB is a derivative
688 of biliverdin in plants, we hypothesized that the chromophore was a precursor or a derivative of
689 biliverdin, or biliverdin itself. To investigate this idea, we deleted two genes in the biliverdin
690 biosynthesis pathway, namely, *HEM14*[147,148], a protoporphyrinogen oxidase needed for heme
691 biosynthesis, or *HMX1*[149], a heme oxygenase that converts heme to biliverdin. Both genes turned
692 out to be needed for *yor1Δ* to enable supplement-free use of PhyB-Pif3 (Fig. 7 C), suggesting that
693 the chromophore is biliverdin or a biliverdin derivative. Further supporting this idea, we found that
694 supplementing biliverdin instead of PCB suffices for PhyB-Pif3 function (Fig. 7 C). The recent
695 discovery that PhyB can covalently incorporate biliverdin *in vitro* and interact with PIF6 provides
696 mechanistic support for our finding[150]. (The ability to substitute lower-cost biliverdin for PCB for use
697 with budding yeast is by itself advantageous.) Additionally, the biliverdin sensor iRFP[151] showed
698 about 70% higher fluorescence in *yor1Δ* versus wild-type *YOR1* cells (Fig. 7 H). To characterize the
699 efficiency with which Yor1 may export biliverdin, we quantified the difference in iRFP fluorescence
700 with and without *YOR1* at different extracellular biliverdin concentrations. The gap in iRFP
701 fluorescence indicates that Yor1 can maintain a substantial difference between intra- and
702 extracellular biliverdin. Together, our results strongly suggest that biliverdin or a biliverdin
703 derivative are exported out of the cytosol by Yor1 and accumulate sufficiently for PhyB-Pif3 function
704 with *yor1Δ* deletion.

705 Going further, we searched for other proteins that might reduce the levels of biliverdin in yeast cells,
706 in addition to Yor1. Eliminating such proteins would further boost PhyB-Pif3 function in the absence
707 of a supplemental chromophore. Our first strategy was to find potential biliverdin-binding proteins.
708 We used Foldseek[152] to find yeast proteins with structural homology to human biliverdin reductase
709 A (BLVRA). This search identified the poorly characterized yeast protein Ymr315w. The ligand
710 identification tool AlphaFill[153] showed that Ymr315w was likely to bind biliverdin. In line with these
711 computational predictions, deleting *YMR315W* enhanced PhyB-Pif3 transcriptional output in a
712 *yor1Δ* background without supplementing a chromophore (Fig. 7 C). (The *ymr315wΔ* deletion alone
713 had a mild effect, which is why our directed evolution campaign may not have caught it.) In a second
714 approach, we tested whether another ABC transporter could also export the PhyB-Pif3
715 chromophore. Among 16 characterized ABC transporters in yeast, Bpt1, a vacuolar importer, has
716 the greatest sequence similarity to Yor1[154]. However, deleting *BPT1* did not enable or improve
717 supplement-free use of PhyB-Pif3 (Fig. 7 C). These results further support our finding that specific
718 cellular pathways can be modified to enable supplement-free PhyB-Pif3 in budding yeast.
719 Optovolution, being an *in vivo* directed evolution method, can access such solutions which originate
720 in the biology of the cell. Depending on the goal, these solutions can be desired or, if undesired,
721 these avenues can also be foreclosed (**Discussion**).

722 ## Directed evolution of a light- and doxycycline- inducible AND gate

723 In our sixth evolutionary campaign, we applied optovolution to a non-optogenetic system. First, we
724 engineered an AND gate based on the transcription factor rtTA, which is controlled by doxycycline.
725 To make rtTA dynamically sensitive to transcriptional input, we destabilized it by fusing its N-
726 terminus with a PEST degron. When *PEST-rtTA* was transcribed under the control of the El222/*LIP*
727 system, transcription from the rtTA-controlled promoter *tetOpr* was very weak.

728 We wished to evolve variants of the logic gate with stronger on (1) state activity. So, we introduced
729 *tetOpr-CLN2*, *tetOpr-CLB5*, and *PEST-rtTA* into the Dajbog1 strain (Fig. 8 A). We then evolved the
730 system by exposing cells to short pulses of blue light, 2 sec on every 100 min, under which they
731 could not proliferate (Fig. 8 B). Before evolution, light pulsing 30 times 30 sec on, 30 sec off every
732 100 min and doxycycline allowed cell proliferation, confirming the AND gate functionality prior to
733 directed evolution (Fig. 8 C). However, the *tetO* promoter is very leaky in budding yeast (*tetOpr-*
734 *yEVenus* expression was at 2% maxGAL1 without *rtTA*) so that even in darkness and without
735 doxycycline, Dajbog1 proliferated, albeit much more slowly. This is why we used the more leakiness-
736 tolerant Dajbog1 strain in this campaign and screened for mutants as soon as small colonies
737 emerged under 2 sec light pulses every 100 min.

738 In principle, mutations in any part of the system could lead to the increased activity. Given that we
739 have already extensively characterized the mutations that boost the activity of the El222/*LIP*
740 optogenetic system, we now focused on screening for mutations in *PEST-rtTA* (**Discussion**). We
741 discovered two mutations, F67C and R253H (numbering is with respect to +1 methionine in rtTA).

742 To characterize the *PEST-rtTA* mutants, we cloned and introduced them as single-copy constructs
743 driven by *PGK1pr* into a reporter strain with a single copy of *tetOpr-yEVenus-PEST* (Fig. 8 D). Both
744 mutations showed increased activity in the presence of doxycycline. The mutated residues are
745 located between the DNA binding domain and the rtTA core domain or in the VP16 transcriptional
746 activation domain, respectively (Fig. 8 E). Relatedly, in previous directed evolution experiments of
747 rtTA, F67S was identified as increasing the sensitivity of rtTA (without a degron) to doxycycline[155].

748 These results demonstrate how the light-driven selection pressure in optovolution can be leveraged
749 for the evolution of non-optogenetic proteins with dynamic, multi-state, and computational
750 properties.

751

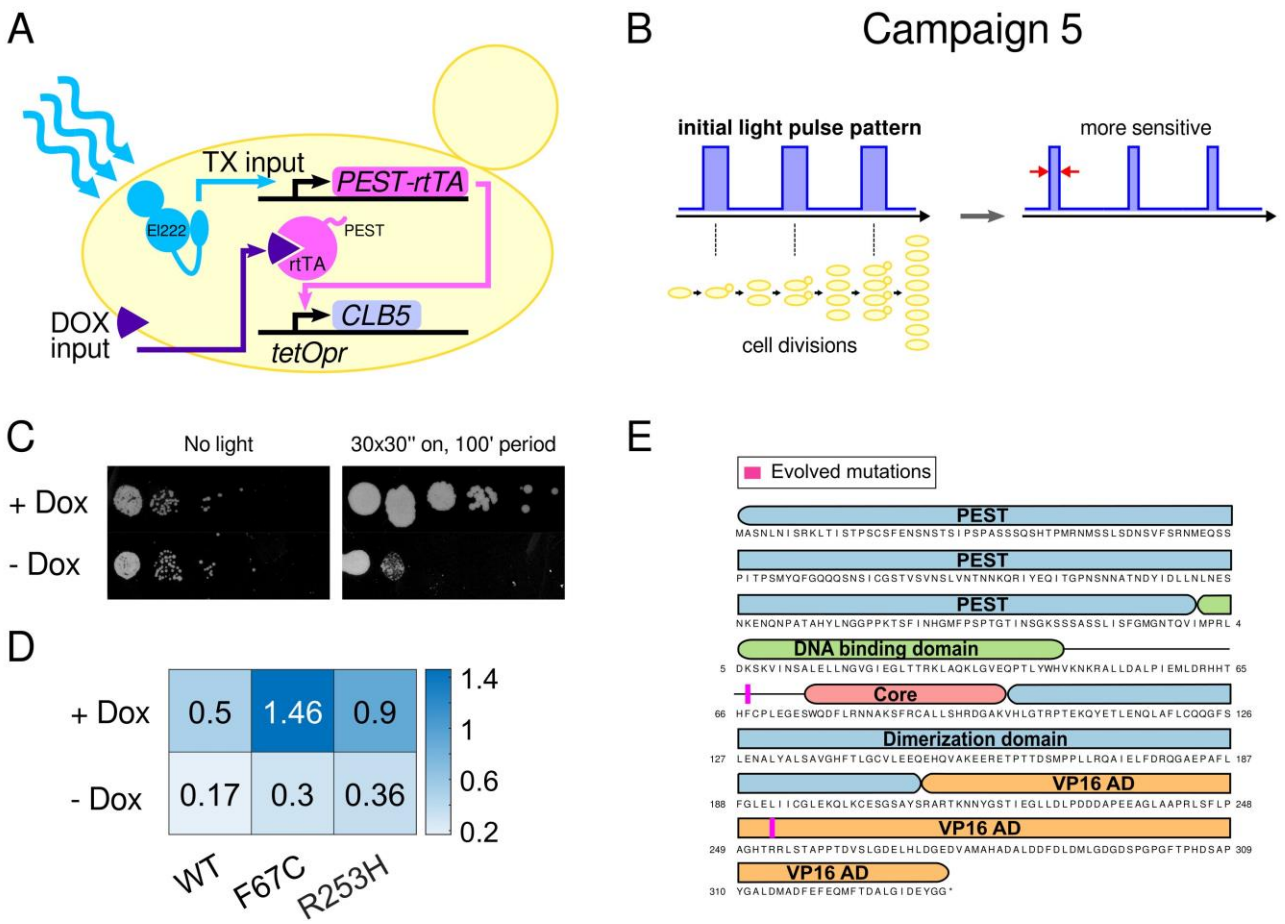

Fig. 8. Directed evolution campaign 6 to improve the AND logic gate function of PEST-rtTA. A. Schematic of wiring diagram relevant for campaign. TX, transcription; DOX, doxycycline. B. Schematic of the campaign. C. Spot test for wild-type Dajbog1 strain with PEST-rtTA system with ten-fold dilutions. D. Expression level of *tetOpr-yEVenus-PEST* under the control of the original or evolved PEST-rtTA in maxGAL1 units. For lowering experimental variability, the original and mutant *PEST-rtTA* were expressed from the *PGK1* promoter. Residue numbers are with respect to +1 methionine of rtTA. Numbers of analyzed cells are given in the Supplementary Table 11. E. Positions of mutations in domain diagram of PEST-rtTA.

Discussion

Two key ideas underlying optovolution

The primary advance of our directed evolution paradigm is the coupling of the POI output to an element of cell cycle control that has to oscillate for cellular replication in the specially engineered Dajbog genetic background. This obviates interventions needed to screen phenotypes or to switch between selection mechanisms after each round of evolution. Instead, both 0-to-1 and 1-to-0 switching of the POI are effectively screened every ≈90 min by the cell cycle control machinery *in vivo*. In addition, the coupling of the desired POI properties to organismal fitness automatically ensures that the evolved variants are functional *in vivo*. Additional *in vitro* screening is not needed.

770 These advantages of our method arise from leveraging cell cycle control, to our knowledge, for the
771 first time for directed evolution.

772 Secondarily, we use optogenetics to cycle through the inputs of the POI. Fundamentally, light control
773 is powerful for directed evolution because it allows communicating with cells rapidly, conveniently,
774 and for extended periods. Thus, new kinds of selection pressures can be created, which require
775 dynamic interaction with cells. As far as we know, this is the first time that optogenetics has been
776 leveraged for continuous directed evolution.

777 Light control also allows straightforwardly shaping the fitness landscape of the POI by tuning the
778 selection pressure. Different evolutionary outcomes can be achieved depending on the light
779 exposure protocol. Input-output relationships can be challenged by administering light input that is
780 too weak or too strong. Directed evolution can be expected then to improve the input-output by
781 mutational adaptations. Similarly, engaging and releasing the POI early or late forces adaptations
782 toward improved POI kinetics. We used the same strain, with *EL222* directly controlling both *CLB5*
783 and *CLN2* in *trans*, for four directed evolution campaigns: enhancement of the 1-output activity of
784 El222 (on agar plates or liquid culture), suppression of the 0-output activity, or green
785 responsiveness.

786 Tolerance toward poor initial POI functionality

787 A general challenge is that a POI may be so poor with respect to a desired function that the directed
788 evolution campaign cannot even be initiated. This is mitigated in two key ways in our method: The
789 selection pressure can be easily tuned by changing the light pulse regime, e.g., shorter, longer,
790 dimmer, or brighter light pulses. Furthermore, the training wheel plasmid allows proliferation in the
791 absence of any POI function, so that directed evolution of the POI can be initiated concomitantly
792 with selection for loss of the training wheel plasmid on 5-FOA.

793 Efficiency and targeted mutagenesis

794 Mutations in the POI gene evolved efficiently and bypass mutations were either rarely observed in
795 Dajbog2 (*sic1Δ*) or were reasonable in number to quickly find the mutation of interest with Dajbog1
796 (wt-*SIC1*). The strains can in principle be further optimized to suppress mutations in the budding
797 yeast genome. After identifying such bypass mutations, one can effectively prevent them by
798 inserting additional copies of the gene. This strategy takes advantage of the tolerance of yeast
799 toward multiple copies of most of its genes[156,157] and the extremely low likelihood of mutations
800 occurring in different copies of the same gene. We demonstrated this strategy with multiple *LIP-*
801 *CLB5* copies in our second directed evolution campaign. Should bypass mutations occur in non-
802 essential genes, one can in principle simply prevent them by deleting the gene.

803 The deep literature on cell cycle control can be used to guide future improvements of optovolution.
804 We leveraged the extensive genetic screens for suppressors of cell cycle arrest performed in the

805 past to create a genetically robust platform. Screens have only revealed *sic1Δ* to bypass *cln1-3Δ*
806 arrest.[133] This bypass relies on *CLB3-6*, which are absent in the Dajbog strains. (It should be noted
807 that *cln1-3Δsic1Δ* cells proliferate poorly, suggesting that bypass mutations do not necessarily affect
808 directed evolution experiment in practice.) Bypass mutations in Cdk1 can be practically ruled out
809 since at least five mutations are required to run the cell cycle oscillator in a *cln1-3Δ clb5,6Δ*
810 background.[131] It is unknown whether even these quintuply mutated Cdk1 could run the Dajbog
811 strains, which have additional deletions of *CLB3,4*.

812 Another potential way to increase the efficiency of our method is to take advantage of the
813 orthogonal advances in targeted mutagenesis methods. These are especially needed when
814 mutations elsewhere in the genome can readily bypass the desired POI functionality. However,
815 Dajbog2 was genetically tight, so it was not necessary to target mutations to the POI gene to achieve
816 our goals. Using *pol3-L523D*, we expected to increase the genome-wide mutation rate to 0.5×10^{-7}
817 per base-pair per generation. This means that in tens of milliliters of log-phase yeast population,
818 about all single mutants of the POI gene should have been present. Straightforward ways to further
819 increase the mutation rates globally involve the use of DNA damaging radiation and chemicals,
820 although not all nucleotide mutations can be attained in this manner. Another common method to
821 achieve very high rates of targeted mutations at the start of the directed evolution campaign is to
822 introduce the POI on mutagenized plasmid libraries, e.g., by error-prone PCR. Our method will also
823 presumably benefit from incorporation of targeted *in vivo* mutagenesis systems such as OrthoRep[10],
824 MutaT7[12,158], or Cas9-[159] or transposon-mediated systems[17], especially when evolutionary goals
825 require multiple mutations at the same time.

826 Ease of use

827 After extensive engineering and testing, the Dajbog strains can now be used without further
828 modification, in principle, including different variants (*SIC1*/*sic1Δ* and with multiple *CLB5* copies).
829 The steps to setting up optovolution (Fig. 3) resemble those of other *in vivo* directed evolution
830 methods, i.e., *CLB5* and *CLN2* must be placed under the control of the POI, similarly to non-
831 continuous directed evolution methods with fluorescent proteins or *URA3*. The key difference is
832 that cumbersome alternating selection mechanisms are obviated by the cell cycle oscillator. The
833 training wheel plasmid further helps exploring which pulsing regimes exert selection pressure, and
834 can be cleanly removed by counter-selection. With Clb5 (and Cln2) being critical for a key biological
835 process and cell cycle phenotypes extensively characterized and easy to interpret, the use and
836 debugging of optovolution is straightforward. Only standard equipment such as LED panels and
837 incubators as well as knowledge of standard techniques in budding yeast maintenance and
838 transformation are needed.

Limitations of optovolution

Limitations on types of POI input: Our directed evolution of PEST-rtTA demonstrated that the POI itself need not be light sensitive. To take advantage of intervention-less optovolution, a non-optogenetic POI has to be wired in a multi-step signaling cascades (optogenetics → POI → Clb5,Cln2). Options for light control of the POI are diverse and rapidly expanding, including light-controlled transcriptional input (used for PEST-rtTA), light-controlled protein-protein interaction (used for PhyB-Pif3), light-controlled degrons, kinases, and mRNA targeting systems. POIs that can only be controlled with chemicals are compatible with our platform but would require intervention, albeit only to cycle through the chemical POI inputs but not to change the selection mechanism.

Limitations on types of POI output: We demonstrated optovolution by evolving POIs that control the transcription of *CLB5* (and simultaneously *CLN2*): two transcription factors, El222 and PEST-rtTA, and an inducible protein-protein interaction system, PhyB-Pif3, which was engineered to control transcription using the yeast two-hybrid system. Many existing continuous directed evolution methods[14,34,35] were similarly initially applied to POIs that control transcription, presumably because transcriptional control can be created in a multitude of ways: The well-established two-hybrid method converts protein-protein interactions into transcriptional output[160]. CRISPR-Cas systems were in many cases evolved by blunting the endonuclease activity of Cas proteins and coupling to transcriptional output.[25,26,161,162] GPCRs were similarly screened by coupling downstream signaling to transcription.[163–165] Thus, transcriptional control does not limit the POI to transcription factors. Furthermore, the crucial element of our method is control of Clb5 activity, which can in principle be coupled to POI activity in other ways.

Limitations on targeting POIs: Even if the cell cycle-coupled selection mechanism is genetically robust, genomic mutations can emerge that are in cellular pathways affecting POI function. An example in our study is *YOR1*, whose mutations allowed PhyB-Pif3 to respond to red light in the absence of PCB. We considered the mutations in *YOR1* to be sufficiently surprising and useful to report in their own right as an endpoint of that campaign, instead of seeking to suppress them.

Requirement of minimal computational functionalities: Optovolution is fundamentally not suited for proteins whose state switching cannot be controlled even by way of intermediates, or for proteins that cannot control Clb5 activity. Essentially, the POI must meet the minimum requirements for computational functionality: controllable inputs and an output that can be read out, specifically, by coupling to Clb5. For example, proteins that stochastically switch between states without input or that are not coupled to an activity that could ultimately control Clb5 are not evolvable with optovolution.

Extendibility to other organisms: Budding yeast provides many advantages for directed evolution of dynamic, multi-state, and computational functionalities, including a relatively short generation time, ease of genetic engineering, and a vast literature on genetics, growth, metabolism, and cell cycle control. As a eukaryote, budding yeast shares many homologous genes with mammals. While

876 this makes budding yeast a well-appreciated platform for protein engineering and subsequent
877 transfer to mammalian cells, proteins optimized for budding yeast may not immediately function as
878 expected in mammalian cells. Further work is often required for adaptation to new hosts[166]. Our
879 *yor1Δ* findings motivate a targeted screen of human ABC transporters and genes in the biliverdin
880 metabolism pathway for enabling PhyB-Pif function in the absence of PCB[167]. To transfer our El222
881 mutants to mammalian cells, one should consider that LOV proteins are temperature sensitive,
882 potentially requiring adaptation to elevated temperatures[54]. While all of our directed evolution
883 campaigns were conducted at 30 °C, which maximized budding yeast growth, the organism is known
884 to tolerate 37 °C as well, with only a mild (<10%) slow-down in the cell cycle[168]. Thus, optovolution
885 can be used to evolve POIs closer to use in mammalian cells. Nevertheless, additional improvements
886 of the POI may be needed beyond temperature adaptation.

887 Green responsive El222 and *yor1Δ*-enabled PhyB-Pif3 function

888 Directed evolution methods rapidly assess an enormous number of mutations (determined by the
889 mutation rate, spectrum, and number of cells) for a desired POI property, beyond what is currently
890 feasible in standard site-directed mutagenesis and *in vitro* analyses. Optovolution substantially
891 simplifies this powerful approach for dynamic, multi-state, and computational functionalities. We
892 used it to uncover a number of practically useful and surprising mutations.

893 Rescuing Dajbog cells under pulses of green light, T83A and G80R El222 mutants, cloned into our
894 reporter strains, showed responses to ≈500-520 nm green light. Comparing the 450±5 nm blue light
895 response at different intensities to the 510±5 nm green light response (Fig. 6 J-M), we observed that
896 the latter was lower but comparable when non-saturating blue light was applied. In contrast, El222
897 was not responsive to any of the light we administered except to the highest intensity of blue light
898 used in this set of experiments (20%), preventing conclusions to be drawn regarding differential
899 color sensitivity. The A157V mutation, which is far from the chromophore, produced a response to
900 all blue light intensities in these experiments but, again, no detectable response to our highest-
901 intensity green light, which was quite bright to the human eye. The *in vivo* data show that T83A and
902 G80R gained green responsiveness that is not simply a consequence of a scaled overall light
903 responsiveness.

904 Our biophysical characterization of T83A shows higher relative sensitivity in the 500-520 nm range
905 compared to 450 nm than in wild type, as assessed by the absorption spectrum and by comparing
906 the activation kinetics in blue and green light (Fig. 6 N-P). Changes to the relative sensitivity to green
907 and blue light are novel and surprising. In contrast, we determined the purified G80R variant to be
908 overall more light sensitive, which at least partially accounts for the greater green sensitivity *in vivo*.
909 In any case, these results highlight the value of *in vivo* directed evolution driving protein engineering
910 alongside biochemical and other approaches: Based on the *in vitro* alone, especially of G80R, the
911 starkly different responsiveness to green light *in vivo* would have been difficult to predict.
912 Irrespective of the underlying mechanism, this observation motivated the creation of a circuit that

913 enables a green-only response (Fig. 6 R), which also demonstrates that the difference in
914 responsiveness to green light suffices in practice. Green responsiveness is not readily found in other
915 LOV domains, for example, it is absent in the phototropin *At*LOV2 module (Fig. 6 T).

916 For the second set of unexpected results, the findings that knock-out of *YOR1* obviates the need for
917 supplemental PCB, we found a well-constrained mechanistic explanation. In particular, the genetic
918 analysis that deletion of *HEM14* and *HMX1* abolish the ability of *yor1Δ* to support PhyB-Pif3 function,
919 together with the established role of Yor1 as a plasma membrane transporter, suggest that
920 biliverdin or a biliverdin derivative, naturally produced by budding yeast, serves as chromophore.
921 Further work is needed, however, to pinpoint the identity of the chromophore precisely.

922 Outlook for evolving computational functionalities

923 Given the appropriate selection pressure, directed evolution can solve challenging engineering
924 problems and uncover unexpected solutions -- such as green-responsive El222 mutants or PCB
925 independence conferred by *yor1Δ*. Here, we present the first method for continuous directed
926 evolution of dynamic, multi-state, and computational protein functionalities. Such capabilities are
927 fundamental to signal transduction -- and thus to life. While much of cellular biochemistry computes
928 decisions, it had been unclear how continuous directed evolution could be adapted to tune these
929 properties. Apart from interest in this as a fundamental problem, a solution is also needed for
930 biological engineering since dynamic, multi-state, and computational properties are of intense
931 current interest, especially, in protein design[169–173].

932 More advanced computational capabilities involve more inputs for more complex input-output
933 relationships. Using optovolution, different colors (UV[174,175], blue[103], green[176], red[108,177]) and
934 optogenetic systems allow administering different inputs to the POI and cycling through input
935 combinations during directed evolution.[99–102,176,178,179] The number of optogenetic effectors is
936 increasing, enabling different kinds of input to the POIs[180]. Single-protein computers would have
937 numerous advantages over multi-gene circuits, including simpler genetic introduction into cells and
938 presumably faster kinetics. However, rational engineering of proteins often leads to poorly
939 performing molecules, underscoring the need for directed evolution approaches. Our motivation
940 for engineering and evolving an AND gate involving PEST-rtTA was to demonstrate that optovolution
941 is well-suited for such systems, beyond light-sensitive proteins.

942 Optovolution is particularly timely for the revolution that is currently taking place in artificial
943 intelligence-based protein design, in which there is substantial interest in dynamic, multi-state, and
944 computational properties[29,181–183]. Prototypes that have been computationally designed can be
945 screened and improved in a high-throughput manner with optovolution. Additionally, machine-
946 learning guided methods will rely on experimentally validated training sets, which can be further
947 enriched through directed evolution. We expect optovolution to provide solutions to previously
948 intractable engineering problems and pave the way for more sophisticated proteins.

949 # Methods

950 ## Media

951 We used synthetic complete media[184] (SCD) with methionine (+Met) or without methionine (-Met)
952 and supplemented with 2% (w/v) glucose. For preparing solid SC plates, we used 2% agar. For
953 experiments with 5-FOA, we used a standard recipe with 0.1% 5-FOA[71,185]. For controlling and
954 evolving the transcriptionally and doxycycline-regulated AND gate (PEST-rtTA), we used 30 µM
955 doxycycline diluted from a 1000x stock in water (Sigma, USA). For characterization of the PEST-rtTA
956 variants, we used 10 µM doxycycline. For experiments with PhyB-Pif3, we used 30 µM PCB, diluted
957 from a 1000x DMSO stock (Sychem, Germany) when supplying exogenous PCB.

958 ## Plasmid construction

959 Cloning was performed using restriction enzyme digestion and ligation with T4 ligase (New England
960 Biolabs) or Gibson assembly (New England Biolabs). Plasmids were propagated in DH5alpha *E. coli*
961 in LB medium supplemented with ampicillin. See Supplementary Table 1 for a list of the plasmids.

962 ## Strain construction and preparation for directed evolution

963 Transformations of budding yeast were performed using the high-efficiency LiAc/DNA carrier/PEG
964 (polyethylene glycol) protocol[186]. All strains are derivatives of W303 (*leu2-3,112 trp1-1 can1-100*
965 *ura3-1 ade2-1 his3-11,15*). A list of strains is provided in Supplementary Table 2.

966 The Dajbog1 (*cln1-3Δ clb3-6Δ*) and Dajbog2 (*cln1-3Δ clb3-6Δ sic1Δ*) strains proliferated in the
967 absence of light pulses in SCD-Met medium plates due to the presence of the *URA3*-marked training
968 wheel plasmid pRD-TW1 (*MET3pr-CLN2, CLB5pr-CLB5, CEN/ARS*), which was built using the pRS416
969 vector[187]. (Lack of methionine induces *MET3pr-CLN2*.) For the different directed evolution
970 campaigns, we built additional strains starting with the Dajbog strains. To evolve *EL222* (first four
971 campaigns), we transformed the strains with *LIP-CLB5*, *LIP-CLN2*, and *PGK1pr-EL222* constructs. For
972 the evolution of the PhyB-Pif3 system (fifth campaign), we transformed them with *ADH1pr-PHYB-*
973 *GALBD*, *ADH1pr-GAL4AD-PIF3*, *GAL1pr-CLN2*, and *GAL1pr-CLB5* constructs. Lastly, for evolving the
974 AND gate (sixth campaign), we transformed the strains with *PGK1pr-EL222*, *LIP-PEST-rtTA*, *tetOpr-*
975 *CLN2*, and *tetOpr-CLB5*. We confirmed transformations by PCR.

976 To prepare the strains for directed evolution experiments, we selected for the loss of the training
977 wheel plasmid as follows: First, cells were spread on fresh SCD+Met plates and placed under pulsing
978 light. Methionine shuts off *MET3pr*, reducing any advantage that the training wheel may confer and
979 thus increasing the fraction of cells that lose the training wheel plasmid. Then, we transferred cells
980 to SCD+Met+5-FOA plates under the same pulsing light regime, so only cells that had lost the
981 training wheel plasmid could proliferate. We picked isolated colonies in which we confirmed the

982 loss of the training wheel plasmid by the lack of growth in darkness on plates lacking methionine.
983 From then on, the strains were propagated under pulsing light.

984 After directed evolution, we characterized the evolved POIs by cloning the mutated POI genes into
985 a backbone for single-copy integration. A W303 strain was transformed with these plasmids as well
986 as plasmids for single-copy integration of constructs in which the transcription of a fluorescent
987 protein was driven by *LIP* (in case of El222) or *tetOpr* (PEST-rtTA). Integration of single copies was
988 confirmed by PCR in all transformants. For measuring the transcriptional rate of PhyB-Pif3 as a split
989 Gal4 system, we used the strain from ref.[110]

990 Light conditions

991 Throughout, we handled cells sensitive to blue and green light under red light and red-responsive
992 cells as well as PCB under green light. Plates were otherwise always wrapped in aluminum foil.

993 For administering blue light to induce El222, we used commercial blue light LED panels (model
994 884667106091218, HQRP, USA). The panels were placed inside incubators at a distance of 20 cm
995 above the agar plates or a spinning wheel of liquid cell culture tubes. For evolving green-responsive
996 El222 variants, we used LEDs with peaks around green (525 nm, model LTL3H3TGRADS), yellow-
997 green (555 nm, model WP710A10PGC), yellow (575 nm, model 3SUGC-F), orange (615 nm, model
998 TLCO5100), and red (660 nm, model TLDR5800) (Mouser, Switzerland). For characterizing the green-
999 responsive El222 variants, we used band-pass filters FBH450-10, FBH500-10, FBH510-10, FBH520-
1000 10, FBH530-10, and FBH650-40 (Thorlabs) placed in the path of the microscope's diascopic light
1001 (Supplementary Figure 1). For administering red and far-red light that switches PhyB-Pif3, we used
1002 red light panels (model TLDR5800, Mouser, Switzerland) with a peak around 650 nm and custom-
1003 made printed circuit boards with 750 nm far-red LEDs (model LED750-33AU, Roithner Lasertechnik,
1004 Austria).

1005 The spectral characteristics of the light sources, measured using an ST-VIS-25 spectrometer (Ocean
1006 Insight, USA) are shown in Supplementary Figure 1.

1007 To control the LEDs or lasers, we used an NI USB 6501 (Texas Instruments, USA) I/O device. The
1008 system was run using a custom Matlab script (**Code availability**). The regime of pulsing light could
1009 be adjusted with a precision of less than one second.

1010 Quantification of the transition from *cln1-3Δ* arrest with optogenetic cell-cycle
1011 control

1012 To score the portion of cells that bud in response to a pulse of light (Fig. 2 B), we tested *cln1-3Δ*
1013 *MET3pr-CLN2* and *cln1-3Δ clb3-6Δ pRD-TW1* cells with additional *EL222* and LIP-controlled Cdk1
1014 cyclins, as indicated. After loading cells into a microfluidic chip (CellASIC ONIX Y04C-02, Sigma-
1015 Aldrich Chemie GmbH, Germany) and growing them for 4-5 hrs, we supplied methionine, which
1016 shuts off *MET3pr*. Two hours after methionine had been added, cells were large and unbudded (G1

1017 arrest). Different optogenetic constructs (*LIP-CLB5* and *LIP-CLN2*) were activated by using diascopic
1018 light from the microscope set to 80% of maximal intensity for 20 min or 40 min, depending on the
1019 experiment. Cells were imaged every 10 min.

1020 Optovolution experiments on agar plates

1021 Prior to evolution, cells were propagated under the light pulsing regime that allowed proliferation
1022 on SCD agar plates until growth saturation. For the El222 campaigns, this was 5 times 25 sec on, 35
1023 sec off every 100 min; for the PhyB-Pif3 campaign, 40 min on, 60 min off; for the PEST-rtTA
1024 campaign, 30 times 30 sec on, 30 sec off every 100 min. To increase the mutational diversity of the
1025 population, cells were then mutagenized by exposing them for 10 sec to UV light with 254 nm
1026 emission peak (model G30T8, Sankyo Denki, Japan). We scraped cells from one plate and
1027 resuspended them in 1 mL of liquid SCD medium prewarmed to 30°C. Then, we plated 100-200 µL
1028 of cell culture on fresh agar plates and chose the desired selection pressure by adjusting the light
1029 pulse regime. After two to three days, we picked isolated colonies and restreaked them on fresh
1030 SCD plates. After two days of growth of the streaks, we extracted genomic DNA and identified the
1031 mutations by Sanger sequencing the POI gene or whole-genome sequencing.

1032 Long-term continuous optovolution in liquid medium

1033 As in the agar plate experiments, cells were propagated on SCD plates and UV-mutagenized. We
1034 scraped cells from one plate and resuspended them in 1 mL of liquid SCD medium. We added 200
1035 µL from this suspension to 100 mL of liquid SCD medium. We used transparent 250 mL Erlenmeyer
1036 flasks (VWR, Switzerland). Cell cultures were placed in an incubator shaker (Infors HT, Switzerland)
1037 set to 250 rotations per minute and 30°C. For administering pulsing light, we used panels of blue
1038 LEDs mounted on a custom rack inside the incubator.

1039 To prevent the cultures from reaching saturation, we diluted them in warm SCD medium to a final
1040 OD_{660} of approximately 0.04-0.1 every 12 hrs, unless the OD had not changed. We performed the
1041 experiment for a week, after which we proceeded to Sanger sequencing bulk culture genomic DNA
1042 for the POI gene.

1043 Mutation identification

1044 To screen for mutations in the genes of interest, we performed Sanger sequencing (Microsynth AG,
1045 Switzerland) using primers that span the coding sequence of interest. The identified mutations were
1046 confirmed by sequencing the plasmids after cloning the POI gene.

1047 For identifying mutations in the genome, we performed paired-end whole genome sequencing of
1048 the evolved and ancestral genomes. The sequencing was performed using 150 bp long reads on the
1049 DNBseq platform with a total data output of 1 Gb. The ancestral and the evolved reads were then
1050 mapped onto the W303 reference genome using Bowtie 2. For variant calling, we used BCFtools.

1051 The mutations were called if they appeared in the evolved but not the ancestral genome, and if they
1052 were sequenced with a depth of at least 10.

1053 Variant characterization

1054 In all cases, strains were grown to saturation for 18-20 h, diluted, and then allowed to reach log
1055 phase. Transcriptional activities were scaled to the maxGAL1 unit, where 1 maxGAL1 corresponds
1056 to the steady-state expression of *GAL1pr* in synthetic complete medium containing 3% raffinose
1057 (w/v) and 2% galactose (w/v)[88].

1058 For characterizing the light-sensitized and *in vivo* green-responsive El222 variants, we cloned the
1059 mutant *EL222* genes into plasmids that inserted as single copies into the genome of strains that
1060 contained a single-copy *LIP-ymScarletI* reporter. While *LIP-ymScarletI* was the reporter of choice for
1061 characterizing light-sensitized variants to avoid excitation light inducing the mutant El222, it has a
1062 comparatively lower sensitivity than a *yEVenus* reporter. Hence, for carefully characterizing the
1063 leakiness of wild-type El222 and low-leakiness variants, we introduced them into a strain containing
1064 a single-copy *LIP-yEVenus* reporter. All variants were induced in log phase in liquid culture for 6 h.
1065 The light-sensitized or low-leakiness variants were tested under two different light pulse regimes,
1066 high or low time-averaged LED intensity (Fig. 5). The low LED regime corresponds to the blue LEDs
1067 (Supplementary Figure 1) pulsed for 10 sec every 5 min. The high LED regime corresponds to 30 sec
1068 on, 30 sec off every minute. For characterizing the dynamics of the evolved variants with timelapse
1069 fluorescence microscopy, we used variants of the reporters in which the corresponding fluorescent
1070 proteins are fused to the PEST degron, reducing the half-life of the reporters. From the measured
1071 fluorescence values, we subtracted the fluorescence levels of cells containing only the
1072 corresponding *LIP*-based reporter, which showed elevated fluorescence levels compared to wild-
1073 type (no-reporter) cells (Supplementary Figure 3).

1074 For characterizing the effect of *yor1Δ* in combination with the PhyB-Pif3 system, we used a strain
1075 from ref. [110] with a *GAL1pr-Venus* reporter. In case PCB was used, cells were incubated with it in
1076 darkness for 1 hr before exposure to red light. We used 30 sec on, 30 sec off red light with an
1077 emission peak around 650 nm delivered for 6 h to cells grown in SCD liquid medium tubes on a
1078 spinning wheel. After that, the level of expression was measured using fluorescence microscopy.
1079 Previous measurements of *GAL1pr* activity in glucose showed that it does not exhibit leakiness that
1080 is distinguishable from wild-type cells without a reporter[88]. Hence, from the measured values, we
1081 subtracted the background fluorescence of a wild-type strain. To convert the expression levels to
1082 maxGAL1 units, we measured the steady-state expression level of *GAL1pr-Venus* in the same strain
1083 by growing it in SC medium with 3% raffinose (w/v) and 2% galactose medium (w/v).

1084 For quantifying the activity of PEST-rtTA mutants, we introduced them into strains with a *tetOpr-*
1085 *yEVenus-PEST* reporter. We grew the strains with or without doxycycline for 6 hrs and then imaged
1086 them by fluorescence microscopy. From the measured values, we subtracted the corresponding

1087 background fluorescence values of the strain containing only a *tetOpr-yEVenus-PEST* reporter in the
1088 corresponding medium.

1089 Microscopy and image analysis

1090 Images were recorded using a Nikon Ti2-E (Nikon, Switzerland) microscope equipped with a 60x oil,
1091 N.A. 1.40 objective and a Hamamatsu Orca-Flash 4.0 camera (Hamamatsu, Japan). The microscope
1092 was controlled using NIS-Elements software and the Nikon Perfect Focus System. When performing
1093 timelapse microscopy to monitor the dynamic properties of El222, we induced with diascopic light,
1094 as described previously. For green-responsive mutants, we inserted bandpass filters into the light
1095 path of the microscope's diascopic light. The characteristics of this light are presented in
1096 Supplementary Figure 1. The diascopic light was set to the intensities indicated in the figures. Image
1097 analysis was performed using YeaZ[137], a deep neural network for analyzing images of yeast cells.

1098 Expression and purification of El222 variants

1099 El222 variants were produced by heterologous expression in *E. coli* and chromatographic
1100 purification according to previous expression protocols for El222[139] and other LOV receptors[188]. In
1101 brief, a pET29b(+) vector encoding the El222 gene with an N-terminal His_{10} tag and under the control
1102 of a T7-lacO promoter was used[139]. The mutations G80R and T83A were introduced into this vector
1103 by site-directed mutagenesis. *E. coli* CmpX13 bacteria[189] harboring the requisite plasmid were grown
1104 at 37 °C and 225 rpm agitation in 2× 800 mL lysogeny broth (LB) medium supplemented with 50 µg
1105 mL^{-1} kanamycin and 50 µM riboflavin. At an optical density at 600 nm of around 0.6, 1 mM isopropyl
1106 β-D-1-thiogalactopyranoside was added, the temperature was lowered to 16 °C, and the incubation
1107 continued overnight. All subsequent steps were carried out under red safe light. Cells were
1108 harvested by centrifugation and resuspended in 20 mM Tris/HCl pH 7.5, 300 mM NaCl; to promote
1109 solubility, in the case of the T83A variant, 500 mM of the osmolyte arginine was included in all
1110 buffers. Following lysis by sonication and centrifugation to remove cell debris, the supernatant was
1111 applied to a Co^{2+} immobilized metal ion chromatography (IMAC) and eluted by imidazole. The eluted
1112 fractions were analyzed by denaturing polyacrylamide gel electrophoresis and pooled based on
1113 protein content and purity. To remove the His_6 tag, TEV protease was added, followed by dialysis
1114 into buffer without imidazole. The sample was again applied to an IMAC column, dialyzed into
1115 storage buffer (20 mM Tris/HCl pH 7.5, 30 mM NaCl, 10% (v/v) glycerol) plus 500 mM arginine for
1116 T83A, and concentrated by spin filtration.

1117 Absorption-spectroscopic analyses of El222 variants

1118 All spectroscopic measurements were carried out on an Agilent Cary 60 UV/vis spectrophotometer
1119 at a temperature of 25 °C maintained by a circulating water bath. To this end, the El222 samples
1120 were diluted into 20 mM Tris/HCl pH 7.5, 500 mM arginine, 30 mM NaCl, 10% (v/v) glycerol. Spectra
1121 recorded on the dark-adapted El222 variants served to determine the concentration of the
1122 holoprotein based on a molar extinction coefficient of 12,500 M^{-1} cm^{-1} at 450 nm for the absorbance

of the flavin-nucleotide cofactor. To record spectra of the light-adapted state, the sample was exposed to an LED with peak emission at 470 and a light power of 36 mW cm^{-2} measured at the position of the protein sample using a Newport model 842-PE power meter and a 918D-UV-OD3 silicon photodiode.

Dark-recovery kinetics were recorded at 25 °C by monitoring the return from the light-adapted state at a wavelength of 450 nm, corrected by the absorbance at 600 nm to account for baseline shifts. The resultant data were fitted by single-exponential functions using the Fit-o-mat software to determine the rate constant k_{-1} of dark recovery[190].

To evaluate the forward kinetics of photoactivation by blue and green light, respectively, dark-adapted El222 samples were irradiated through (450 ± 5) nm and (510 ± 5) nm filters (Thorlabs) using a fiber-optic lamp. Measured at the sample position, the area intensities of the 450-nm and 510-nm light amounted to 0.75 mW cm^{-2} and 1.5 mW cm^{-2}, respectively. The gradual transition to the light-adapted state during illumination was tracked by absorbance measurements at 450 nm, corrected by the reading at 600 nm. Control experiments showed that the probe light of the spectrophotometer did not promote detectable photoactivation in itself. The resultant absorbance data were fitted to single-exponential functions to determine observable rate constants k_o. As recovery to the dark-adapted state takes place during the experiment, the rate constant k_o is the sum of k_{-1} (see above) and the light-dependent forward rate constant k_1 of photoactivation.

Statistics and reproducibility

No statistical method was used to predetermine sample size. The values in the heatmaps in Figs. 4 and 6 are rounded based on the first significant digit of the standard error of the mean.

Data and material availability

The characteristics of the systems measured in this study have been added to the Inducible Transcriptional Systems Database (https://promoter-benchmark.epfl.ch/)[88]. Any additional data that support the findings of this study are available from the corresponding author upon request.

Code availability

The Matlab code for controlling the light pulses is available at:

https://github.com/rahi-lab/optogenetic_controller_script/.

1152 # References

1153 1. Mills, D. R., Peterson, R. L. & Spiegelman, S. An extracellular Darwinian experiment with a self-
1154 duplicating nucleic acid molecule. *Proc. Natl. Acad. Sci. U.S.A.* **58**, 217–224 (1967).
1155 2. Kuchner, O. & Arnold, F. H. Directed evolution of enzyme catalysts. *Trends in Biotechnology* **15**,
1156 523–530 (1997).
1157 3. Schmidt-Dannert, C. & Arnold, F. H. Directed evolution of industrial enzymes. *Trends in*
1158 *Biotechnology* **17**, 135–136 (1999).
1159 4. Packer, M. S. & Liu, D. R. Methods for the directed evolution of proteins. *Nat Rev Genet* **16**, 379–
1160 394 (2015).
1161 5. Wang, Y., Xue, P., Cao, M., Yu, T., Lane, S. T. & Zhao, H. Directed Evolution: Methodologies and
1162 Applications. *Chem. Rev.* **121**, 12384–12444 (2021).
1163 6. Crameri, A., Whitehorn, E. A., Tate, E. & Stemmer, W. P. C. Improved Green Fluorescent Protein
1164 by Molecular Evolution Using DNA Shuffling. *Nat Biotechnol* **14**, 315–319 (1996).
1165 7. Campbell, R. E., Tour, O., Palmer, A. E., Steinbach, P. A., Baird, G. S., Zacharias, D. A. & Tsien, R.
1166 Y. A monomeric red fluorescent protein. *Proc. Natl. Acad. Sci. U.S.A.* **99**, 7877–7882 (2002).
1167 8. Li, Y., Moysey, R., Molloy, P. E., Vuidepot, A.-L., Mahon, T., Baston, E., Dunn, S., Liddy, N., Jacob,
1168 J., Jakobsen, B. K. & Boulter, J. M. Directed evolution of human T-cell receptors with picomolar
1169 affinities by phage display. *Nat Biotechnol* **23**, 349–354 (2005).
1170 9. Xu, L., Aha, P., Gu, K., Kuimelis, R. G., Kurz, M., Lam, T., Lim, A. C., Liu, H., Lohse, P. A., Sun, L.,
1171 Weng, S., Wagner, R. W. & Lipovsek, D. Directed Evolution of High-Affinity Antibody Mimics
1172 Using mRNA Display. *Chemistry & Biology* **9**, 933–942 (2002).
1173 10. Ravikumar, A., Arzumanyan, G. A., Obadi, M. K. A., Javanpour, A. A. & Liu, C. C. Scalable,
1174 Continuous Evolution of Genes at Mutation Rates above Genomic Error Thresholds. *Cell* **175**,
1175 1946-1957.e13 (2018).

1176 11. Yi, X., Khey, J., Kazlauskas, R. J. & Travisano, M. Plasmid hypermutation using a targeted artificial
1177 DNA replisome. *Sci. Adv.* **7**, eabg8712 (2021).
1178 12. Moore, C. L., Papa, L. J. & Shoulders, M. D. A Processive Protein Chimera Introduces Mutations
1179 across Defined DNA Regions *In Vivo*. *J. Am. Chem. Soc.* **140**, 11560–11564 (2018).
1180 13. Arnold, F. H. Design by Directed Evolution. *Acc. Chem. Res.* **31**, 125–131 (1998).
1181 14. Esvelt, K. M., Carlson, J. C. & Liu, D. R. A system for the continuous directed evolution of
1182 biomolecules. *Nature* **472**, 499–503 (2011).
1183 15. Badran, A. H. & Liu, D. R. In vivo continuous directed evolution. *Current Opinion in Chemical*
1184 *Biology* **24**, 1–10 (2015).
1185 16. Molina, R. S., Rix, G., Mengiste, A. A., Álvarez, B., Seo, D., Chen, H., Hurtado, J. E., Zhang, Q.,
1186 García-García, J. D., Heins, Z. J., Almhjell, P. J., Arnold, F. H., Khalil, A. S., Hanson, A. D., Dueber,
1187 J. E., Schaffer, D. V., Chen, F., Kim, S., Fernández, L. Á., Shoulders, M. D. & Liu, C. C. In vivo
1188 hypermutation and continuous evolution. *Nat Rev Methods Primers* **2**, 36 (2022).
1189 17. Crook, N., Abatemarco, J., Sun, J., Wagner, J. M., Schmitz, A. & Alper, H. S. In vivo continuous
1190 evolution of genes and pathways in yeast. *Nat Commun* **7**, 13051 (2016).
1191 18. Morrison, M. S., Podracky, C. J. & Liu, D. R. The developing toolkit of continuous directed
1192 evolution. *Nat Chem Biol* **16**, 610–619 (2020).
1193 19. Hubbard, B. P., Badran, A. H., Zuris, J. A., Guilinger, J. P., Davis, K. M., Chen, L., Tsai, S. Q., Sander,
1194 J. D., Joung, J. K. & Liu, D. R. Continuous directed evolution of DNA-binding proteins to improve
1195 TALEN specificity. *Nat Methods* **12**, 939–942 (2015).
1196 20. Pu, J., Zinkus-Boltz, J. & Dickinson, B. C. Evolution of a split RNA polymerase as a versatile
1197 biosensor platform. *Nat Chem Biol* **13**, 432–438 (2017).
1198 21. Xie, V. C., Pu, J., Metzger, B. P., Thornton, J. W. & Dickinson, B. C. Contingency and chance erase
1199 necessity in the experimental evolution of ancestral proteins. *eLife* **10**, e67336 (2021).

1200 22. Doyon, J. B., Pattanayak, V., Meyer, C. B. & Liu, D. R. Directed Evolution and Substrate Specificity
1201 Profile of Homing Endonuclease I-SceI. *J. Am. Chem. Soc.* **128**, 2477–2484 (2006).
1202 23. Kleinstiver, B. P., Prew, M. S., Tsai, S. Q., Topkar, V. V., Nguyen, N. T., Zheng, Z., Gonzales, A. P.
1203 W., Li, Z., Peterson, R. T., Yeh, J.-R. J., Aryee, M. J. & Joung, J. K. Engineered CRISPR-Cas9
1204 nucleases with altered PAM specificities. *Nature* **523**, 481–485 (2015).
1205 24. Lee, J. K., Jeong, E., Lee, J., Jung, M., Shin, E., Kim, Y., Lee, K., Jung, I., Kim, D., Kim, S. & Kim, J.-S.
1206 Directed evolution of CRISPR-Cas9 to increase its specificity. *Nat Commun* **9**, 3048 (2018).
1207 25. Spisak, S., O'Brien, B. & Ostermeier, M. A bacterial dual positive and negative selection system
1208 for dCas9 activity. *PLoS ONE* **17**, e0269270 (2022).
1209 26. Goldberg, G. W., Spencer, J. M., Giganti, D. O., Camellato, B. R., Agmon, N., Ichikawa, D. M.,
1210 Boeke, J. D. & Noyes, M. B. Engineered dual selection for directed evolution of SpCas9 PAM
1211 specificity. *Nat Commun* **12**, 349 (2021).
1212 27. Casini, A., Olivieri, M., Petris, G., Montagna, C., Reginato, G., Maule, G., Lorenzin, F., Prandi, D.,
1213 Romanel, A., Demichelis, F., Inga, A. & Cereseto, A. A highly specific SpCas9 variant is identified
1214 by in vivo screening in yeast. *Nat Biotechnol* **36**, 265–271 (2018).
1215 28. Sadeghi, A., Dervey, R., Gligorovski, V., Labagnara, M. & Rahi, S. J. The optimal strategy balancing
1216 risk and speed predicts DNA damage checkpoint override times. *Nat. Phys.* (2022)
1217 doi:10.1038/s41567-022-01601-3.
1218 29. Chen, Z., Kibler, R. D., Hunt, A., Busch, F., Pearl, J., Jia, M., VanAernum, Z. L., Wicky, B. I. M.,
1219 Dods, G., Liao, H., Wilken, M. S., Ciarlo, C., Green, S., El-Samad, H., Stamatoyannopoulos, J.,
1220 Wysocki, V. H., Jewett, M. C., Boyken, S. E. & Baker, D. De novo design of protein logic gates.
1221 *Science* **368**, 78–84 (2020).
1222 30. Gao, X. J., Chong, L. S., Kim, M. S. & Elowitz, M. B. Programmable protein circuits in living cells.
1223 *Science* **361**, 1252–1258 (2018).

1224 31. Fink, T., Lonzarić, J., Praznik, A., Plaper, T., Merljak, E., Leben, K., Jerala, N., Lebar, T., Strmšek,
1225 Ž., Lapenta, F., Benčina, M. & Jerala, R. Design of fast proteolysis-based signaling and logic
1226 circuits in mammalian cells. *Nat Chem Biol* **15**, 115–122 (2019).
1227 32. Omersa, N., Aden, S., Kisovec, M., Podobnik, M. & Anderluh, G. Design of Protein Logic Gate
1228 System Operating on Lipid Membranes. *ACS Synth. Biol.* **9**, 316–328 (2020).
1229 33. Vishweshwaraiah, Y. L., Chen, J., Chirasani, V. R., Tabdanov, E. D. & Dokholyan, N. V. Two-input
1230 protein logic gate for computation in living cells. *Nat Commun* **12**, 6615 (2021).
1231 34. Berman, C. M., Papa, L. J., Hendel, S. J., Moore, C. L., Suen, P. H., Weickhardt, A. F., Doan, N.-D.,
1232 Kumar, C. M., Uil, T. G., Butty, V. L., Hoeben, R. C. & Shoulders, M. D. An Adaptable Platform for
1233 Directed Evolution in Human Cells. *J. Am. Chem. Soc.* **140**, 18093–18103 (2018).
1234 35. English, J. G., Olsen, R. H. J., Lansu, K., Patel, M., White, K., Cockrell, A. S., Singh, D., Strachan, R.
1235 T., Wacker, D. & Roth, B. L. VEGAS as a Platform for Facile Directed Evolution in Mammalian
1236 Cells. *Cell* **178**, 748-761.e17 (2019).
1237 36. Groseclose, T. M., Rondon, R. E., Herde, Z. D., Aldrete, C. A. & Wilson, C. J. Engineered systems
1238 of inducible anti-repressors for the next generation of biological programming. *Nat Commun* **11**,
1239 4440 (2020).
1240 37. Sanchez, M. I. & Ting, A. Y. Directed evolution improves the catalytic efficiency of TEV protease.
1241 *Nat Methods* **17**, 167–174 (2020).
1242 38. Tominaga, M., Nozaki, K., Umeno, D., Ishii, J. & Kondo, A. Robust and flexible platform for
1243 directed evolution of yeast genetic switches. *Nat Commun* **12**, 1846 (2021).
1244 39. Klauser, B., Atanasov, J., Siewert, L. K. & Hartig, J. S. Ribozyme-Based Aminoglycoside Switches
1245 of Gene Expression Engineered by Genetic Selection in *S. cerevisiae*. *ACS Synth. Biol.* **4**, 516–525
1246 (2015).
1247 40. Skjoedt, M. L., Snoek, T., Kildegaard, K. R., Arsovska, D., Eichenberger, M., Goedecke, T. J.,
1248 Rajkumar, A. S., Zhang, J., Kristensen, M., Lehka, B. J., Siedler, S., Borodina, I., Jensen, M. K. &

1249 Keasling, J. D. Engineering prokaryotic transcriptional activators as metabolite biosensors in
1250 yeast. *Nat Chem Biol* **12**, 951–958 (2016).
1251 41. Snoek, T., Chaberski, E. K., Ambri, F., Kol, S., Bjørn, S. P., Pang, B., Barajas, J. F., Welner, D. H.,
1252 Jensen, M. K. & Keasling, J. D. Evolution-guided engineering of small-molecule biosensors.
1253 *Nucleic Acids Research* **48**, e3–e3 (2020).
1254 42. Usherenko, S., Stibbe, H., Muscó, M., Essen, L.-O., Kostina, E. A. & Taxis, C. Photo-sensitive
1255 degron variants for tuning protein stability by light. *BMC Syst Biol* **8**, 128 (2014).
1256 43. Lu, H., Mazumder, M., Jaikaran, A. S. I., Kumar, A., Leis, E. K., Xu, X., Altmann, M., Cochrane, A.
1257 & Woolley, G. A. A Yeast System for Discovering Optogenetic Inhibitors of Eukaryotic Translation
1258 Initiation. *ACS Synth. Biol.* **8**, 744–757 (2019).
1259 44. Wang, W., Wildes, C. P., Pattarabanjird, T., Sanchez, M. I., Glober, G. F., Matthews, G. A., Tye, K.
1260 M. & Ting, A. Y. A light- and calcium-gated transcription factor for imaging and manipulating
1261 activated neurons. *Nat Biotechnol* **35**, 864–871 (2017).
1262 45. Woloschuk, R. M., Reed, P. M. M., McDonald, S., Uppalapati, M. & Woolley, G. A. Yeast Two-
1263 Hybrid Screening of Photoswitchable Protein–Protein Interaction Libraries. *Journal of Molecular*
1264 *Biology* **432**, 3113–3126 (2020).
1265 46. Taslimi, A., Zoltowski, B., Miranda, J. G., Pathak, G. P., Hughes, R. M. & Tucker, C. L. Optimized
1266 second-generation CRY2–CIB dimerizers and photoactivatable Cre recombinase. *Nat Chem Biol*
1267 **12**, 425–430 (2016).
1268 47. Huang, Z., Li, Z., Zhang, X., Kang, S., Dong, R., Sun, L., Fu, X., Vaisar, D., Watanabe, K. & Gu, L.
1269 Creating Red Light-Switchable Protein Dimerization Systems as Genetically Encoded Actuators
1270 with High Specificity. *ACS Synth. Biol.* **9**, 3322–3333 (2020).
1271 48. Guntas, G., Hallett, R. A., Zimmerman, S. P., Williams, T., Yumerefendi, H., Bear, J. E. & Kuhlman,
1272 B. Engineering an improved light-induced dimer (iLID) for controlling the localization and activity
1273 of signaling proteins. *Proc. Natl. Acad. Sci. U.S.A.* **112**, 112–117 (2015).

1274 49. Reis, J. M., Xu, X., McDonald, S., Woloschuk, R. M., Jaikaran, A. S. I., Vizeacoumar, F. S., Woolley,
1275 G. A. & Uppalapati, M. Discovering Selective Binders for Photoswitchable Proteins Using Phage
1276 Display. *ACS Synth. Biol.* **7**, 2355–2364 (2018).
1277 50. Wang, H., Vilela, M., Winkler, A., Tarnawski, M., Schlichting, I., Yumerefendi, H., Kuhlman, B.,
1278 Liu, R., Danuser, G. & Hahn, K. M. LOVTRAP: an optogenetic system for photoinduced protein
1279 dissociation. *Nat Methods* **13**, 755–758 (2016).
1280 51. Kawano, F., Aono, Y., Suzuki, H. & Sato, M. Fluorescence Imaging-Based High-Throughput
1281 Screening of Fast- and Slow-Cycling LOV Proteins. *PLoS ONE* **8**, e82693 (2013).
1282 52. Yokobayashi, Y., Weiss, R. & Arnold, F. H. Directed evolution of a genetic circuit. *Proc. Natl. Acad.*
1283 *Sci. U.S.A.* **99**, 16587–16591 (2002).
1284 53. Maranhao, A. C. & Ellington, A. D. Evolving Orthogonal Suppressor tRNAs To Incorporate
1285 Modified Amino Acids. *ACS Synth. Biol.* **6**, 108–119 (2017).
1286 54. Baumschlager, A., Weber, Y., Cánovas, D., Dionisi, S. & Khammash, M. *Enhancing the*
1287 *Performance of Magnets Photosensors through Directed Evolution*.
1288 http://biorxiv.org/lookup/doi/10.1101/2022.11.14.516313 (2022)
1289 doi:10.1101/2022.11.14.516313.
1290 55. Meyer, A. J., Segall-Shapiro, T. H., Glassey, E., Zhang, J. & Voigt, C. A. Escherichia coli
1291 "Marionette" strains with 12 highly optimized small-molecule sensors. *Nat Chem Biol* **15**, 196–
1292 204 (2019).
1293 56. Tashiro, Y., Fukutomi, H., Terakubo, K., Saito, K. & Umeno, D. A nucleoside kinase as a dual
1294 selector for genetic switches and circuits. *Nucleic Acids Research* **39**, e12–e12 (2011).
1295 57. Taylor, N. D., Garruss, A. S., Moretti, R., Chan, S., Arbing, M. A., Cascio, D., Rogers, J. K., Isaacs,
1296 F. J., Kosuri, S., Baker, D., Fields, S., Church, G. M. & Raman, S. Engineering an allosteric
1297 transcription factor to respond to new ligands. *Nat Methods* **13**, 177–183 (2016).

1298 58. Tang, S.-Y., Fazelinia, H. & Cirino, P. C. AraC Regulatory Protein Mutants with Altered Effector
1299 Specificity. *J. Am. Chem. Soc.* **130**, 5267–5271 (2008).
1300 59. Lee, S. K., Chou, H. H., Pfleger, B. F., Newman, J. D., Yoshikuni, Y. & Keasling, J. D. Directed
1301 Evolution of AraC for Improved Compatibility of Arabinose- and Lactose-Inducible Promoters.
1302 *Appl Environ Microbiol* **73**, 5711–5715 (2007).
1303 60. Shong, J., Huang, Y.-M., Bystroff, C. & Collins, C. H. Directed Evolution of the Quorum-Sensing
1304 Regulator EsaR for Increased Signal Sensitivity. *ACS Chem. Biol.* **8**, 789–795 (2013).
1305 61. Nomura, Y. & Yokobayashi, Y. Dual selection of a genetic switch by a single selection marker.
1306 *Biosystems* **90**, 115–120 (2007).
1307 62. Muranaka, N., Sharma, V., Nomura, Y. & Yokobayashi, Y. An efficient platform for genetic
1308 selection and screening of gene switches in Escherichia coli. *Nucleic Acids Research* **37**, e39–e39
1309 (2009).
1310 63. Sharma, V., Nomura, Y. & Yokobayashi, Y. Engineering Complex Riboswitch Regulation by Dual
1311 Genetic Selection. *J. Am. Chem. Soc.* **130**, 16310–16315 (2008).
1312 64. Richter, F., Fonfara, I., Bouazza, B., Schumacher, C. H., Bratovič, M., Charpentier, E. & Möglich,
1313 A. Engineering of temperature- and light-switchable Cas9 variants. *Nucleic Acids Research* **44**,
1314 gkw930 (2013).
1315 65. Tominaga, M., Ike, K., Kawai-Noma, S., Saito, K. & Umeno, D. Rapid and Liquid-Based Selection
1316 of Genetic Switches Using Nucleoside Kinase Fused with Aminoglycoside Phosphotransferase.
1317 *PLoS ONE* **10**, e0120243 (2015).
1318 66. Saeki, K., Tominaga, M., Kawai-Noma, S., Saito, K. & Umeno, D. Rapid Diversification of BetI-
1319 Based Transcriptional Switches for the Control of Biosynthetic Pathways and Genetic Circuits.
1320 *ACS Synth. Biol.* **5**, 1201–1210 (2016).

1321 67. Ike, K., Arasawa, Y., Koizumi, S., Mihashi, S., Kawai-Noma, S., Saito, K. & Umeno, D. Evolutionary
1322 Design of Choline-Inducible and -Repressible T7-Based Induction Systems. *ACS Synth. Biol.* **4**,
1323 1352–1360 (2015).
1324 68. Guntas, G., Mansell, T. J., Kim, J. R. & Ostermeier, M. Directed evolution of protein switches and
1325 their application to the creation of ligand-binding proteins. *Proc. Natl. Acad. Sci. U.S.A.* **102**,
1326 11224–11229 (2005).
1327 69. Tashiro, Y., Kimura, Y., Furubayashi, M., Tanaka, A., Terakubo, K., Saito, K., Kawai-Noma, S. &
1328 Umeno, D. Directed evolution of the autoinducer selectivity of *Vibrio fischeri* LuxR. *J. Gen. Appl.*
1329 *Microbiol.* **62**, 240–247 (2016).
1330 70. Ellefson, J. W., Ledbetter, M. P. & Ellington, A. D. Directed evolution of a synthetic phylogeny of
1331 programmable Trp repressors. *Nat Chem Biol* **14**, 361–367 (2018).
1332 71. Boeke, J. D., Trueheart, J., Natsoulis, G. & Fink, G. R. [10] 5-Fluoroorotic acid as a selective agent
1333 in yeast molecular genetics. in *Methods in Enzymology* vol. 154 164–175 (Elsevier, 1987).
1334 72. Tague, N., Coriano-Ortiz, C., Sheets, M. B. & Dunlop, M. J. *Light Inducible Protein Degradation in*
1335 *E. Coli with the LOVdeg Tag*. https://elifesciences.org/reviewed-preprints/87303v2 (2024)
1336 doi:10.7554/eLife.87303.2.
1337 73. Nguyen, N. T., Liu, S., Han, G., Zhou, Y. & Huang, K. Nano-optogenetic CAR-T Cell
1338 Immunotherapy. in *Cancer Immunotherapy* (eds. Siciliano, V. & Ceroni, F.) vol. 2748 267–278
1339 (Springer US, New York, NY, 2024).
1340 74. Song, G., Tian, C., Li, J., Zhang, F., Peng, Y., Gao, X. & Tian, Y. Rapid characterization of anti-
1341 CRISPR proteins and optogenetically engineered variants using a versatile plasmid interference
1342 system. *Nucleic Acids Research* **51**, 12381–12396 (2023).
1343 75. Levskaya, A., Weiner, O. D., Lim, W. A. & Voigt, C. A. Spatiotemporal control of cell signalling
1344 using a light-switchable protein interaction. *Nature* **461**, 997–1001 (2009).

1345 76. Cui, M., Lee, S., Ban, S. H., Ryu, J. R., Shen, M., Yang, S. H., Kim, J. Y., Choi, S. K., Han, J., Kim, Y.,
1346 Han, K., Lee, D., Sun, W., Kwon, H.-B. & Lee, D. A single-component, light-assisted uncaging
1347 switch for endoproteolytic release. *Nat Chem Biol* (2023) doi:10.1038/s41589-023-01480-6.
1348 77. Nzigou Mombo, B., Bijonowski, B. M., Raab, C. A., Niland, S., Brockhaus, K., Müller, M., Eble, J.
1349 A. & Wegner, S. V. Reversible photoregulation of cell-cell adhesions with opto-E-cadherin. *Nat*
1350 *Commun* **14**, 6292 (2023).
1351 78. Legnini, I., Emmenegger, L., Zappulo, A., Rybak-Wolf, A., Wurmus, R., Martinez, A. O., Jara, C. C.,
1352 Boltengagen, A., Hessler, T., Mastrobuoni, G., Kempa, S., Zinzen, R., Woehler, A. & Rajewsky, N.
1353 Spatiotemporal, optogenetic control of gene expression in organoids. *Nat Methods* **20**, 1544–
1354 1552 (2023).
1355 79. Ho, E. K., Oatman, H. R., McFann, S. E., Yang, L., Johnson, H. E., Shvartsman, S. Y. & Toettcher, J.
1356 E. Dynamics of an incoherent feedforward loop drive ERK-dependent pattern formation in the
1357 early *Drosophila* embryo. *Development* **150**, dev201818 (2023).
1358 80. Pal, A. A., Benman, W., Mumford, T. R., Huang, Z., Chow, B. Y. & Bugaj, L. J. Optogenetic
1359 clustering and membrane translocation of the BcLOV4 photoreceptor. *Proc. Natl. Acad. Sci.*
1360 *U.S.A.* **120**, e2221615120 (2023).
1361 81. Mahlandt, E. K., Palacios Martínez, S., Arts, J. J., Tol, S., Van Buul, J. D. & Goedhart, J. Opto-
1362 RhoGEFs, an optimized optogenetic toolbox to reversibly control Rho GTPase activity on a global
1363 to subcellular scale, enabling precise control over vascular endothelial barrier strength. *eLife* **12**,
1364 RP84364 (2023).
1365 82. Lim, C. K., Yeoh, J. W., Kunartama, A. A., Yew, W. S. & Poh, C. L. A biological camera that captures
1366 and stores images directly into DNA. *Nat Commun* **14**, 3921 (2023).
1367 83. Elsaid, R., Mikdache, A., Diabangouaya, P., Gros, G. & Hernández, P. P. *A Non-Invasive*
1368 *Photoactivatable Split-Cre Recombinase System for Genome Engineering in Zebrafish*.

1369 http://biorxiv.org/lookup/doi/10.1101/2023.06.23.546268 (2023)
1370 doi:10.1101/2023.06.23.546268.
1371 84. De Belly, H., Yan, S., Borja Da Rocha, H., Ichbiah, S., Town, J. P., Zager, P. J., Estrada, D. C., Meyer,
1372 K., Turlier, H., Bustamante, C. & Weiner, O. D. Cell protrusions and contractions generate long-
1373 range membrane tension propagation. *Cell* **186**, 3049-3061.e15 (2023).
1374 85. Benisch, M., Benzinger, D., Kumar, S., Hu, H. & Khammash, M. Optogenetic closed-loop feedback
1375 control of the unfolded protein response optimizes protein production. *Metabolic Engineering*
1376 **77**, 32–40 (2023).
1377 86. Sheets, M. B., Tague, N. & Dunlop, M. J. An optogenetic toolkit for light-inducible antibiotic
1378 resistance. *Nat Commun* **14**, 1034 (2023).
1379 87. Zoltowski, B. D., Vaccaro, B. & Crane, B. R. Mechanism-based tuning of a LOV domain
1380 photoreceptor. *Nat Chem Biol* **5**, 827–834 (2009).
1381 88. Gligorovski, V., Sadeghi, A. & Rahi, S. J. Multidimensional characterization of inducible
1382 promoters and a highly light-sensitive LOV-transcription factor. *Nat Commun* **14**, 3810 (2023).
1383 89. Pudasaini, A., El-Arab, K. K. & Zoltowski, B. D. LOV-based optogenetic devices: light-driven
1384 modules to impart photoregulated control of cellular signaling. *Front. Mol. Biosci.* **2**, (2015).
1385 90. Benman, W., Huang, Z., Iyengar, P., Wilde, D., Mumford, T. R. & Bugaj, L. J. A temperature-
1386 inducible protein module for control of mammalian cell fate. *Nat Methods* **22**, 539–549 (2025).
1387 91. Dietler, J., Schubert, R., Krafft, T. G. A., Meiler, S., Kainrath, S., Richter, F., Schweimer, K.,
1388 Weyand, M., Janovjak, H. & Möglich, A. A Light-Oxygen-Voltage Receptor Integrates Light and
1389 Temperature. *Journal of Molecular Biology* **433**, 167107 (2021).
1390 92. Adir, O., Albalak, M. R., Abel, R., Weiss, L. E., Chen, G., Gruber, A., Staufer, O., Kurman, Y.,
1391 Kaminer, I., Shklover, J., Shainsky-Roitman, J., Platzman, I., Gepstein, L., Shechtman, Y., Horwitz,
1392 B. A. & Schroeder, A. Synthetic cells with self-activating optogenetic proteins communicate with
1393 natural cells. *Nat Commun* **13**, 2328 (2022).

1394 93. Pan, H., Li, L., Pang, G., Han, C., Liu, B., Zhang, Y., Shen, Y., Sun, T., Liu, J., Chang, J. & Wang, H.
1395 Engineered NIR light-responsive bacteria as anti-tumor agent for targeted and precise cancer
1396 therapy. *Chemical Engineering Journal* **426**, 130842 (2021).
1397 94. Wang, Z., Yan, Y. & Zhang, H. Design and Characterization of an Optogenetic System in *Pichia*
1398 *pastoris*. *ACS Synth. Biol.* **11**, 297–307 (2022).
1399 95. Zhao, E. M., Zhang, Y., Mehl, J., Park, H., Lalwani, M. A., Toettcher, J. E. & Avalos, J. L. Optogenetic
1400 regulation of engineered cellular metabolism for microbial chemical production. *Nature* **555**,
1401 683–687 (2018).
1402 96. Motta-Mena, L. B., Reade, A., Mallory, M. J., Glantz, S., Weiner, O. D., Lynch, K. W. & Gardner,
1403 K. H. An optogenetic gene expression system with rapid activation and deactivation kinetics. *Nat*
1404 *Chem Biol* **10**, 196–202 (2014).
1405 97. Baaske, J., Gonschorek, P., Engesser, R., Dominguez-Monedero, A., Raute, K., Fischbach, P.,
1406 Müller, K., Cachat, E., Schamel, W. W. A., Minguet, S., Davies, J. A., Timmer, J., Weber, W. &
1407 Zurbriggen, M. D. Dual-controlled optogenetic system for the rapid down-regulation of protein
1408 levels in mammalian cells. *Sci Rep* **8**, 15024 (2018).
1409 98. LaBelle, J., Ramos-Martinez, A., Shen, K., Motta-Mena, L. B., Gardner, K. H., Materna, S. C. &
1410 Woo, S. TAEL 2.0: An Improved Optogenetic Expression System for Zebrafish. *Zebrafish* **18**, 20–
1411 28 (2021).
1412 99. Akagi, H., Shimizu, H. & Toya, Y. Multicolor optogenetics for regulating flux ratio of three
1413 glycolytic pathways using EL222 and CcaSR in *Escherichia coli*. *Biotech & Bioengineering*
1414 bit.28628 (2023) doi:10.1002/bit.28628.
1415 100. Kramer, M. M., Mühlhäuser, W. W. D., Weber, W. & Radziwill, G. Multichromatic Control of
1416 Signaling Pathways in Mammalian Cells. *Advanced Biology* **5**, 2000196 (2021).
1417 101. Ochoa-Fernandez, R., Abel, N. B., Wieland, F.-G., Schlegel, J., Koch, L.-A., Miller, J. B.,
1418 Engesser, R., Giuriani, G., Brandl, S. M., Timmer, J., Weber, W., Ott, T., Simon, R. & Zurbriggen,

1419 M. D. Optogenetic control of gene expression in plants in the presence of ambient white light.
1420 *Nat Methods* **17**, 717–725 (2020).
1421 102. Redchuk, T. A., Karasev, M. M., Verkhusha, P. V., Donnelly, S. K., Hülsemann, M., Virtanen,
1422 J., Moore, H. M., Vartiainen, M. K., Hodgson, L. & Verkhusha, V. V. Optogenetic regulation of
1423 endogenous proteins. *Nat Commun* **11**, 605 (2020).
1424 103. Losi, A., Gardner, K. H. & Möglich, A. Blue-Light Receptors for Optogenetics. *Chem. Rev.* **118**,
1425 10659–10709 (2018).
1426 104. Remeeva, A., Nazarenko, V. V., Kovalev, K., Goncharov, I. M., Yudenko, A., Astashkin, R.,
1427 Gordeliy, V. & Gushchin, I. Insights into the mechanisms of light-oxygen-voltage domain color
1428 tuning from a set of high-resolution X-ray structures. *Proteins* **89**, 1005–1016 (2021).
1429 105. Nikolaev, A., Yudenko, A., Smolentseva, A., Bogorodskiy, A., Tsybrov, F., Borshchevskiy, V.,
1430 Bukhalovich, S., Nazarenko, V. V., Kuznetsova, E., Semenov, O., Remeeva, A. & Gushchin, I. Fine
1431 spectral tuning of a flavin-binding fluorescent protein for multicolor imaging. *Journal of*
1432 *Biological Chemistry* **299**, 102977 (2023).
1433 106. Toettcher, J. E., Gong, D., Lim, W. A. & Weiner, O. D. Light-based feedback for controlling
1434 intracellular signaling dynamics. *Nat Methods* **8**, 837–839 (2011).
1435 107. Yang, X., Jost, A. P.-T., Weiner, O. D. & Tang, C. A light-inducible organelle-targeting system
1436 for dynamically activating and inactivating signaling in budding yeast. *MBoC* **24**, 2419–2430
1437 (2013).
1438 108. Shimizu-Sato, S., Huq, E., Tepperman, J. M. & Quail, P. H. A light-switchable gene promoter
1439 system. *Nat Biotechnol* **20**, 1041–1044 (2002).
1440 109. Pathak, G. P., Strickland, D., Vrana, J. D. & Tucker, C. L. Benchmarking of optical dimerizer
1441 systems. *ACS Synth. Biol.* **3**, 832–838 (2014).

1442 110. Milias-Argeitis, A., Summers, S., Stewart-Ornstein, J., Zuleta, I., Pincus, D., El-Samad, H.,
1443 Khammash, M. & Lygeros, J. *In silico* feedback for in vivo regulation of a gene expression circuit.
1444 *Nat Biotechnol* **29**, 1114–1116 (2011).
1445 111. Oda, S., Sato-Ebine, E., Nakamura, A., Kimura, K. D. & Aoki, K. *Optogenetic Control of Cell*
1446 *Signaling with Red/Far-Red Light-Responsive Optogenetic Tools in* Caenorhabditis Elegans.
1447 http://biorxiv.org/lookup/doi/10.1101/2022.08.12.503710 (2022)
1448 doi:10.1101/2022.08.12.503710.
1449 112. Uda, Y., Goto, Y., Oda, S., Kohchi, T., Matsuda, M. & Aoki, K. Efficient synthesis of
1450 phycocyanobilin in mammalian cells for optogenetic control of cell signaling. *Proc. Natl. Acad.*
1451 *Sci. U.S.A.* **114**, 11962–11967 (2017).
1452 113. Müller, K., Engesser, R., Timmer, J., Nagy, F., Zurbriggen, M. D. & Weber, W. Synthesis of
1453 phycocyanobilin in mammalian cells. *Chem. Commun.* **49**, 8970 (2013).
1454 114. Hochrein, L., Machens, F., Messerschmidt, K. & Mueller-Roeber, B. PhiReX: a programmable
1455 and red light-regulated protein expression switch for yeast. *Nucleic Acids Research* **45**, 9193–
1456 9205 (2017).
1457 115. Gossen, M., Freundlieb, S., Bender, G., Müller, G., Hillen, W. & Bujard, H. Transcriptional
1458 Activation by Tetracyclines in Mammalian Cells. *Science* **268**, 1766–1769 (1995).
1459 116. Mateus, C. & Avery, S. V. Destabilized green fluorescent protein for monitoring dynamic
1460 changes in yeast gene expression with flow cytometry. *Yeast* **16**, 1313–1323 (2000).
1461 117. Leopold, A. V., Chernov, K. G. & Verkhusha, V. V. Optogenetically controlled protein kinases
1462 for regulation of cellular signaling. *Chem. Soc. Rev.* **47**, 2454–2484 (2018).
1463 118. de Mena, L., Rizk, P. & Rincon-Limas, D. E. Bringing light to transcription: the optogenetics
1464 repertoire. *Front. Genet.* **9**, 518 (2018).

1465 119. Niopek, D., Benzinger, D., Roensch, J., Draebing, T., Wehler, P., Eils, R. & Di Ventura, B.
1466 Engineering light-inducible nuclear localization signals for precise spatiotemporal control of
1467 protein dynamics in living cells. *Nat Commun* **5**, 4404 (2014).
1468 120. Renicke, C., Schuster, D., Usherenko, S., Essen, L.-O. & Taxis, C. A LOV2 Domain-Based
1469 Optogenetic Tool to Control Protein Degradation and Cellular Function. *Chemistry & Biology* **20**,
1470 619–626 (2013).
1471 121. Dagliyan, O., Tarnawski, M., Chu, P.-H., Shirvanyants, D., Schlichting, I., Dokholyan, N. V. &
1472 Hahn, K. M. Engineering extrinsic disorder to control protein activity in living cells. *Science* **354**,
1473 1441–1444 (2016).
1474 122. Chen, J., Vishweshwaraiah, Y. L., Mailman, R. B., Tabdanov, E. D. & Dokholyan, N. V. A
1475 noncommutative combinatorial protein logic circuit controls cell orientation in
1476 nanoenvironments. *Sci. Adv.* **9**, eadg1062 (2023).
1477 123. Rahi, S. J., Pecani, K., Ondracka, A., Oikonomou, C. & Cross, F. R. The CDK-APC/C oscillator
1478 predominantly entrains periodic cell-cycle transcription. *Cell* **165**, 475–487 (2016).
1479 124. Richardson, H., Lew, D. J., Henze, M., Sugimoto, K. & Reed, S. I. Cyclin-B homologs in
1480 Saccharomyces cerevisiae function in S phase and in G2. *Genes Dev.* **6**, 2021–2034 (1992).
1481 125. Wäsch, R. & Cross, F. R. APC-dependent proteolysis of the mitotic cyclin Clb2 is essential for
1482 mitotic exit. *Nature* **418**, 556–562 (2002).
1483 126. Rahi, S. J., Larsch, J., Pecani, K., Katsov, A. Y., Mansouri, N., Tsaneva-Atanasova, K., Sontag,
1484 E. D. & Cross, F. R. Oscillatory stimuli differentiate adapting circuit topologies. *Nat Methods* **14**,
1485 1010–1016 (2017).
1486 127. Epstein, C. B. & Cross, F. R. CLB5: a novel B cyclin from budding yeast with a role in S phase.
1487 *Genes Dev.* **6**, 1695–1706 (1992).
1488 128. Schwob, E. & Nasmyth, K. CLB5 and CLB6, a new pair of B cyclins involved in DNA replication
1489 in Saccharomyces cerevisiae. *Genes & Development* **7**, 1160–1175 (1993).

1490 129. Loog, M. & Morgan, D. O. Cyclin specificity in the phosphorylation of cyclin-dependent kinase
1491 substrates. *Nature* **434**, 104–108 (2005).
1492 130. Morgan, D. O. *The Cell Cycle: Principles of Control*. (Published by New Science Press in
1493 association with Oxford University Press ; Distributed inside North America by Sinauer
1494 Associates, Publishers, London : Sunderland, MA, 2007).
1495 131. Levine, K., Kiang, L., Jacobson, M. D., Fisher, R. P. & Cross, F. R. Directed Evolution to Bypass
1496 Cyclin Requirements for the Cdc28p Cyclin-Dependent Kinase. *Molecular Cell* **4**, 353–363 (1999).
1497 132. Kozholianko, G. SOLAR CULT OF ANCIENT UKRAINIANS. *nz* **139**, 57–64 (2018).
1498 133. Tyers, M. The cyclin-dependent kinase inhibitor p40SIC1 imposes the requirement for Cln G1
1499 cyclin function at Start. *Proc. Natl. Acad. Sci. U.S.A.* **93**, 7772–7776 (1996).
1500 134. Jin, Y. H., Garg, P., Stith, C. M. W., Al-Refai, H., Sterling, J. F., Murray, L. J. W., Kunkel, T. A.,
1501 Resnick, M. A., Burgers, P. M. & Gordenin, D. A. The Multiple Biological Roles of the 3′→5′
1502 Exonuclease of *Saccharomyces cerevisiae* DNA Polymerase δ Require Switching between the
1503 Polymerase and Exonuclease Domains. *Molecular and Cellular Biology* **25**, 461–471 (2005).
1504 135. Lang, G. I. & Murray, A. W. Estimating the Per-Base-Pair Mutation Rate in the Yeast
1505 *Saccharomyces cerevisiae*. *Genetics* **178**, 67–82 (2008).
1506 136. Wildenberg, G. A. & Murray, A. W. Evolving a 24-hr oscillator in budding yeast. *eLife* **3**,
1507 e04875 (2014).
1508 137. Dietler, N., Minder, M., Gligorovski, V., Economou, A. M., Joly, D. A. H. L., Sadeghi, A., Chan,
1509 C. H. M., Koziński, M., Weigert, M., Bitbol, A.-F. & Rahi, S. J. A convolutional neural network
1510 segments yeast microscopy images with high accuracy. *Nat Commun* **11**, 5723 (2020).
1511 138. Jang, J. & Woolley, G. A. Directed evolution approaches for optogenetic tool development.
1512 *Biochemical Society Transactions* **49**, 2737–2748 (2021).

1513 139. Nash, A. I., McNulty, R., Shillito, M. E., Swartz, T. E., Bogomolni, R. A., Luecke, H. & Gardner,
1514 K. H. Structural basis of photosensitivity in a bacterial light-oxygen-voltage/helix-turn-helix
1515 (LOV-HTH) DNA-binding protein. *Proc. Natl. Acad. Sci. U.S.A.* **108**, 9449–9454 (2011).
1516 140. Zoltowski, B. D., Motta-Mena, L. B. & Gardner, K. H. Blue light-induced dimerization of a
1517 bacterial LOV–HTH DNA-binding protein. *Biochemistry* **52**, 6653–6661 (2013).
1518 141. Ziegler, T. & Möglich, A. Photoreceptor engineering. *Front. Mol. Biosci.* **2**, (2015).
1519 142. García De Fuentes, A. & Möglich, A. Reduction midpoint potential of a paradigm light–
1520 oxygen–voltage receptor and its modulation by methionine residues. *RSC Chem. Biol.* **5**, 530–
1521 543 (2024).
1522 143. Glantz, S. T., Carpenter, E. J., Melkonian, M., Gardner, K. H., Boyden, E. S., Wong, G. K.-S. &
1523 Chow, B. Y. Functional and topological diversity of LOV domain photoreceptors. *Proc. Natl. Acad.*
1524 *Sci. U.S.A.* **113**, (2016).
1525 144. Allard, C. A. H., Decker, F., Weiner, O. D., Toettcher, J. E. & Graziano, B. R. A size-invariant
1526 bud-duration timer enables robustness in yeast cell size control. *PLoS ONE* **13**, e0209301 (2018).
1527 145. Cui, Z., Hirata, D., Tsuchiya, E., Osada, H. & Miyakawa, T. The Multidrug Resistance-
1528 associated Protein (MRP) Subfamily (Yrs1/Yor1) of *Saccharomyces cerevisiae* Is Important for
1529 the Tolerance to a Broad Range of Organic Anions. *Journal of Biological Chemistry* **271**, 14712–
1530 14716 (1996).
1531 146. Szczypka, M. S., Wemmie, J. A., Moye-Rowley, W. S. & Thiele, D. J. A yeast metal resistance
1532 protein similar to human cystic fibrosis transmembrane conductance regulator (CFTR) and
1533 multidrug resistance-associated protein. *Journal of Biological Chemistry* **269**, 22853–22857
1534 (1994).
1535 147. Camadro, J.-M. & Labbe, P. Cloning and Characterization of the Yeast HEM14 Gene Coding
1536 for Protoporphyrinogen Oxidase, the Molecular Target of Diphenyl Ether-type Herbicides.
1537 *Journal of Biological Chemistry* **271**, 9120–9128 (1996).

1538 148. Glerum, D. M., Shtanko, A., Tzagoloff, A., Gorman, N. & Sinclair, P. R. Cloning and
1539 identification of HEM14, the yeast gene for mitochondrial protoporphyrinogen oxidase. *Yeast*
1540 **12**, 1521–1425 (1996).
1541 149. Auclair, K., Huang, H.-W., Moënne-Loccoz, P. & Ortiz De Montellano, P. R. Cloning and
1542 expression of a heme binding protein from the genome of Saccharomyces cerevisiae. *Protein*
1543 *Expression and Purification* **28**, 340–349 (2003).
1544 150. Möglich, A., Yi, C., Golonka, D., Meier, S., Tang, K., Ihalainen, J. & Zurbriggen, M.
1545 Commutability of Bilin Chromophores in Plant Phytochromes. Preprint at
1546 https://doi.org/10.21203/rs.3.rs-6196749/v1 (2025).
1547 151. Sakai, K., Kondo, Y., Fujioka, H., Kamiya, M., Aoki, K. & Goto, Y. Near-infrared imaging in
1548 fission yeast using a genetically encoded phycocyanobilin biosynthesis system. *Journal of Cell*
1549 *Science* **134**, jcs259315 (2021).
1550 152. Van Kempen, M., Kim, S. S., Tumescheit, C., Mirdita, M., Lee, J., Gilchrist, C. L. M., Söding, J.
1551 & Steinegger, M. Fast and accurate protein structure search with Foldseek. *Nat Biotechnol* **42**,
1552 243–246 (2024).
1553 153. Hekkelman, M. L., De Vries, I., Joosten, R. P. & Perrakis, A. AlphaFill: enriching AlphaFold
1554 models with ligands and cofactors. *Nat Methods* **20**, 205–213 (2023).
1555 154. Jungwirth, H. & Kuchler, K. Yeast ABC transporters – A tale of sex, stress, drugs and aging.
1556 *FEBS Letters* **580**, 1131–1138 (2006).
1557 155. Zhou, X., Vink, M., Klaver, B., Berkhout, B. & Das, A. T. Optimization of the Tet-On system for
1558 regulated gene expression through viral evolution. *Gene Ther* **13**, 1382–1390 (2006).
1559 156. Makanae, K., Kintaka, R., Makino, T., Kitano, H. & Moriya, H. Identification of dosage-
1560 sensitive genes in *Saccharomyces cerevisiae* using the genetic tug-of-war method. *Genome Res.*
1561 **23**, 300–311 (2013).

1562 157. Robinson, D., Place, M., Hose, J., Jochem, A. & Gasch, A. P. Natural variation in the
1563 consequences of gene overexpression and its implications for evolutionary trajectories. *eLife* **10**,
1564 e70564 (2021).
1565 158. Cravens, A., Jamil, O. K., Kong, D., Sockolosky, J. T. & Smolke, C. D. Polymerase-guided base
1566 editing enables in vivo mutagenesis and rapid protein engineering. *Nat Commun* **12**, 1579
1567 (2021).
1568 159. Skrekas, C., Limeta, A., Siewers, V. & David, F. Targeted *In Vivo* Mutagenesis in Yeast Using
1569 CRISPR/Cas9 and Hyperactive Cytidine and Adenine Deaminases. *ACS Synth. Biol.* **12**, 2278–2289
1570 (2023).
1571 160. Fields, S. & Song, O. A novel genetic system to detect protein–protein interactions. *Nature*
1572 **340**, 245–246 (1989).
1573 161. Hu, J. H., Miller, S. M., Geurts, M. H., Tang, W., Chen, L., Sun, N., Zeina, C. M., Gao, X., Rees,
1574 H. A., Lin, Z. & Liu, D. R. Evolved Cas9 variants with broad PAM compatibility and high DNA
1575 specificity. *Nature* **556**, 57–63 (2018).
1576 162. Miller, S. M., Wang, T., Randolph, P. B., Arbab, M., Shen, M. W., Huang, T. P., Matuszek, Z.,
1577 Newby, G. A., Rees, H. A. & Liu, D. R. Continuous evolution of SpCas9 variants compatible with
1578 non-G PAMs. *Nat Biotechnol* **38**, 471–481 (2020).
1579 163. Di Roberto, R. B., Chang, B. & Peisajovich, S. G. The directed evolution of ligand specificity in
1580 a GPCR and the unequal contributions of efficacy and affinity. *Sci Rep* **7**, 16012 (2017).
1581 164. Scott, B. M., Chen, S. K., Bhattacharyya, N., Moalim, A. Y., Plotnikov, S. V., Heon, E.,
1582 Peisajovich, S. G. & Chang, B. S. W. Coupling of Human Rhodopsin to a Yeast Signaling Pathway
1583 Enables Characterization of Mutations Associated with Retinal Disease. *Genetics* **211**, 597–615
1584 (2019).
1585 165. Ladds, G., Goddard, A. & Davey, J. Functional analysis of heterologous GPCR signalling
1586 pathways in yeast. *Trends in Biotechnology* **23**, 367–373 (2005).

1587 166. Nevozhay, D., Zal, T. & Balázsi, G. Transferring a synthetic gene circuit from yeast to
1588 mammalian cells. *Nat Commun* **4**, 1451 (2013).
1589 167. Rees, D. C., Johnson, E. & Lewinson, O. ABC transporters: the power to change. *Nat Rev Mol*
1590 *Cell Biol* **10**, 218–227 (2009).
1591 168. Vanoni, M., Vai, M. & Frascotti, G. Effects of temperature on the yeast cell cycle analyzed by
1592 flow cytometry. *Cytometry* **5**, 530–533 (1984).
1593 169. Alberstein, R. G., Guo, A. B. & Kortemme, T. Design principles of protein switches. *Current*
1594 *Opinion in Structural Biology* **72**, 71–78 (2022).
1595 170. Pillai, A., Idris, A., Philomin, A., Weidle, C., Skotheim, R., Leung, P. J. Y., Broerman, A.,
1596 Demakis, C., Borst, A. J., Praetorius, F. & Baker, D. *De Novo Design of Allosterically Switchable*
1597 *Protein Assemblies*. http://biorxiv.org/lookup/doi/10.1101/2023.11.01.565167 (2023)
1598 doi:10.1101/2023.11.01.565167.
1599 171. Glasgow, A. A., Huang, Y.-M., Mandell, D. J., Thompson, M., Ritterson, R., Loshbaugh, A. L.,
1600 Pellegrino, J., Krivacic, C., Pache, R. A., Barlow, K. A., Ollikainen, N., Jeon, D., Kelly, M. J. S., Fraser,
1601 J. S. & Kortemme, T. Computational design of a modular protein sense-response system. *Science*
1602 **366**, 1024–1028 (2019).
1603 172. Kretschmer, S., Perry, N., Zhang, Y. & Kortemme, T. Multi-input Drug-Controlled Switches of
1604 Mammalian Gene Expression Based on Engineered Nuclear Hormone Receptors. *ACS Synth. Biol.*
1605 **12**, 1924–1934 (2023).
1606 173. Jefferson, R. E., Oggier, A., Füglistaler, A., Camviel, N., Hijazi, M., Villarreal, A. R., Arber, C. &
1607 Barth, P. Computational design of dynamic receptor—peptide signaling complexes applied to
1608 chemotaxis. *Nat Commun* **14**, 2875 (2023).
1609 174. Ouyang, X., Ren, H. & Huang, X. Optogenetic tools controlled by ultraviolet-B light. *aBIOTECH*
1610 **2**, 170–175 (2021).

1611 175. Rizzini, L., Favory, J.-J., Cloix, C., Faggionato, D., O'Hara, A., Kaiserli, E., Baumeister, R.,
1612 Schäfer, E., Nagy, F., Jenkins, G. I. & Ulm, R. Perception of UV-B by the *Arabidopsis* UVR8 Protein.
1613 *Science* **332**, 103–106 (2011).
1614 176. Jang, J., Tang, K., Youn, J., McDonald, S., Beyer, H. M., Zurbriggen, M. D., Uppalapati, M. &
1615 Woolley, G. A. Engineering of bidirectional, cyanobacteriochrome-based light-inducible dimers
1616 (BICYCL)s. *Nat Methods* **20**, 432–441 (2023).
1617 177. Kaberniuk, A. A., Baloban, M., Monakhov, M. V., Shcherbakova, D. M. & Verkhusha, V. V.
1618 Single-component near-infrared optogenetic systems for gene transcription regulation. *Nat*
1619 *Commun* **12**, 3859 (2021).
1620 178. Bugaj, L. J. & Lim, W. A. High-throughput multicolor optogenetics in microwell plates. *Nat*
1621 *Protoc* **14**, 2205–2228 (2019).
1622 179. Meier, S. S. M., Multamäki, E., Ranzani, A. T., Takala, H. & Möglich, A. Multimodal Control of
1623 Bacterial Gene Expression by Red and Blue Light. in *Synthetic Biology* (ed. Braman, J. C.) vol.
1624 2760 463–477 (Springer US, New York, NY, 2024).
1625 180. Kolar, K., Knobloch, C., Stork, H., Žnidarič, M. & Weber, W. OptoBase: A Web Platform for
1626 Molecular Optogenetics. *ACS Synth. Biol.* **7**, 1825–1828 (2018).
1627 181. Ng, A. H., Nguyen, T. H., Gómez-Schiavon, M., Dods, G., Langan, R. A., Boyken, S. E., Samson,
1628 J. A., Waldburger, L. M., Dueber, J. E., Baker, D. & El-Samad, H. Modular and tunable biological
1629 feedback control using a de novo protein switch. *Nature* **572**, 265–269 (2019).
1630 182. Langan, R. A., Boyken, S. E., Ng, A. H., Samson, J. A., Dods, G., Westbrook, A. M., Nguyen, T.
1631 H., Lajoie, M. J., Chen, Z., Berger, S., Mulligan, V. K., Dueber, J. E., Novak, W. R. P., El-Samad, H.
1632 & Baker, D. De novo design of bioactive protein switches. *Nature* **572**, 205–210 (2019).
1633 183. Shui, S., Scheller, L. & Correia, B. E. *Rationally Designed Protein Bandpass Filters for*
1634 *Controlling Cellular Signaling with Chemical Inputs*.

1635 http://biorxiv.org/lookup/doi/10.1101/2023.02.10.528077 (2023)
1636 doi:10.1101/2023.02.10.528077.
1637 184. Synthetic complete (SC) medium. *Cold Spring Harb Protoc* **2016**, pdb.rec090589 (2016).
1638 185. 5-Fluoroorotic Acid (5-FOA) Plates. *Cold Spring Harb Protoc* **2016**, pdb.rec086637 (2016).
1639 186. Gietz, R. D. & Schiestl, R. H. High-efficiency yeast transformation using the LiAc/SS carrier
1640 DNA/PEG method. *Nat Protoc* **2**, 31–34 (2007).
1641 187. Sikorski, R. S. & Hieter, P. A system of shuttle vectors and yeast host strains designed for
1642 efficient manipulation of DNA in Saccharomyces cerevisiae. *Genetics* **122**, 19–27 (1989).
1643 188. Dietler, J., Gelfert, R., Kaiser, J., Borin, V., Renzl, C., Pilsl, S., Ranzani, A. T., García De Fuentes,
1644 A., Gleichmann, T., Diensthuber, R. P., Weyand, M., Mayer, G., Schapiro, I. & Möglich, A. Signal
1645 transduction in light-oxygen-voltage receptors lacking the active-site glutamine. *Nat Commun*
1646 **13**, 2618 (2022).
1647 189. Mathes, T., Vogl, C., Stolz, J. & Hegemann, P. In Vivo Generation of Flavoproteins with
1648 Modified Cofactors. *Journal of Molecular Biology* **385**, 1511–1518 (2009).
1649 190. Möglich, A. An Open-Source, Cross-Platform Resource for Nonlinear Least-Squares Curve
1650 Fitting. *J. Chem. Educ.* **95**, 2273–2278 (2018).
1651 191. Swartz, T. E., Corchnoy, S. B., Christie, J. M., Lewis, J. W., Szundi, I., Briggs, W. R. & Bogomolni,
1652 R. A. The Photocycle of a Flavin-binding Domain of the Blue Light Photoreceptor Phototropin.
1653 *Journal of Biological Chemistry* **276**, 36493–36500 (2001).
1654 192. Rivera-Cancel, G., Motta-Mena, L. B. & Gardner, K. H. Identification of natural and artificial
1655 DNA substrates for light-activated LOV–HTH transcription factor EL222. *Biochemistry* **51**, 10024–
1656 10034 (2012).
1657 193. Quail, P. H. Phytochromes. *Current Biology* **20**, R504–R507 (2010).
1658 194. Quail, P. H., Boylan, M. T., Parks, B. M., Short, T. W., Xu, Y. & Wagner, D. Phytochromes:
1659 Photosensory Perception and Signal Transduction. *Science* **268**, 675–680 (1995).

1660 195. Liu, C., Fu, Y., Lin, L., Elson, E. L. & Wang, J. Understanding Cellular Noise with Optical
1661 Perturbation and Deep Learning. (2024) doi:10.48550/ARXIV.2401.12498.
1662 196. Sharrock, R. A. The phytochrome red/far-red photoreceptor superfamily. *Genome Biol* **9**, 230
1663 (2008).
1664 197. Baron, U. & Bujard, H. Tet repressor-based system for regulated gene expression in
1665 eukaryotic cells: Principles and advances. in *Methods in Enzymology* vol. 327 401–421 (Elsevier,
1666 2000).
1667 198. Orlando, D. A., Lin, C. Y., Bernard, A., Wang, J. Y., Socolar, J. E. S., Iversen, E. S., Hartemink,
1668 A. J. & Haase, S. B. Global control of cell-cycle transcription by coupled CDK and network
1669 oscillators. *Nature* **453**, 944–947 (2008).
1670 199. Yang, X., Lau, K.-Y., Sevim, V. & Tang, C. Design Principles of the Yeast G1/S Switch. *PLoS Biol*
1671 **11**, e1001673 (2013).
1672 200. Lengronne, A. & Schwob, E. The Yeast CDK Inhibitor Sic1 Prevents Genomic Instability by
1673 Promoting Replication Origin Licensing in Late G1. *Molecular Cell* **9**, 1067–1078 (2002).
1674 201. Dahmann, C., Diffley, J. F. X. & Nasmyth, K. A. S-phase-promoting cyclin-dependent kinases
1675 prevent re-replication by inhibiting the transition of replication origins to a pre-replicative state.
1676 *Current Biology* **5**, 1257–1269 (1995).
1677 202. Nguyen, V. Q., Co, C. & Li, J. J. Cyclin-dependent kinases prevent DNA re-replication through
1678 multiple mechanisms. *Nature* **411**, 1068–1073 (2001).
1679 203. Jacobson, M. D., Gray, S., Yuste-Rojas, M. & Cross, F. R. Testing cyclin specificity in the exit
1680 from mitosis. *Mol Cell Biol* **20**, 4483–4493 (2000).
1681 204. Sakai, K., Kondo, Y., Fujioka, H., Kamiya, M., Aoki, K. & Goto, Y. Near-infrared imaging in
1682 fission yeast using a genetically encoded phycocyanobilin biosynthesis system. *Journal of Cell*
1683 *Science* **134**, jcs259315 (2021).

1684 205. Zhu, Y. O., Siegal, M. L., Hall, D. W. & Petrov, D. A. Precise estimates of mutation rate and
1685 spectrum in yeast. *Proc. Natl. Acad. Sci. U.S.A.* **111**, (2014).
1686
1687

1688 # Acknowledgments

1689 We thank Roxane Dervey for help with strain construction and media preparation; Dr. Kyle Douglass,
1690 Dr. Hélène Lambert, Dr. Matthew Lycas, and Prof. Suliana Manley for sharing resources; Prof. Peter
1691 Quail, Prof. Hana El-Samad, and Dr. Brian Graziano for providing PhyB-Pif3 strains and constructs;
1692 Prof. Yuhei Goto for sharing iRFP budding yeast strains; Prof. Mathieu Coppey for sharing a PhyB-
1693 PIF6 mammalian cell line; Prof. Kazuhiro Aoki for sharing plasmids; Prof. Wilfried Weber and Prof.
1694 Gerald Radziwill for sharing plasmids for transcriptional PhyB-PIF6 control; Prof. José L. Avalos and
1695 Dr. Evan Zhao for providing the *EL222* plasmid; Prof. Andrew Murray for providing the *pol3-L523D*
1696 strain; and Dr. Enrico Tenaglia for help with molecular cloning. We thank the mechanical and
1697 electronics workshops of the Institute of Physics in the Cubotron building at EPFL for help building
1698 the hardware for optogenetic stimulation. We acknowledge support for VG, ML, LS, and SJR
1699 provided by SNSF grants CRSK-3_190526, 310030_204938, and CRSK-3_221036 awarded to SJR. LS
1700 is also supported by the EPFLglobaLeaders doctoral fellowship. A.M. acknowledges support through
1701 grant DFG MO2192/10-1 by the Deutsche Forschungsgemeinschaft.

1702 # Author contributions

1703 VG, ML, LS, MB, AM, NM, and SJR designed the experiments and analyzed the data. VG constructed
1704 the strains used for evolution. VG performed the directed evolution experiments. VG and ML
1705 characterized the evolved variants, including reporter strain construction. LS constructed and tested
1706 the multiplexing system, aided by VG. VG, MB, and AM purified proteins and performed *in vitro*
1707 biophysical characterization. VG, AM, and SJR wrote the manuscript. NM supervised the
1708 experiments in mammalian cells. AM supervised the *in vitro* experiments. SJR supervised the overall
1709 project and acquired funding.

1710 # Competing interests

1711 VG and SJR have filed a provisional patent application for the method reported in this manuscript
1712 through EPFL.

1713

1714 # Supplementary Material

1715 ## Supplementary Note 1: List of previous multiple-goal continuous
1716 directed evolution campaigns

Publication	Molecular target	Details	Host	Ref.
Continuous directed evolution of DNA-binding proteins to improve TALEN specificity Hubbard et al., 2015	TALENs	Based on the PACE platform[14] Positive selection: DNA binding domain of TALENs coupled to phage propagation by way of bacterial RNA polymerase Negative selection: Promiscuous phage activity coupled to pIII-neg that inhibits phage propagation	*E. coli*	19
Evolution of a split RNA polymerase as a versatile biosensor platform Pu et al., 2017	T7 RNAP	Based on the PACE platform[14] Positive selection: Desired interaction between the halves of RNAP linked to phage propagation Negative selection: Interaction with alternative domains counterselected by linking promiscuous activity to dominant negative pIII-neg	*E. coli*	20
Contingency and chance erase necessity in the experimental evolution of ancestral proteins Xie et al., 2021	BCL-2 coregulators	Based on the PACE platform[14] Positive selection: The interaction of interest drives the expression of pIII necessary for phage propagation Negative selection: Unwanted interaction is counterselected by linking its activity to dominant negative pIII-neg	*E. coli*	21
Directed Evolution and Substrate Specificity Profile of Homing Endonuclease I-SceI Doyon et al., 2006	I-SceI	Positive selection: Endonuclease activity of I-SceI rescues the host cell by digesting a plasmid with a toxic gene (*ccdB*) Negative selection: Promiscuous substrate recognition suppressed using an antibiotic-resistance plasmid that must not be cut by I-SceI	*E. coli*	22
Engineered CRISPR-Cas9 nucleases with altered PAM specificities Kleinstiver et al., 2015	Cas9	Positive selection: Survival requires Cas9-mediated cleavage of a plasmid harboring a toxic gene Negative selection: Unwanted recognition of PAM sequences is suppressed using an antibiotic resistance plasmid whose cleavage by Cas9 leads to cell death	*E. coli*	23
Directed evolution of CRISPR-Cas9 to increase its specificity Lee et al., 2018	Cas9	Positive selection: Survival requires Cas9-mediated cleavage of a plasmid harboring a toxic gene Negative selection: Off-target cleavage is suppressed by introducing potential recognition sequences into *E. coli* genome that if cut lead to cell death	*E. coli*	24
A bacterial dual positive and negative selection system for dCas9 activity	Cas9	Positive selection: dCas9- and LacI-mediated derepression of antibiotic resistance genes Negative selection: dCas9-mediated repression of essential genes	*E. coli*	25

Spisak et al., 2022				
Engineered dual selection for directed evolution of SpCas9 PAM specificity Goldberg et al., 2021	Cas9	Positive selection: dCas9-mediated expression of *HIS3* auxotrophic gene, essential in media without histidine Negative selection: off-target binding leads to repression of *HIS3*	*E. coli*	[26]
A highly specific SpCas9 variant is identified by in vivo screening in yeast Casini et al., 2018	Cas9	Positive selection: On-target cleavage leads to reconstitution of functional auxotrophic marker *TRP1* Negative selection: Off-target cleavage leads to reconstitution of *ADE2*, which causes color change of yeast colony	Budding yeast	[27]

Supplementary Note 2: List of previous selection/counterselection directed evolution campaigns

Publication	Molecular target	Selection mechanism	Organism	Timing of selection cycles	Mutagenesis	Selection environ-ment	Ref.
Robust and flexible platform for directed evolution of yeast genetic switches Tominaga et al., 2021	Tet-ON system and biosensors for DAPG and Camphor	Positive selection: *BLE* expression (Zeocin resistance) Negative selection: hsvTK activity in the presence of specific substrates leads to toxic products	Budding yeast	24 h of negative selection followed by 24 h induction and final positive selection for 24 h	Error-prone PCR	Liquid	[38]
Ribozyme-Based Aminoglycoside Switches of Gene Expression Engineered by Genetic Selection in *S. cerevisiae* Klauser et al., 2015	RNA switches	Positive selection: *HIS3* auxotrophic marker expression Negative selection: *URA3* expression in medium with 5-fluoroorotic acid (5-FOA)	Budding yeast	Not specified	Randomized library	Solid	[39]
Engineering prokaryotic transcriptional activators as metabolite biosensors in yeast Skjoedt et al., 2016	Transcriptional biosensor based on LTTR family of proteins	FACS (Fluorescence activated cell sorting)-based screening	Budding yeast	Cells grown for 24 h without inducer were subjected to negative selection followed by a 24 h induction and positive selection	Error-prone PCR	Liquid	[40]
Evolution-guided engineering of small-molecule biosensors Snoek et al., 2020	Transcriptional sensors for *cis,cis*-muconic acid	FACS-based screening	Budding yeast	Single round of FACS-selection for desired phenotype with cells grown under inducing or non-inducing conditions for 22 h	Error-prone PCR	Liquid	[41]

Photo-sensitive degron variants for tuning protein stability by light Usherenko et al., 2014	Photosensitive degron	Manual screen for different fluorescence in darkness/light	Budding yeast	Replicas of colonies screened under inducing and non-inducing conditions separately after 24 h of growth	Error-prone PCR	Solid	[42]
A Yeast System for Discovering Optogenetic Inhibitors of Eukaryotic Translation Initiation Lu et al., 2019	Optogenetic inhibitors of translation	Positive selection based on translation inhibition	Budding yeast	Replicas of colonies screened under inducing and non-inducing conditions separately after 2 days of growth	Error-prone PCR	Solid	[43]
A light- and calcium-gated transcription factor for imaging and manipulating activated neurons Wang et al., 2017	Light- and calcium-gated transcription factor	FACS-based screen	Budding yeast	Six rounds of alternating positive and negative selection with 2-3 days of growth between each round	Error-prone PCR	Liquid	[44]
Yeast Two-Hybrid Screening of Photoswitchable Protein–Protein Interaction Libraries Woloschuk et al., 2020	Proteins that interact with photoswitcha-ble proteins	Positive selection based on yeast-two-hybrid driven expression of *HIS3* auxotrophic marker	Budding yeast	Positive selection for 72 h after the transformation followed by separate screens of replicas under inducing and non-inducing conditions grown for 48 h	Site-directed mutagenesis	Solid	[45]
Optimized second-generation CRY2-CIB dimerizers and photoactivatable Cre recombinase Taslimi et al., 2016	CRY2	Dual selection based on yeast-two-hybrid driven expression of *URA3* gene on -uracil (positive) or +5-FOA plates (negative)	Budding yeast	For identifying light-sensitized variants, cells were subjected to low light on -uracil plates and then replica-plated in darkness onto 5-FOA plates. For identifying low-leakiness variants, cells were subjected to selection under low light on 5-FOA plates and then replica-plated onto -uracil plates under a high-light regime. Timing not fully specified.	Error-prone PCR	Solid	[46]
Creating Red Light-Switchable Protein Dimerization Systems as Genetically Encoded Actuators with High Specificity Huang et al., 2020	Binders of bacterial phytochrome	The library enriched by phage display was further screened in budding yeast using the yeast two-hybrid method	Budding yeast	Growth of budding yeast under positive selection conditions for 4-5 days followed by separate screening of replica colonies under inducing and non-inducing conditions for 24 h to exclude constitutively active mutants	Randomized library	Solid	[47]

Engineering an improved light-induced dimer (iLID) for controlling the localization and activity of signaling proteins Guntas et al., 2015	LOV domains	Positive selection: binding under light Negative selection: elution in darkness	Phage display	Four rounds of the following steps: 1 h light induction, selection, 10 min in darkness, and counter-selection	Rationally designed library	*Ex vivo*	[48]
Discovering Selective Binders for Photoswitchable Proteins Using Phage Display Reis et al., 2018	Binders of PYP and LOV2	Selection for binding of either darkness- or light-adapted form of the protein, with washouts designed to reduce constitutive binding	Phage display *E. coli* (used for protein expres-sion)	Three rounds of selection and counterselection with 1 h exposure to light or 1 h in darkness for proteins to adopt their light- or dark-states, respectively.	Site-directed mutagenesis	*Ex vivo*	[49]
LOVTRAP: an optogenetic system for photoinduced protein dissociation Wang et al., 2016	LOV domains	mRNA display (Selection for binding in darkness with washouts designed to reduce constitutive binding)	*E. coli* (used for protein expressio n)	12 rounds of selection. Timing not specified.	Randomized library	*Ex vivo*	[50]
Fluorescence Imaging-Based High-Throughput Screening of Fast- and Slow-Cycling LOV Proteins Kawano et al., 2013	LOV domains	Manual screen of mutant colonies	*E. coli*	Transient induction followed by timelapse imaging of bacterial colonies for three hours	Site-directed mutageneis	Solid	[51]
Directed evolution of a genetic circuit Yokobayashi et al., 2002	Logic gate based on constitutive bacterial regulators	Manual screen of colonies	*E. coli*	Not specified	Error-prone PCR	Solid	[52]
Evolving Orthogonal Suppressor tRNAs To Incorporate Modified Amino Acids Maranhao and Ellington, 2017	tRNA	Positive selection: compartmentalized partnered replication (CPR) Negative selection: incorporation of toxic *p*-Cl-phenylalanine (p-Cl-Phe)	*E. coli*	Three rounds of CPR, each including 3 h of growth, then 4 h of incubation with p-Cl-Phe for negative selection, followed by a final round of CPR	Randomized library	Liquid	[53]
Enhancing the performance of Magnets photosensors through directed evolution Baumschlager et al., 2022	LOV domains	FACS-based selection	*E. coli*	For each selection step, cells were grown in inducing or non-inducing conditions for 4 h. Three rounds of selection in total: two positive with one negative in-between	Error-prone PCR	Liquid	[54]
Escherichia coli "Marionette" strains with 12 highly optimized small-molecule sensors	12 prokaryotic chemically-responsive biosensors	Positive selection: expression of DNA Polymerase for compartmentalized partnered replication	*E. coli*	Alternating negative selection for 12-16 h, followed by positive selection for 4 h, with 4-23 total rounds of selection	Randomized library of biosensors with intermittent	Liquid	[55]

Meyer et al., 2019		Negative selection: incorporation of lethal *p*-Cl-phenylalanine (p-Cl-Phe)			library shuffling		
A nucleoside kinase as a dual selector for genetic switches and circuits Tashiro et al., 2011	Logic gate protein circuits	Positive and negative selection based on activity of *hsvTK* gene	*E. coli*	12-15 h of positive selection followed by 12 h of negative selection	N/A	Liquid and solid	[56]
Engineering an allosteric transcription factor to respond to new ligands Taylor et al., 2016	LacI	Positive selection: FACS of fluorescently labeled cells Negative selection: Expression of the toxin importer *tolC* gene	*E. coli*	Overnight negative selection followed by a FACS-based positive selection	Rationally designed mutation library combined with error-prone PCR	Liquid	[57]
AraC Regulatory Protein Mutants with Altered Effector Specificity Tang et al., 2008	AraC	FACS-based selection	*E. coli*	Positive selection after overnight induction followed by negative selection (no timing specified for negative selection)	Error-prone PCR	Liquid	[58]
Directed evolution of AraC for improved compatibility of arabinose- and lactose-inducible promoters Lee et al., 2007	AraC	FACS-based positive selection	*E. coli*	Only positive selection with FACS after 6 h of induction	Error-prone PCR	Liquid	[59]
Directed Evolution of the Quorum-Sensing Regulator EsaR for Increased Signal Sensitivity Shong et al., 2013	EsaR	Semi-automated screen using pin replicator and luminescence measurements	*E. coli*	24 h of incubation under non-inducing conditions, then negative selection, followed by overnight incubation under inducing conditions and positive selection for 24 h	Error-prone PCR	Solid	[60]
Dual selection of a genetic switch by a single selection marker Nomura and Yokobayashi, 2007	*lac* promoter	Proof of principle that a single selection marker (*tetA*) can be used for both positive and negative selection. *tetA* is essential for tetracycline resistance but renders cells more sensitive to $NiCl_2$	*E. coli*	20-24 h in $NiCl_2$, followed by a 1.5 h incubation period and 17-24 h of selection by tetracycline	N/A	Solid	[61]
An efficient platform for genetic selection and screening of gene switches in *Escherichia coli* Muranaka et al., 2009	Thiamine riboswitches	Positive and negative selection based on *tetA* expression	*E. coli*	8 h of induction, then 24 h of positive selection, followed by washout, 8 h of growth under non-inducing conditions and 24 h of negative selection	Randomized library	Liquid	[62]

Engineering Complex Riboswitch Regulation by Dual Genetic Selection Sharma et al., 2008	Theophylline and Thiamine riboswitches	Positive and negative selection based on *tetA* expression	*E. coli*	Two cycles of selection for each of the input combinations. Each selection step lasted 24 h	Rationally constructed library	Solid	[63]
Engineering of temperature- and light-switchable Cas9 variants Ritches et al., 2013	dCas9	FACS-based selection	*E. coli*	Positive selection followed by negative selection with induction time dependent on the temperature (4-19 h)	Rationally designed library	Liquid	[64]
Rapid and Liquid-Based Selection of Genetic Switches Using Nucleoside Kinase Fused with Aminoglycoside Phosphotransferase Tominaga et al., 2015	Lux promoter variants	Positive selection based on two different antibiotic resistance genes Negative selection based on *hsvTK* gene	*E. coli*	Negative selection overnight followed by a washout and 4-6 h of positive selection in the presence of the inducer	Site-directed mutagenesis	Liquid	[65]
Rapid Diversification of BetI-Based Transcriptional Switches for the Control of Biosynthetic Pathways and Genetic Circuits Saeki et al., 2016	Choline-inducible transcription factor BetI	Positive selection based on two different antibiotic resistance genes Negative selection based on *hsvTK* gene	*E. coli*	1 h of incubation, then 3 h of negative selection followed by 1 h of incubation and 3 h of positive selection. Depending on the desired outcome, the inducer was added during the incubation time, either before positive or negative selection	Error-prone PCR	Liquid	[66]
Evolutionary Design of Choline-Inducible and -Repressible T7-Based Induction Systems Ike et al., 2015	Choline-inducible transcription factor BetI	Screen for and against fluorescence under inducing and non-inducing conditions	*E. coli*	Selection of colonies that fluoresce under inducible conditions followed by a screen of liquid culture replicates separately under inducing and non-inducing conditions to exclude constitutive variants. Each incubation step was performed overnight.	Error-prone PCR	Solid	[67]
Directed evolution of protein switches and their application to the creation of ligand-binding proteins Guntas et al., 2005	Beta-lactamase	Selection of cells that survive under maltose and beta-lactamase antibiotic targets	*E. coli*	Cells selected for survival on plates containing maltose and ampicillin were further screened for maltose-dependence. Timing not specified.	Random domain insertion and random circular permutation	Solid	[68]
Directed evolution of the autoinducer selectivity of *Vibrio fischeri* LuxR	LuxR	Dual selection based on the *hsvTK* gene	*E. coli*	2 h of negative selection, followed by a washout, induction of 6 h and positive selection of 20 h	Site-directed mutagenesis	Liquid	[69]

Tashiro et al., 2016							
Directed evolution of a synthetic phylogeny of programmable Trp repressors Ellefson et al., 2018	TrpR	Dual selection based on compartmentalized partnered replication	*E. coli*	Variants obtained from the first CPR round of positive selection were cloned into another plasmid that allowed negative CPR selection. Before each CPR, cells were grown for 1 h, followed by 4 h of growth in inducing conditions	Randomized library	Liquid	[70]
Engineered systems of inducible anti-repressors for the next generation of biological programming Groseclose et al., 2020	Several classes of antirepressors	FACS-based selection	*E. coli*	Positive selection followed by negative selection. Timing not specified.	Error-prone PCR	Liquid	[36]

Supplementary Note 3: El222 optogenetic system

El222 is a transcription factor from marine bacterium *Erythrobacter litoralis*.[140] El222 has been adapted for use in eukaryotes by way of a tandem fusion of the prokaryotic El222 transcription factor, a nuclear localization signal, and the VP16 transcriptional activation domain. In darkness, the interaction of the helix-turn-helix (HTH) DNA binding domain with DNA is sterically hindered by the light-sensing LOV-domain[139]. Upon blue light illumination, a covalent bond is formed between the Cys-75 residue and the flavin chromophore[191]. (All references to mutant residue numbers in El222 are given with respect to bacterial El222 to match the numbering used in previous work[88,139,140].) This leads to a conformational change, which dislocates the Jα helix of the LOV domain. Subsequently, the protein forms a homodimer and binds to the DNA substrate using its exposed HTH domain. In the absence of blue light, the protein reverts to its ground state. For brevity, we refer to the promoter consisting of 5 El222 binding sites[192] upstream of a minimal eukaryotic promoter as *LIP*.

1735 # Supplementary Note 4: PhyB-Pif3 optogenetic system

1736 Phytochromes are photosensors in plants, bacteria, and fungi[193]. Phytochrome B and its interaction
1737 partner Pif3 are used by plants to adapt gene expression to environmental light conditions[194].

1738 The light-inducible PhyB-Pif3 interaction has been extensively used in organisms other than
1739 plants[106–109]. By fusing one protein to PhyB and another to Pif3, one can induce protein-protein
1740 interactions in a temporarily and spatially precise manner, for example, in order to sequester
1741 proteins to specific cellular compartments[107]. In the yeast two-hybrid version of the system, it is
1742 used for light-inducible transcriptional control in budding yeast.[108,195] Typically, PhyB and Pif3 are
1743 fused to the Gal4 DNA binding domain and the Gal4 transcriptional activation domain,
1744 respectively.[108] When bound to its chromophore and activated by red light (≈650 nm), PhyB binds
1745 Pif3, thereby, bringing the transcriptional activation and DNA binding domains close together, which
1746 leads to the expression of the *GAL* family of genes. In the presence of far-red light (≈ 740 nm) or
1747 prolonged darkness, PhyB changes conformation again and dissociates from Pif3.

1748 The photoreceptive core of the PhyB protein contains a linear tetrapyrrole chromophore.[196] In
1749 plants, this chromophore is phytochromobilin. However, phytochromobilin is not produced in many
1750 model organisms. Thus, to use PhyB-Pif3, one adds phycocyanobilin (PCB), which is the
1751 chromophore in algal phytochromes, to the incubation medium prior to optogenetic experiments.
1752 It has been shown that bacterial and fungal phytochromes can carry biliverdin, another tetrapyrrole
1753 molecule, as a chromophore.[196]

1754

1755 # Supplementary Note 5: Tetracycline-regulated gene expression
1756 systems

1757 Tetracycline-responsive systems, originally identified in bacteria as part of a feedback loop that
1758 mediates resistance to the antibiotic tetracycline, are widely used for controlling transcription. The
1759 system is made up of the tTA regulator, which binds the *tetO* DNA sequence. In its original form, tTA
1760 is part of the Tet-Off system that is inhibited by tetracycline or the closely related molecule
1761 doxycycline[197]. Mutations that reverse tTA activity with respect to the inducer have been used to
1762 construct rtTA.[115] To function as a transcriptional activator in eukaryotes, rtTA is typically fused to
1763 the VP16 transcriptional activation domain. To construct an inducible eukaryotic promoter, the
1764 binding sites for rtTA, *tetO*, are placed next to a minimal promoter. However, this system, called the
1765 Tet-On system, exhibits high basal activity in the absence of the inducer. To circumvent this, we
1766 fused the PEST degron to rtTA, which leads to increased degradation of rtTA.

1767

Supplementary Note 6: Summary of cell cycle biology relevant to optovolution

Wild-type cell cycle control

In this note, we briefly summarize the wild-type model of cell cycle control in budding yeast.[130] In the next section, we focus on how the cell cycle runs in the Dajbog strains.

At the biochemical level, the rhythm of the cell-cycle oscillator is predominantly generated by a negative feedback loop[126]. In this loop, cyclin-dependent kinase (CDK) and the anaphase-promoting complex/cyclosome (APC/C) alternate in activity and drive cell cycle progression.

In budding yeast, there is a single cyclin-dependent kinase, Cdk1 (also known as Cdc28). Processes that Cdk1 controls include the transcription of hundreds of cell cycle-periodic genes, DNA replication, spindle pole body duplication, and spindle formation. Activity and specificity of Cdk1 towards different substrates is mainly regulated through its interaction with regulatory proteins called cyclins. Different cyclins generally promote distinct cell-cycle events and are expressed at different stages of the cell cycle. In *S. cerevisiae*, cyclins are commonly classified into four groups: G1, G1/S, S, and M cyclins. Each cyclin-Cdk complex promotes the activation of the next group of cyclins.

The G1 cyclin Cln3 activates G1/S cyclins Cln1 and Cln2 and has a role in cell-cycle entry in response to growth. Cln1-3 are responsible for the initiation of formation of the daughter cell and expression of the 100s of genes of the Start regulon. At the onset of S phase, levels of S cyclins Clb5 and Clb6 rise. Their association with Cdk1 is primarily responsible for the initiation of DNA replication by triggering the activation of origins of replication. Approaching mitosis, the concentrations of the remaining B-type cyclins increase. In budding yeast, there are four such cyclins, Clb1, Clb2, Clb3, and Clb4. Their association with Cdk1 enables assembly of the mitotic spindle and attachment of chromosomes to the spindle.

In order to enable mitotic exit and reset the state of the cell for new cell cycles, cyclins have to be inactivated. While the activity G1/S cyclins is brought down by degradation and inhibition of the transcription factor SBF, S and M phase cyclins are not degraded until anaphase. At least two different mechanisms help repress Clb cyclin activity. The first one is through the activation of APC/C by the proteins Cdc20 and Cdh1. APC/C is a ubiquitin ligase complex that marks cyclins for degradation by the proteasome. The second mechanism is through the protein Sic1, which stoichiometrically inhibits Cdk1-Clb complexes, thereby effectively reducing their activity.

Rewired cell cycle control in the Dajbog strains

Although cyclins are specialized for certain phases of the cell cycle, the functions of some cyclins overlap. For example, when overexpressed, S phase cyclin Clb5 can initiate budding in a *cln1-3Δ*

1802 block[127]. Similarly, the M-phase cyclins Clb1[198]or Clb2[123]can assume the roles of all other Clb cyclins
1803 in a *clb1-6Δ* background. Endogenous *CLB3-6* genes also suffice for cell cycle start when the Clb-
1804 cyclin inhibitor *SIC1* is deleted, rendering *cln1-3Δ sic1Δ* cells viable[133].

1805 While G1/S cyclin and S cyclin expression initiates at about the same time under the control of
1806 transcription factors Sbf and Mbf[130], respectively, S cyclins are inactive until G1/S cyclins have
1807 sufficiently degraded Sic1 and Cdh1. Thus, in wild-type cells, although *CLN2* and *CLB5* are
1808 simultaneously transcriptionally activated, there is a delay between G1/S-Cdk and S-Cdk
1809 activity[130,199]. We expect this delay to persist in Dajbog1 cells. Deleting *SIC1* in Dajbog2 cells is
1810 expected to cause an increase in chromosomal rearrangements due to premature S-Cdk activity[200]
1811 but this did not noticeably interfere with our directed evolution experiments.

1812 Clb5-Cdk1 leads to the firing of origins of replication in S phase. Overexpression of destruction box
1813 deficient Clb5db in galactose medium arrests the cell cycle by inhibiting the formation of pre-
1814 replicative origins, a process known as origin of replication relicensing[201–203]. This represents the
1815 expected mechanism for the lethality of *CLB5* overexpression in glucose medium. This observation
1816 led us to further sensitize Dajbog1 cells to continuous Clb5 activity by deleting *SIC1*, resulting in
1817 Dajbog2 strains.

1818

Supplementary Figures

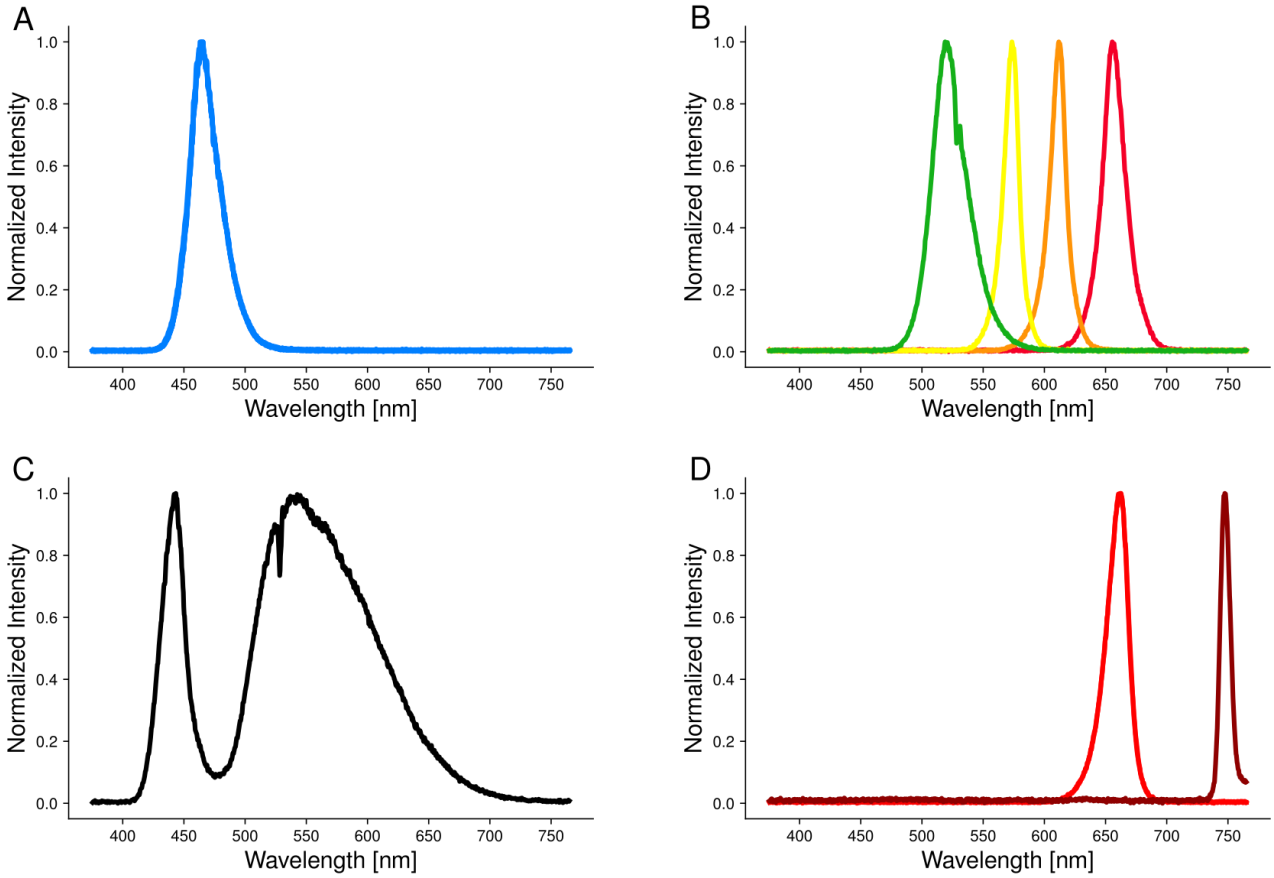

Supplementary Figure 1. Emission spectra of light sources used. A. Blue LED panel used for evolving and inducing El222 and its variants (light intensity 8.3 mW/cm^2). B. LEDs used to evolve *in vivo* green responsive El222 variants from left to right: 24 mW/cm^2, 0.12 mW/cm^2, 2.6 mW/cm^2, 0.46 mW/cm^2. C. Diascopic LED light used for inducing El222 and its variants for microscopy. The intensity of the light is 8.4 mW/cm^2 when set to 20% of the maximal power and 97 mW/cm^2 when set to 80% of maximal power. D. Red and far-red LEDs used for switching the PhyB-Pif3 system. Light intensity of the red LEDs is 36 mW/cm^2, and the light intensity of the far-red LEDs is 26 mW/cm^2. The reported intensities in panels A, B, and D are total intensities and are for the location of the agar plates.

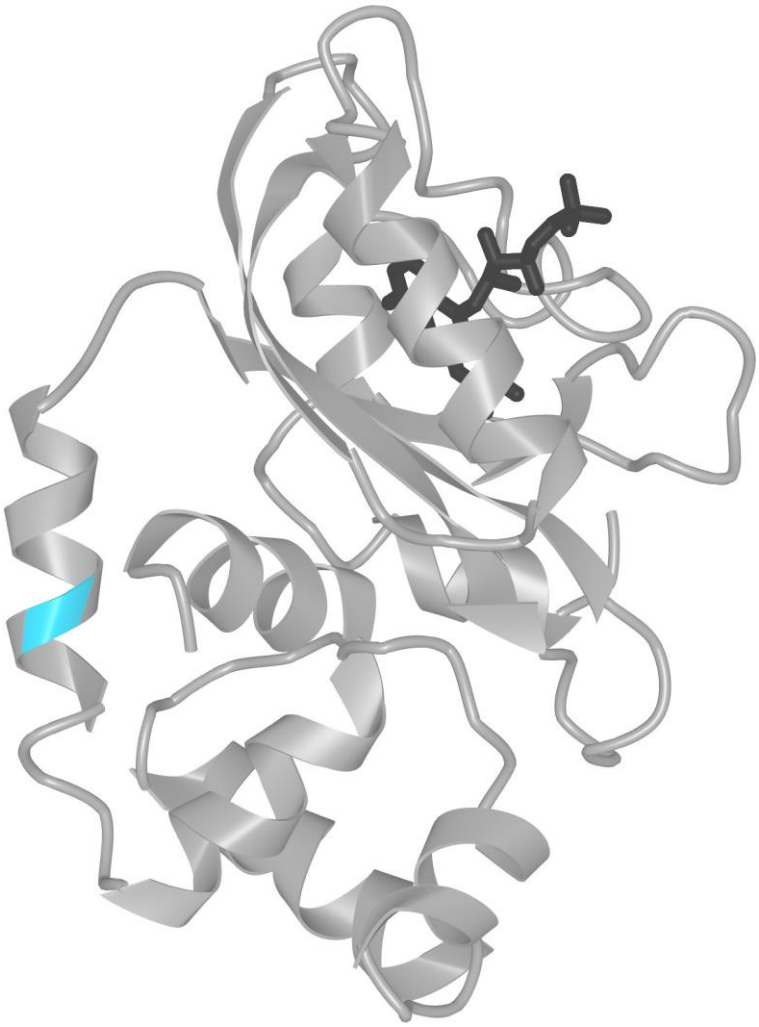

Supplementary Figure 2. Location of A157 residue marked in teal in the dark state EI222 structure (PDB: 3P7N). The chromophore is in black.

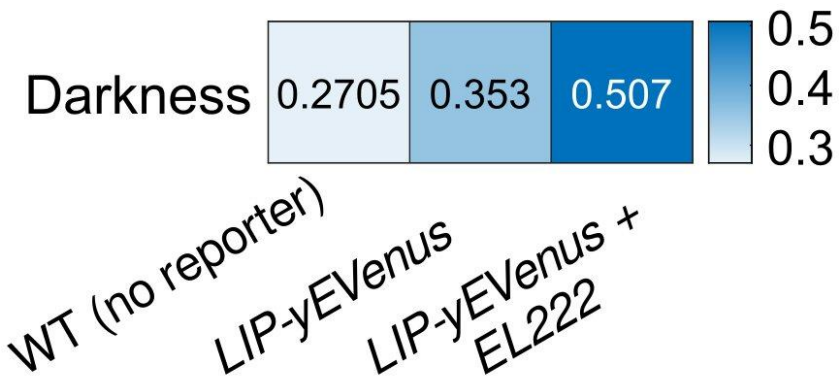

1835

1836 Supplementary Figure 3. Baseline leakiness of the reporter sets the minimum leakiness attainable in optovolution.
1837 Comparison of fluorescence in no-reporter (WT), reporter-only (*LIP-yEVenus*), and reporter plus El222 strains (*LIP-*
1838 *yEVenus + EL222*) in darkness. Cells that contain a transcriptional reporter for El222 (*LIP-yEVenus*) but not the
1839 transcription factor (e.g., *PGK1pr-EL222*) showed elevated fluorescence compared to wild-type budding yeast cells. This
1840 suggests that other transcription factors might weakly drive the transcription from *LIP* and set the lower bound for
1841 leakiness of *LIP*. The leakiness reported for all El222 variants is the difference between the reporter-only and the
1842 reporter plus variant strains. Numbers of analyzed cells are given in the Supplementary Table 12.

1843

1844

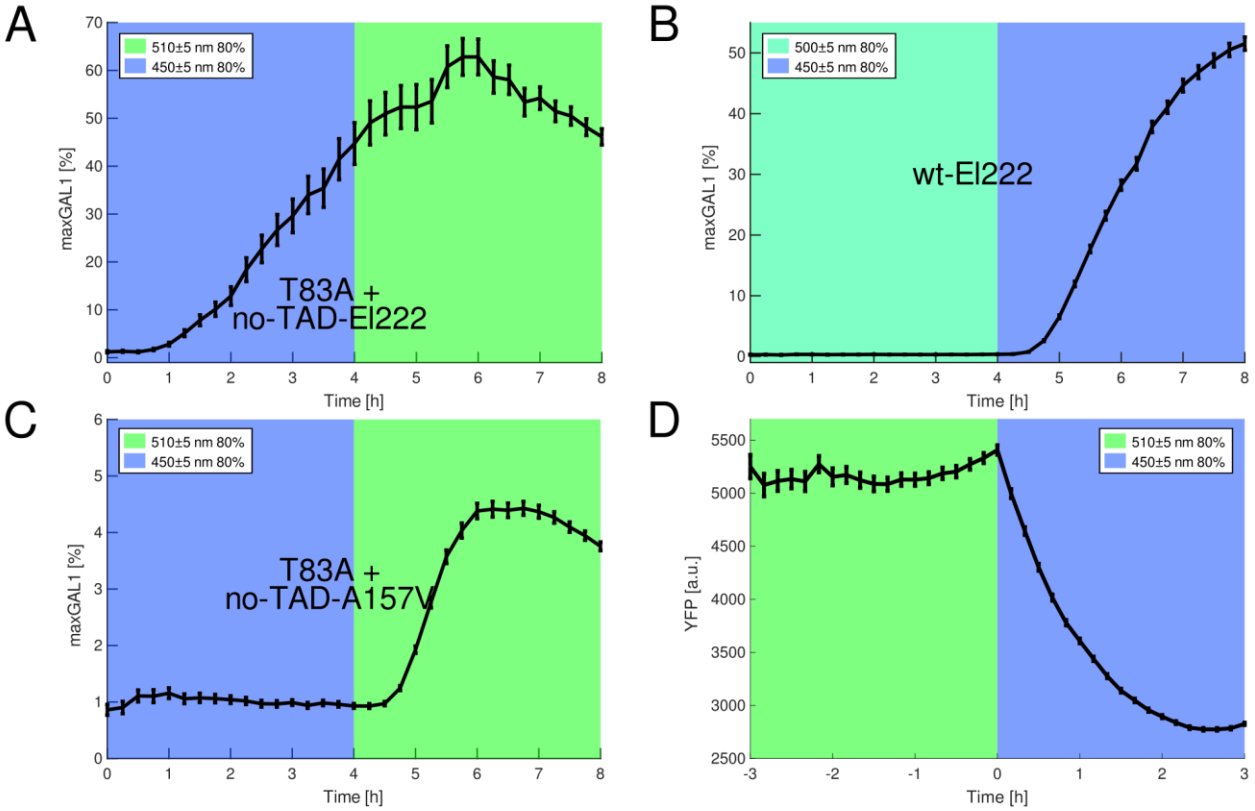

Supplementary Figure 4. Related to Figure 6. A. no-TAD-El222 does not suffice to suppress El222(T83A). In the same reporter cells, *GAL1*-promoter-driven no-TAD-El222 is expressed in raffinose plus galactose medium but does not clearly inhibit the activity of *PGK1* promoter-driven El222(T83A) in blue 450±5 nm light. B. Wild-type El222 remains inducible in raffinose plus galactose medium in 450±5 nm light only. C. T83A response in the presence of no-TAD-A157V in 510±5 nm and 450±5 nm light. The combination of T83A and no-TAD-A157V produces a smaller response in 510±5 nm light than in 500±5 nm (Fig. 6 R). D. psd does not activate in 510±5 nm light but does activate in 450±5 nm. All error bars indicate the standard error of the mean (SEM).

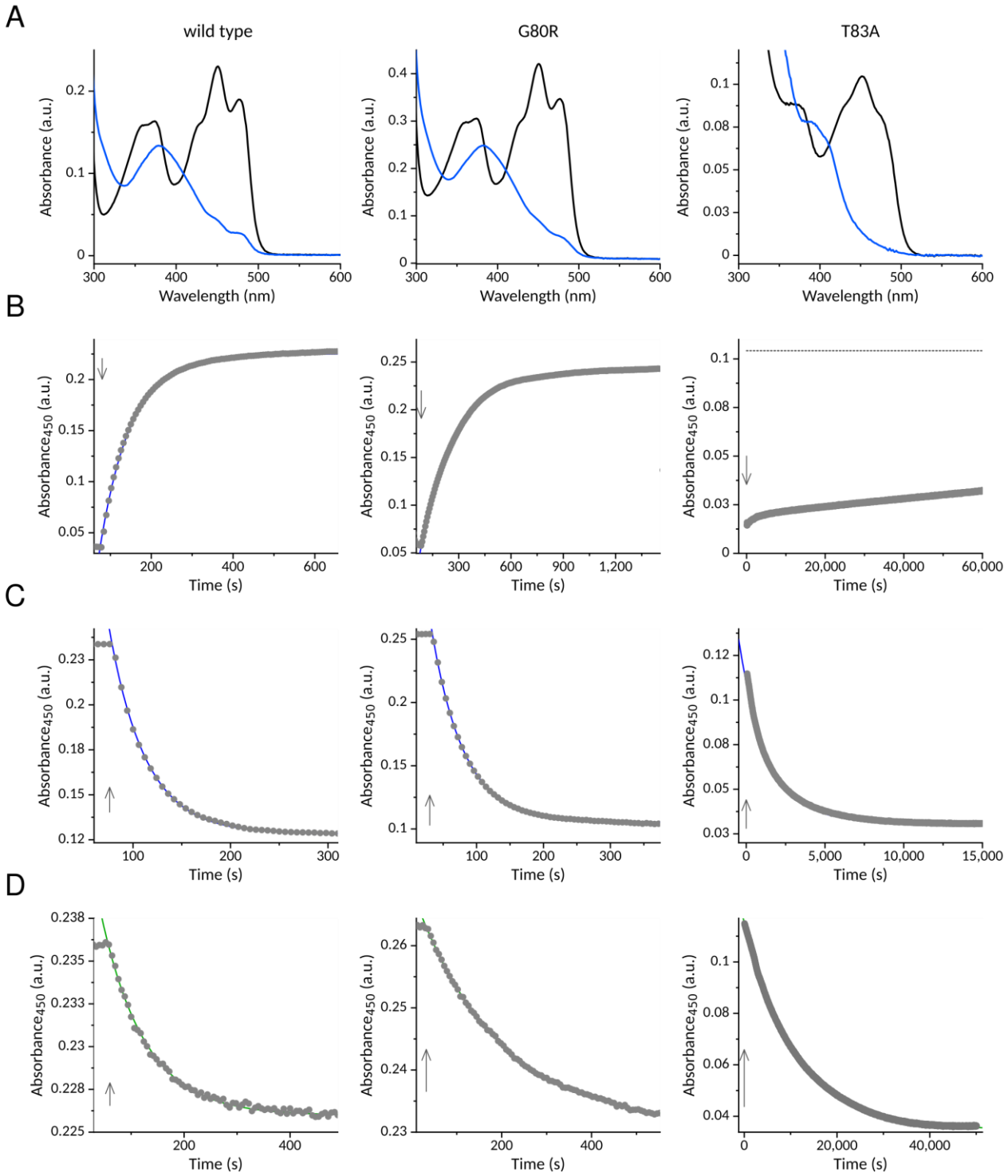

Supplementary Figure 5. Absorption-spectroscopic characterization of wild-type El222 and the G80R and T83A variants. A. UV/vis absorption spectra of El222 receptors in their dark-adapted states (black lines) and upon exposure to blue light (450 nm, 36 mW cm^{-2}) (blue lines). B. The El222 receptors were exposed to saturating 450-nm light to populate the light-adapted state. Upon cessation of illumination (marked by arrow), the thermal recovery to the dark-adapted state was monitored by tracking the absorbance at 450 nm. C. The El222 receptors were irradiated through an interference filter at (450 ± 5) nm at a power of 0.75 mW cm^{-2} while monitoring the photoconversion to the light-adapted state by the absorbance at 450 nm. D. As in panel C but the samples were irradiated through an interference filter at (510 ± 5) nm at a power of 1.5 mW cm^{-2}.

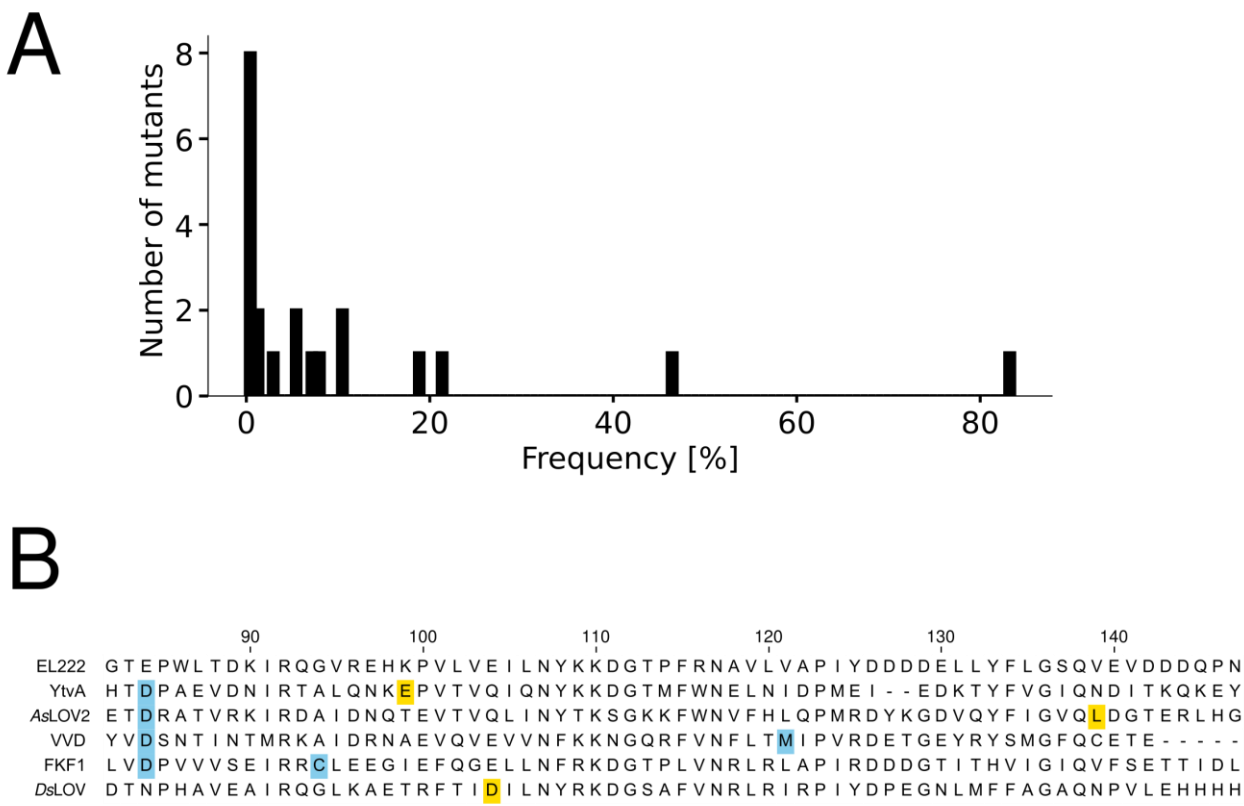

Supplementary Figure 6. Analysis of El222 mutations found by optovolution in existing LOV domains. A. Histogram of the frequency with which the mutations from our three campaigns are found in putative LOV domains identified in ref.[143]. B. Searching for the mutations from our three campaigns in LOV domains with characterized dark-reversion kinetics[89] (FKF1 from *Arabidopsis thaliana*, VVD from *Neurospora crassa*, YtvA from *Bacillus subtilis*, *Ds*LOV from *Dinoroseobacter shibae*, and the LOV2 domain of phot1 from *Avena sativa*) identifies the light-sensitizing (blue squares) and low-leakiness mutations (yellow squares) but not the *in vivo* green-responsive mutations.

1873 # Supplementary Tables

1874 Supplementary Table 1. Plasmids used in the study

Plasmid name	Insert	Type of plasmid	Yeast selection marker	Bacterial selection marker	Source of the plasmid
EZL105	*PGK1pr-EL222*	For integration in a single copy	*CgHIS3*	*AmpR*	Ref. [95]
pVG117	*PGK1pr-EL222 (Asp18Tyr, Val139Leu)*	For integration in a single copy	*CgHIS3*	*AmpR*	This study
pVG118	*PGK1pr-EL222 (Asp18Tyr)*	For integration in a single copy	*CgHIS3*	*AmpR*	This study
pVG119	*PGK1pr-EL222 (Val139Leu)*	For integration in a single copy	*CgHIS3*	*AmpR*	This study
pVG135	*PGK1pr-EL222 (Lys99Glu)*	For integration in a single copy	*CgHIS3*	*AmpR*	This study
pVG136	*PGK1pr-EL222 (Pro165Ser)*	For integration in a single copy	*CgHIS3*	*AmpR*	This study
pVG137	*PGK1pr-EL222 (Val201Leu)*	For integration in a single copy	*CgHIS3*	*AmpR*	This study
pML81	*PGK1pr-EL222 (Glu104Asp)*	For integration in a single copy	*CgHIS3*	*AmpR*	This study
pML82	*PGK1pr-EL222 (Ile124Phe)*	For integration in a single copy	*CgHIS3*	*AmpR*	This study
pVG120	*PGK1pr-EL222 (Asp89Tyr)*	For integration in a single copy	*CgHIS3*	*AmpR*	This study
pVG147	*PGK1pr-EL222 (Gly94Cys)*	For integration in a single copy	*CgHIS3*	*AmpR*	This study
pVG122	*PGK1pr-strongLOV*	For integration in a single copy	*CgHIS3*	*AmpR*	Ref. [88]
pVG143	*PGK1pr-EL222 (Leu87Ile)*	For integration in a single copy	*CgHIS3*	*AmpR*	This study
pVG123	*PGK1pr-EL222 (Ala157Val)*	For integration in a single copy	*CgHIS3*	*AmpR*	This study
pVG286	*PGK1pr-EL222 (Gly80Glu)*	For integration in a single copy	*CgHIS3*	*AmpR*	This study

pVG121	*PGK1pr-EL222 (Gly82Val)*	For integration in a single copy	*CgHIS3*	*AmpR*	This study
pVG124	*PGK1pr-EL222 (Thr83Ser)*	For integration in a single copy	*CgHIS3*	*AmpR*	This study
pVG310	*PGK1pr-AQTrip* (yeast codon-optimized)	For integration in a single copy	*CgHIS3*	*AmpR*	This study
pVG150	*PGK1pr-EL222 (Ser137Asn)*	For integration in a single copy	*CgHIS3*	*AmpR*	This study
pVG144	*PGK1pr-EL222 (Val121Met)*	For integration in a single copy	*CgHIS3*	*AmpR*	This study
pVG298	*PGK1pr-EL222 (Thr83Ala)*	For integration in a single copy	*CgHIS3*	*AmpR*	This study
pVG173	*PGK1pr-EL222 (Gly83Arg)*	For integration in a single copy	*CgHIS3*	*AmpR*	This study
pVG443	*GAL1pr-NLS-LOV-HTH*	2 u	*LEU2*	*AmpR*	This study
pVG444	*GAL1pr-NLS-LOV-HTH (A157V)*	2 u	*LEU2*	*AmpR*	This study
pVG101	*PGK1pr-EL222, LIP-CLN2, LIP-CLB5*	For integration	*NatMX*	*AmpR*	This study
pVG104	*ADH1pr-PHYB, ADH1pr-PIF3, GAL1-CLB5*	For integration	*NatMX*	*AmpR*	This study
pVG329	*YOR1 3'UTR and YOR1 5'UTR*	For ORF replacement	*HphMX*	*AmpR*	This study
pVG369	*HMX1 3' UTR and HMX1 5'UTR*	For ORF deletion by pop-in/op-out	*URA3, LEU2*	*AmpR*	This study
pVG371	*BPT1 3' UTR and BPT1 5'UTR*	For ORF deletion by pop-in/op-out	*URA3, LEU2*	*AmpR*	This study
pVG372	*HEM14 3' UTR and HEM14 5'UTR*	For ORF deletion by pop-in/op-out	*URA3, LEU2*	*AmpR*	This study

pVG373	*YMR315W 3' UTR and YMR315W 5'UTR*	For ORF deletion by pop-in/op-out	*URA3, LEU2*	*AmpR*	This study
pVG84	*GAL1pr-CLN2*	For integration	*PatMX*	*AmpR*	This study
pVG49	*GAL1pr-yEVenus-PEST*	For integration in a single copy	*URA3*	*AmpR*	Ref. [88]
pVG9	*LIP-yEVenus-PEST*	For integration in a single copy	*URA3*	*AmpR*	Ref. [88]
pVG175	*LIP-ymScarletI*	For integration in a single copy	*URA3*	*AmpR*	This study
pVG176	*LIP-ymScarletI-PEST*	For integration in a single copy	*URA3*	*AmpR*	This study
pVG295	*PGK1pr-EL222, LIP-PEST-rtTA, tetOpr-CLN2*	For integration	*NatMX*	*AmpR*	This study
pRD-TW1 (pRD13)	*MET3pr-CLN2, CLB5pr-CLB5*	*CEN/ARS*	*URA3*	*AmpR*	This study
pRD70	*tetOpr-CLB5*	For integration	*PatMX*	*AmpR*	This study
pVG336	*PGK1pr-PEST-rtTA*	For integration in a single copy	*HIS3*	*AmpR*	This study
pVG337	*PGK1pr-PEST-rtTA (Phe67Cys)*	For integration in a single copy	*HIS3*	*AmpR*	This study
pVG338	*PGK1pr-PEST-rtTA (Arg253His)*	For integration in a single copy	*HIS3*	*AmpR*	This study
pVG188	*PGK1pr-EL222, LIP-CLN2*	For integration in a single copy	*NatMX*	*AmpR*	This study
pVG189	*PGK1pr-EL222, LIP-CLB5*	For integration in a single copy	*NatMX*	*AmpR*	This study
pVG70	*PGK1pr-EL222, LIP-CDC20*	For integration	*NatMX*	*AmpR*	This study
pVG15k	*PGK1pr-EL222, LIP-CLB2kd*	For integration	*NatMX*	*AmpR*	This study
pVG47	*tetOpr-yEVenus-PEST*	For integration in a single copy	*URA3*	*AmpR*	Ref. [88]
pVG349	*PGK1pr-yEVenus-psd*	For integration in a single copy	*URA3*	*AmpR*	This study

pVG177	*His$_{10}$-EL222*	For bacterial expression	*None*	*KanR*	This study
pVG332	*His$_{10}$-EL222 (Gly80Arg)*	For bacterial expression	*None*	*KanR*	This study
pVG335	*His$_{10}$-EL222 (Thr83Ala)*	For bacterial expression	*None*	*KanR*	This study

1875

1876

1877 Supplementary Table 2. Strains used in the study

Strain name	Genotype	Source
yVG602	*cln1,3Δ cln2Δ::MET3pr-CLN2 clb1Δ clb2Δ::GALL-CLB2::URA3 HTB2::HTB2-mCherry::HIS3 PGK1pr::PGK1pr-EL222, LIP-CLB2::NatMX*	This study
yVG173	*clb1Δ clb2Δ::GALL-CLB2::URA3 clb3Δ::TRP1 clb4Δ::his3::kanMX clb5Δ::kanMX clb6Δ::kanMX swe1Δ::TRP1 PGK1pr::PGK1pr-EL222, LIP-CLB2kd::NatMX ADE2*	This study
yVG604	*cdh1Δ::LEU2 cdc20Δ::MET3pr-CDC20::TRP1 CLN2pr-GFP-CLN2pest::HIS3 PGK1pr::PGK1pr-EL222, LIP-CDC20::NatMX*	This study
yVG152	*cln1Δ cln2Δ::CLN2pr-Venus::TRP1 cln3Δ::LEU2 trp1Δ::MET3-CLN2::TRP1 clb3Δ::TRP1 clb4Δ::his3::KanMX clb6Δ::KanMX HTB2::HTB2-mCherry::HIS5 PGK1pr::PGK1pr-EL222, LIP-CLB5::NatMX*	This study
yVG2371	*cln1Δ cln2Δ cln3Δ::LEU2 trp1Δ::MET3pr::CLN2 ycr051wΔ::PGL1pr-EL222, LIP-CLN2::NatMX*	This study
yVG2374	*cln1Δ cln2Δ cln3Δ::LEU2 trp1Δ::MET3pr::CLN2 ycr051wΔ::PGL1pr-EL222, LIP-CLB5::NatMX*	This study
yVG2390	*cln1Δ cln2Δ cln3Δ::LEU2 clb3Δ::TRP1 clb4Δ::his3::KanMX clb5Δ::HIS3 clb6Δ::KanMX HTB2::HTB2-mCherry::HIS5 POL3::POL3 (Leu523Asp)::hphMX EFB1pr::PGK1pr-EL222, LIP-CLB5::NatMX* *pRD-TW1 (CEN/ARS)*	This study
yVG1247	*cln1Δ cln2Δ cln3Δ::LEU2 clb3Δ::TRP1 clb4Δ::his3::KanMX clb5Δ::HIS3 clb6Δ::KanMX HTB2::HTB2-mCherry::HIS5 POL3::POL3 (Leu523Asp)::hphMX EFB1pr::PGK1pr-EL222, LIP-CLN2, LIP-CLB5::NatMX* (single copy)	This study
yVG1358	*cln1Δ cln2Δ cln3Δ::LEU2 clb3Δ::TRP1 clb4Δ::his3Δ::KanMX clb5Δ::HIS3 clb6Δ::KanMX HTB2::HTB2-mCherry::HIS5 POL3::POL3 (Leu523Asp)::hphMX sic1Δ::URA3 EFB1pr::PGK1pr-EL222, LIP-CLN2, LIP-CLB5::NatMX* (single copy)	This study

yVG1623	*ura3Δ::LIP-yEVenus::KanMX* (single copy)	Ref. [88]
yVG2850	*his3Δ::PGK1pr-EL222::HIS3* (single copy) *ycr051wΔ::LIP-ymScarletI::URA3* (single copy)	This study
yVG2852	*his3Δ::PGK1pr-EL222::HIS3* (single copy) *ycr051wΔ::LIP-ymScarletI-PEST::URA3* (single copy)	This study
yVG1637	*his3Δ::PGK1pr-EL222::HIS3* (single copy) *ura3Δ::LIP-yEVenus::KanMX* (single copy)	Ref. [88]
yVG2854	*his3Δ::PGK1pr-EL222 (Asp18Tyr, Val139Leu)::HIS3* (single copy) *ura3Δ::LIP-yEVenus::KanMX* (single copy)	This study
yVG2856	*his3Δ::PGK1pr-EL222 (Asp18Tyr)::HIS3* (single copy) *ura3Δ::LIP-yEVenus::KanMX* (single copy)	This study
yVG2858	*his3Δ::PGK1pr-EL222 (Val139Leu)::HIS3* (single copy) *ura3Δ::LIP-yEVenus::KanMX* (single copy)	This study
yVG2860	*his3Δ::PGK1pr-EL222 (Lys99Glu)::HIS3* (single copy) *ura3Δ::LIP-yEVenus::KanMX* (single copy)	This study
yVG2862	*his3Δ::PGK1pr-EL222 (Pro165Ser)::HIS3* (single copy) *ura3Δ::LIP-yEVenus::KanMX* (single copy)	This study
yVG2864	*his3Δ::PGK1pr-EL222 (Val201Leu)::HIS3* (single copy) *ura3Δ::LIP-yEVenus::KanMX* (single copy)	This study
yML196	*his3Δ::PGK1pr-EL222 (Glu104Asp)::HIS3 (single copy)* *ura3Δ::LIP-yEVenus-PEST::URA3 (single copy)*	This study
yML197	*his3Δ::PGK1pr-EL222 (Ile124Phe)::HIS3 (single copy)* *ura3Δ::LIP-yEVenus-PEST::URA3 (single copy)*	This study
yVG2701	*his3Δ::PGK1pr-EL222 (Asp89Tyr)::HIS3* (single copy) *ycr051wΔ::LIP-ymScarletI::URA3* (single copy)	This study
yVG2750	*his3Δ::PGK1pr-EL222 (Gly94Cys)::HIS3* (single copy) *ycr051wΔ::LIP-ymScarletI::URA3* (single copy)	This study

yVG2704	*his3Δ::PGK1pr-strongLOV::HIS3* (single copy) *ycr051wΔ::LIP-ymScarletI::URA3* (single copy)	This study
yVG2726	*his3Δ::PGK1pr-EL222 (Leu87Ile)::HIS3* (single copy) *ycr051wΔ::LIP-ymScarletI::URA3* (single copy)	This study
yVG1645	*his3Δ::PGK1pr-EL222 (Ala157Val)::HIS3* (single copy) *ura3Δ::LIP-yEVenus::KanMX* (single copy)	This study
yVG2759	*his3Δ::PGK1pr-EL222 (Gly80Glu)::HIS3* (single copy) *ycr051wΔ::LIP-ymScarletI::URA3* (single copy)	This study
yVG2703	*his3Δ::PGK1pr-EL222 (Gly82Val)::HIS3* (single copy) *ycr051wΔ::LIP-ymScarletI::URA3* (single copy)	This study
yVG2706	*his3Δ::PGK1pr-EL222 (Thr83Ser)::HIS3* (single copy) *ycr051wΔ::LIP-ymScarletI::URA3* (single copy)	This study
yVG2761	*his3Δ::PGK1pr-AQTrip (yeast codon optimized)::HIS3* (single copy) *ycr051wΔ::LIP-ymScarletI::URA3* (single copy)	This study
yVG2752	*his3Δ::PGK1pr-EL222 (Ser137Asn)::HIS3* (single copy) *ycr051wΔ::LIP-ymScarletI::URA3* (single copy)	This study
yVG2727	*his3Δ::PGK1pr-EL222 (Val121Met)::HIS3* (single copy) *ycr051wΔ::LIP-ymScarletI::URA3* (single copy)	This study
yVG2699	*his3Δ::PGK1pr-EL222 (Thr83Ala)::HIS3* (single copy) *ycr051wΔ::LIP-ymScarletI::URA3* (single copy)	This study
yVG2745	*his3Δ::PGK1pr-EL222 (Gly80Arg)::HIS3* (single copy) *ycr051wΔ::LIP-ymScarletI::URA3* (single copy)	This study
yVG2796	*his3Δ::PGK1pr-EL222 (Thr83Ala)::HIS3* (single copy) *ycr051wΔ::LIP-ymScarletI-PEST::URA3* (single copy)	This study

yVG2818	*his3Δ::PGK1pr-EL222 (Gly80Arg)::HIS3* (single copy) *ycr051wΔ::LIP-ymScarletI-PEST::URA3* (single copy)	This study
yLS2000	*his3Δ::PGK1pr-EL222 (Thr83Ala)::HIS3* (single copy) *ycr051wΔ::LIP-ymScarletI::URA3* (single copy) *GAL1pr-NLS-LOV-HTH::LEU2 (CEN/ARS)*	This study
yLS2001	*his3Δ::PGK1pr-EL222 (Thr83Ala)::HIS3* (single copy) *ycr051wΔ::LIP-ymScarletI::URA3* (single copy) *GAL1pr-NLS-LOV(A157V)-HTH::LEU2 (CEN/ARS)*	This study
yML153	*ycr051wΔ::LIP-yEVenus-psd::URA3* (single copy)	This study
yVG1031	*ura3Δ::GAL1pr-yEVenus::KanMX*	Ref. [88]
yVG301	*ura3Δ::GAL1pr-yEVenus-PEST::URA3*	Ref. [88]
yVG151	*PHYB-mCherry-Tom7::LEU2; Bem1-mCitrine-PIF::HIS3*	Ref. [144]
yVG2849	*PHYB-mCherry-Tom7::LEU2; Bem1-mCitrine-PIF::HIS3 yor1::hphMX*	This study
yVG2847	*leu2Δ::ADH1pr-GADPIF3::LEU2, trp1::ADH1pr-PHYB-GDBD::TRP1, his3Δ::GAL1pr-YFP::HIS3, ade2::ADE2*	Ref. [110]
yVG2848	*leu2Δ::ADH1pr-GADPIF3::LEU2, trp1::ADH1pr-PHYB-GDBD::TRP1, his3Δ::GAL1pr-YFP::HIS3, ade2::ADE2 yor1::hphMX*	This study
yML200	*leu2Δ::ADH1pr-GADPIF3::LEU2, trp1::ADH1pr-PHYB-GDBD::TRP1, his3Δ::GAL1pr-YFP::HIS3, ade2::ADE2, bpt1Δ*	This study
yML201	*leu2Δ::ADH1pr-GADPIF3::LEU2, trp1::ADH1pr-PHYB-GDBD::TRP1, his3Δ::GAL1pr-YFP::HIS3, ade2::ADE2, hem14Δ*	This study
yML202	*leu2Δ::ADH1pr-GADPIF3::LEU2, trp1::ADH1pr-PHYB-GDBD::TRP1, his3Δ::GAL1pr-YFP::HIS3, ade2::ADE2, hmx1Δ*	This study
yML203	*leu2Δ::ADH1pr-GADPIF3::LEU2, trp1::ADH1pr-PHYB-GDBD::TRP1, his3Δ::GAL1pr-YFP::HIS3, ade2::ADE2, ymr315wΔ*	This study
yML204	*leu2Δ::ADH1pr-GADPIF3::LEU2, trp1::ADH1pr-PHYB-GDBD::TRP1, his3Δ::GAL1pr-YFP::HIS3, ade2::ADE2, yor1Δ::hphMX bpt1Δ*	This study

yML205	*leu2Δ::ADH1pr-GADPIF3::LEU2, trp1::ADH1pr-PHYB-GDBD::TRP1, his3Δ::GAL1pr-YFP::HIS3, ade2::ADE2, yor1Δ::hphMX hem14Δ*	This study
yML206	*leu2Δ::ADH1pr-GADPIF3::LEU2, trp1::ADH1pr-PHYB-GDBD::TRP1, his3Δ::GAL1pr-YFP::HIS3, ade2::ADE2, yor1Δ::hphMX hmx1Δ*	This study
yML208	*leu2Δ::ADH1pr-GADPIF3::LEU2, trp1::ADH1pr-PHYB-GDBD::TRP1, his3Δ::GAL1pr-YFP::HIS3, ade2::ADE2, yor1Δ::hphMX ymr315wΔ*	This study
yVG2691	*cln1Δ cln2Δ cln3Δ::LEU2 clb3::TRP1 clb4Δ::his3Δ::KanMX clb5Δ::HIS3 clb6Δ::KanMX HTB2::HTB2-mCherry::HIS5 ycr051wΔ::PGK1pr-EL222, LIP-PEST-rtTA, tetOpr-CLN2::NatMX BUD23::tetOpr-CLB5::PatMX*	This study
yVG2866	*his3Δ::PGK1pr-PEST-rtTA::HIS3* (single copy) *ura3Δ::tetOpr-yEVenus-PEST::URA3* (single copy)	This study
yVG2867	*his3Δ::PGK1pr-PEST-rtTA (Phe67Cys)::HIS3* (single copy) *ura3Δ::tetOpr-yEVenus-PEST::URA3* (single copy)	This study
yVG2868	*his3Δ::PGK1pr-PEST-rtTA (Arg253Hys)::HIS3* (single copy) *ura3Δ::tetOpr-yEVenus-PEST::URA3* (single copy)	This study
SK418	*his3Δ1, leu2Δ0, met15Δ0, ura3Δ0, TRP1::TEFp-NLS-iRFP-NLS::NatMX BY4741 background*	Ref. [204]
yML164	*his3Δ1, leu2Δ0, met15Δ0, ura3Δ0, TRP1::TEFp-NLS-iRFP-NLS::NatMX, yor1Δ*	This study

1880 Supplementary Table 3. Number of cells analyzed in Fig. 2 B

Experiment	Number of scored cells
LIP-CLB5 cln1-3Δ 20 min pulse	53
LIP-CLB5 cln1-3Δ 40 min pulse	30
LIP-CLN2 cln1-3Δ 20 min pulse	27
LIP-CLN2 cln1-3Δ 40 min pulse	20
LIP-CLB5 cln1-3Δ clb3-6Δ pRD-TW1 20 min	129
LIP-CLB5 LIP-CLN2 cln1-3Δ clb3-6Δ pRD-TW1 40 min	42

1881

1882

1883 Supplementary Table 4. Distribution of mutation types across campaigns 1-3 for *EL222* compared to
1884 the WT budding yeast mutation spectrum from ref.[205]

Mutation	Count	Percentage	WT budding yeast mutation spectrum[205]
T>C	2	10%	14%
T>A	3	14%	6%
T>G	2	10%	11%
C>A	7	33%	18%
C>G	0	0%	15%
C>T	7	33%	35%
Total transitions	9	43%	49%
Total transversions	12	57%	51%

1885

1886

1887 Supplementary Table 5. Number of cells analyzed in Fig. 5 B

	wt-EL222	G94C	V121M	A157V	S137N	G80E	D89Y	AQTrip	T83S	E84K	strongLOV	G82V	L87I
Darkness	246	234	424	144	206	341	341	275	126	227	478	239	248
Low blue LED	329	48	344	155	76	117	151	58	107	81	84	93	93
High blue LED	374	60	320	283	67	58	88	83	95	274	100	43	57

1888

1889

1890 Supplementary Table 6. Number of cells analyzed in Fig. 5 C, G, H and Fig. 6 B-G, J-M, R-T

	Strain	Number of cells at 3.5 h	Fig.
Sensitized and low-leakiness variants			
Sensitized			
	wt-El222	248	5C
	T83S	105	5C
	G82V	77	5C
	L87I	119	5C
	G80R	79	5C
	A157V	92	5C
Low leakiness 20% light			
	wt-El222	248	5G
	E104D	247	5G
	K99E	138	5G
	V201L	36	5G
Low leakiness 80% light			
	wt-El222	93	5H
	E104D	186	5H
	K99E	68	5H
	V201L	31	5H
Green-responsiveness variants			
Different wavelengths			
	T83A darkness	150	6B
	T83A 450 nm	146	6B
	T83A 500 nm	204	6B
	T83A 510 nm	130	6B, E
	T83A 520 nm	110	6B
	T83A 530 nm	50	6B
	G80R darkness	141	6C
	G80R 450 nm	207	6C
	G80R 500 nm	157	6C
	G80R 510 nm	248	6C, F
	G80R 520 nm	154	6C
	G80R 530 nm	137	6C
	WT EL222 darkness	284	6D
	WT EL222 450 nm	218	6D, G
	WT EL222 500 nm	93	6D
	WT EL222 510 nm	74	6D
Blue-to-green comparison			
	T83A 450 nm 5%	159	6J
	T83A 450 nm 10%	218	6J
	T83A 450 nm 20%	554	6J
	T83A 510 nm 80%	111	6J
	G80R 450 nm 5%	159	6K
	G80R 450 nm 10%	274	6K
	G80R 450 nm 20%	359	6K
	G80R 510 nm 80%	24	6K
	WT EL222 450 nm 5%	204	6L
	WT EL222 450 nm 10%	127	6L
	WT EL222 450 nm 20%	292	6L
	WT EL222 510 nm 80%	132	6L
	A157V 450 nm 5%	229	6M
	A157V 450 nm 10%	184	6M
	A157V 450 nm 20%	166	6M
	A157V 510 nm 80%	376	6M
Multiplexing			
	El222(T83A) + no-TAD-El222(A157V)	179	6R
	A157V	171	6S

1891

1892 Supplementary Table 7. Number of cells analyzed in Fig. 5 F

	V201L	D31Y, V139L	K99E	P165S	D31Y	I124F	V139L	E104D	wt-El222
Darkness	112	479	188	238	208	439	362	398	246
Low blue LED	325	203	330	81	419	486	209	603	329
High blue LED	209	382	321	98	466	736	441	731	374

1893

1894

1895 Supplementary Table 8. Number of cells analyzed in Fig. 7 C

	WT	+PCB	+BV	*yor1Δ*	*yor1Δ hem14Δ*	*hem14Δ*	*yor1Δ hmx1Δ*	*hmx1Δ*	*yor1Δ bpt1Δ*	*bpt1Δ*	*yor1Δ ymr315wΔ*	*ymr315wΔ*
Darkness	579	438	507	392	429	246	421	174	317	210	407	70
Red LEDs	797	488	589	461	436	249	381	352	295	317	338	261

1896

1897

1898

1899 Supplementary Table 9. Number of cells analyzed in Fig. 7 F, G

Strain	PCB	Number of cells
wt-YOR1	-	210
wt-YOR1	+	164
yor1Δ	-	238
yor1Δ	+	292

1900

1901

1902 Supplementary Table 10. Number of cells analyzed in Fig. 7 H

Strain	BV concentration [µM]	Number of cells
wt-YOR1	0	679
wt-YOR1	25	322
wt-YOR1	50	731
wt-YOR1	75	806
wt-YOR1	100	480
wt-YOR1	125	822
wt-YOR1	150	123
yor1Δ	0	573
yor1Δ	25	446
yor1Δ	50	252
yor1Δ	75	274
yor1Δ	100	256
yor1Δ	125	236
yor1Δ	125	218

1903

1904

1905 Supplementary Table 11. Number of cells analyzed in Fig. 8 D

	WT	F67C	R253H
+ Dox	220	506	467
- Dox	178	273	321

1906

1907

1908

1909 Supplementary Table 12. Number of cells analyzed in Supplementary Figure 3.

	AX42	LIP-yEVenus	WT EL222
Darkness	229	433	246

1910

1911